NAIST-IS-DT0161203

Doctor's Thesis

Studies on Performance Analysis of Network Architectures for Wavelength Division Multiplexing

Takuji Tachibana

July 5, 2004

Department of Information Systems
Graduate School of Information Science
Nara Institute of Science and Technology

Doctor's Thesis
submitted to Graduate School of Information Science,
Nara Institute of Science and Technology
in partial fulfillment of the requirements for the degree of
DOCTOR of ENGINEERING

Takuji Tachibana

Thesis committee: Kenji Sugimoto, Professor
Hirokazu Nishitani, Professor
Shoji Kasahara, Associate Professor

Studies on Performance Analysis of Network Architectures for Wavelength Division Multiplexing*

Takuji Tachibana

Abstract

Wavelength division multiplexing (WDM) is attractive for the infrastructure of the next generation Internet, since it supports huge bandwidth by multiplexing several wavelengths into a single optical fiber. In order to transmit Internet data over WDM networks, network architectures with photonic technologies, such as wavelength routing, optical burst switching (OBS), and optical packet switching (OPS) have been studied and developed.

Currently, it is difficult to store data in optical domain because optical random access memory has still been in development phase. It is also well known that the cost of wavelength conversion is much expensive, while the conversion capability is quite limited. Therefore, it is important to develop WDM network architectures under those constraints, and the evaluation of performance measures such as loss probability, throughput, and wavelength utilization plays a crucial role for quantitative characterization of the developed network architectures. This dissertation focuses on two network architectures: the wavelength routing and OBS.

The dissertation firstly considers the wavelength routing network with dynamic lightpath configuration where a lightpath supports multiple label switched paths (LSPs). In this network, lightpaths are established according to the congestion state of a node and are released after some holding time. For the performance evaluation, the system is modeled as a multiple queueing system in light

* Doctor's Thesis, Department of Information Systems, Graduate School of Information Science, Nara Institute of Science and Technology, NAIST-IS-DT0161203, July 5, 2004.

and heavy traffic cases, and the connection loss probability and wavelength utilization factor are derived. Numerical examples show that the analytical models in both cases are effective for the performance evaluation in comparison with the simulation results, and show how the holding time affects the connection loss probability.

Secondly, to provide the multiple service classes for the connection loss probability, QoS-guaranteed wavelength allocation and shared wavelength allocation are proposed. In the first method, the pre-determined number of wavelengths are allocated to each QoS class depending on the priority of loss probability. Here, a wavelength set for a QoS class is a proper subset of other sets for higher classes. In the second method, wavelengths are classified into multiple dedicated wavelength sets and a shared wavelength set which is utilized by all classes. Both the methods can be utilized in the wavelength routing network with limited-range wavelength conversion. Both methods are modeled and analyzed with queueing theory, and numerical examples show the effectiveness of the methods.

Finally, the dissertation considers a timer-based burst assembly and slotted transmission scheduling for the OBS network. In the method, bursts are assembled in round-robin manner and are transmitted in accordance with slotted scheduling. A loss model with two independent arrival streams is constructed for the performance evaluation, and the burst loss probability, burst throughput, and data throughput are explicitly derived. The usefulness of the analysis is discussed with several numerical examples.

Currently, the WDM networks are deploying world-wide and the research for the realization of all-optical Internet has become more active than ever before. The author expects that the proposed methods and their performance analysis will be significantly utilized in order to construct the WDM networks for the next generation Internet.

Keywords:

WDM Network, Queueing analysis, Wavelength routing, Optical burst switching, Performance evaluation, Wavelength conversion

波長分割多重方式におけるネットワークアーキテクチャの性能解析に関する研究*

橘 拓至

内容梗概

次世代インターネットの基盤技術として, 複数波長の多重化により広帯域伝送を実現する波長分割多重 (WDM) 伝送方式の利用が検討されている. インターネットトラヒックを WDM 方式によって伝送するために, 波長ルーティング, 光バースト交換, 光パケット交換などの光技術を用いたネットワークアーキテクチャの研究開発が盛んに行われている.

現在 WDM 網では, 光ランダムアクセスメモリが依然として開発段階であるため, 光領域でデータを蓄積することが困難である. また波長変換コストが非常に高いために, WDM 網内で使用される波長変換機能が大幅に制限されてしまうことが指摘されている. したがって, WDM を基にした光ネットワークアーキテクチャの研究開発においては上述の技術的制約を十分考慮することが必要である. このとき棄却率, スループット, 波長利用率などの性能指標がネットワークアーキテクチャの定量的特徴を示す上で重要な役割を果たす. 本論文では特に, 波長ルーティングと光バースト交換の 2 つのネットワークアーキテクチャに注目する.

本論文ではまず, 各波長を使って複数の Label switched path (LSP) を設定可能な動的光パス設定手法について検討する. 本手法では各ノードの輻輳状態に応じて光パスが設定され, 光パス保持期間が経過すると解放される. 提案手法の性能評価を行うために, 低負荷および高負荷トラヒックの場合に対して複数待ち行列でモデル化を行い、コネクション棄却率と波長利用率を導出する。数値例では, シミュレーション結果との比較より解析モデルの妥当性を示し, さらに光パス保持期間が光パス棄却率に与える影響について検討する.

* 奈良先端科学技術大学院大学 情報科学研究科 情報システム学専攻 博士論文, NAIST-IS-DT0161203, 2004 年 7 月 5 日.

次に, 光パス棄却率に関して複数サービスクラスを提供する QoS 保証型波長割当方式と共有波長割当方式を提案する. QoS 保証型波長割当方式では, 優先度に応じて異なる数の波長を各 QoS クラスに対して割り当てる. このとき, 各波長集合は真部分集合を構成する. 一方共有波長割当方式では, 複数の専用波長集合と 1 つの共有波長集合に分類される. 各専用波長集合は特定クラスのみ利用可能で, 専用波長集合は全クラスが共有して利用する. ここで, 両手法とも波長変換機能に制約がある波長ルーティング網に適用可能である. 本論文では両手法のモデル化及び待ち行列理論による性能解析を行い, 解析及びシミュレーション結果より提案手法の有効性を示す.

本論文の最後では, ラウンドロビン型バースト生成方式とスロット伝送スケジューリングを組み合わせた光バースト伝送方式を検討する. 本方式では光バーストがラウンドロビンに従って生成され, 生成されたバーストはスロット型スケジューリングに従って送信される. 本方式の性能を評価するため, 2 つの独立な到着流をもつ有限待ち行列システムでモデル化を行い, バースト棄却率, バーストスループット, データスループットを明示的に導出する. 数値例において, 本性能解析の有効性について議論する.

現在 WDM 網は世界中で構築及び利用され始めたところであり, さらに次世代インターネットに向けた全光ネットワーキング技術の研究はこれまで以上に活発に行われている. それゆえ本論文で検討したネットワークアーキテクチャ及び性能解析が, 次世代インターネットに適した WDM 網の構築に広く利用されることが期待される.

キーワード

WDM 網, 待ち行列解析, 波長ルーティング, 光バースト交換, 性能評価, 波長変換

List of Publications

Journal Papers

1. T. Tachibana and S. Kasahara, "QoS-Guaranteed Wavelength Allocation for WDM Networks with Limited-Range Wavelength Conversion," *IEICE Transactions on Communications*, vol. E87-B, no. 6, pp. 1439-1450, June 2004.

2. T. Tachibana and S. Kasahara, "QoS Provisioning with Shared Wavelength Allocation for Limited-range Wavelength Conversion," To appear in *Broadband Networks*.

3. T. Tachibana and S. Kasahara, "Performance Analysis of Dynamic Lightpath Configuration for Symmetric WDM Ring Networks," To appear in *Journal of the Operations Research Society of Japan*.

4. T. Tachibana and S. Kasahara, "Performance Analysis of Timer-Based Burst Assembly with Slotted Scheduling for Optical Burst Switching Networks," Submitted to *IEEE Journal on Selected Areas in Communications*.

International Conference Papers

1. T. Tachibana and S. Kasahara, "Performance Analysis of Dynamic Lightpath Configuration for WDM Asymmetric Ring Networks," in *Proc. IFIP TC6 Networking 2002*, Pisa, Italy, May 2002, pp. 972–983.

2. T. Tachibana and S. Kasahara, "Performance Analysis of Dynamic Lightpath Configuration for WDM Tandem Networks," in *Proc. 10th Interna-*

tional Conference on Telecommunication Systems: Modeling and Analysis, Monterey, CA, USA, October 2002, pp. 679–688.

3. T. Tachibana, T. Ajima, and S. Kasahara, "Round-Robin Burst Assembly and Constant Transmission Scheduling for Optical Burst Switching Networks," in *Proc. IEEE Globecom 2003*, San Francisco, CA, USA, December 2003, pp. 2772–2776.

4. T. Tachibana, M. Ueda, and S. Kasahara, "A Preemptive Scheme with Two-Way Release Message Transmission in Optical Burst Switching Networks," To be presented in *IEEE Globecom 2004*.

Domestic Conference Papers

1. T. Tachibana and S. Kasahara, "Performance Analysis of Dynamic Wavelength-path Configuration for MPLS-based WDM Networks," *Technical Report of IEICE*, SSE2000–295, pp. 427–434, March 2001. (in Japanese)

2. T. Tachibana and S. Kasahara, "Performance Evaluation of Light-path Configuration with GMPLS for WDM Ring Networks: Impact of Access Network Traffic on Packet Loss Probability," *Technical Report of IEICE*, NS2001–140, pp. 37–42, October 2001.

3. T. Tachibana and S. Kasahara, "Queueing Analysis of Dynamic Lightpath Configuration Method for WDM Symmetric Ring Networks," *Proceedings of the Symposium on Queueing Theory and Its Applications: "Queueing theory in the 21st Century"*, pp. 11–20, January 2002.

4. T. Tachibana and S. Kasahara, "On the Performance of Dynamic Lightpath Configuration Method for Asymmetric WDM Ring Networks," *Technical Report of IEICE*, NS2002–14, pp. 53–56, April 2002.

5. T. Tachibana and S. Kasahara, "On the Performance of Shared Wavelengths for Wavelength Routing Network with Multiple QoS Classes," *Technical Report of IEICE*, IN2002–13, pp. 7–12, June 2002. (in Japanese)

6. T. Tachibana and S. Kasahara, "QoS-based Wavelength Allocation in Wavelength Routing Networks," *Technical Report of IEICE*, NS2002–184, PS2002 –58, pp. 9–12, December 2002. (in Japanese)

7. T. Tachibana and S. Kasahara, "Performance Analysis of QoS-Guaranteed Wavelength Allocation for WDM Networks," *Proceedings of the Queueing Symposium: Stochastic Models and their Applications*, pp. 239–248, January 2003.

8. T. Tachibana and S. Kasahara, "Performance Analysis of Optical Crossconnect with Optical Packet Switch: Optical Packet Loss Probability at Core Node," *Technical Report of IEICE*, NS2002–281, IN2002–254, pp. 125–128, March 2003. (in Japanese)

9. T. Tachibana, T. Ajima, and S. Kasahara, "Performance Evaluation of Round-Robin Burst Assembly in OBS switch with Fiber Delay Lines," *The 2003 Spring National Conference of ORSJ, Abstracts*, pp. 158–159, March 2003.

10. T. Tachibana and S. Kasahara, "Performance Evaluation of Shared Wavelength Allocation for WDM Networks with Limited-Range Wavelength Conversion," *Technical Report of IEICE*, CS2003–55, pp. 7–12, July 2003.

11. T. Tachibana and S. Kasahara, "Burst Transmission Scheduling for QoS Guarantee in JIT Protocol," *The 2003 Communications Society Conference of IEICE*, B–6–76, September 2003 (in Japanese).

12. T. Tachibana and S. Kasahara, "QoS-Based Optical burst transmission for JIT Protocol," *Technical Report of IEICE*, NS2003–216, PN2003–44, pp. 37–40, December 2003.

13. T. Tachibana, M. Ueda, and S. Kasahara, "A Preemptive Scheme with Two-Way Release Message Transmission in Optical Burst Switching: Impact of Wavelength Selection Rule on Burst Loss Probability," *Technical Report of IEICE*, CS2004–25, OCS2004-35, PN2004-30, pp. 49–52, May 2004.

Technical Reports

1. T. Tachibana and S. Kasahara, "QoS Provisioning with Shared Wavelength Allocation for Limited-range Wavelength Conversion," *NAIST-IS-TR2002014, Graduate School of Information Science, Nara Institute of Science and Technology*, August 2002.

2. T. Tachibana and S. Kasahara, "QoS-Guaranteed Wavelength Allocation for WDM Networks with Limited-Range Wavelength Conversion," *NAIST-IS-TR2002016, Graduate School of Information Science, Nara Institute of Science and Technology*, November 2002.

3. T. Tachibana and S. Kasahara, "Performance Analysis of Dynamic Lightpath Configuration for Symmetric WDM Ring Networks," *NAIST-IS-TR 2003001, Graduate School of Information Science, Nara Institute of Science and Technology*, February 2003.

4. T. Tachibana, T. Ajima, and S. Kasahara, "Round-Robin Burst Assembly and Constant Transmission Scheduling for Optical Burst Switching Networks," *NAIST-IS-TR2003003, Graduate School of Information Science, Nara Institute of Science and Technology*, April 2003.

Awards

1. The 20th ORSJ Prize for Distinguished Student Paper, Operations Research Society of Japan, September 2002.

2. The 18th TELECOM System Technology Award for Student, The Telecommunications Advancement Foundation, March 2003.

Acknowledgements

I express my gratitude to Professor Kenji Sugimoto of Nara Institute of Science and Technology for his support and constant encouragement. He taught me much about research.

I address thanks to Professor Hirokazu Nishitani for his helpful comments and discussions.

I am also deeply grateful to Associate Professor Shoji Kasahara of Nara Institute of Science and Technology for his kind support in completing this work. He offered me lots of enthusiastic guidance for my research and valuable comments about queueing model for proposed scheme. I managed to accomplish under his guidance and I really appreciate his support.

I address thanks to Assistant Professor Atsushi Satoh of Nara Institute of Science and Technology for his kindness and helpfulness. He gave me good advices about my research.

I address thanks to Assistant Professor Naotoshi Adachi of Nara Institute of Science and Techonology for his helpful comments and feedback. I followed his good example, and hence I could complete my doctorates.

Last but not least, I address thanks to all members of Systems Science Laboratory, Yuiki Kamiishi, Takahiro Miyaura, Natsuki Itaya, Junro Okubo, Yoshito Kikkawa, Hiroaki Sakurai, Shingo Yamane, Tomoya Ajima, Ken Aida, Takayuki Arai, Takafumi Ueno, Masakazu Kurimoto, Yoshiki Koumori, Misato Takei, Kazuma Nishizawa, Masuhiro Nitta, Satoshi Arima, Tomohiro Ikeda, Masayuki Ueda, Yuzo Takahashi, Masahiro Tsujie, Takamitsu Matsubara, Basel Al-Ali, Shuichi Inada, Masayuki Kudo, Kaori Kurita, Yukinori Nakamura, Michiyuki Magono, Chi Ying Jin, Sachiko Mita, Yuka Kai, Yukiko Tsukamoto, Ikuyo Matsumura, and Yoko Hashimoto.

Contents

List of Figures

List of Tables

Chapter 1

Introduction

1.1. Wavelength Division Multiplexing

Optical fiber offers much higher bandwidth than copper cable and is less susceptible to various kinds of electromagnetic interferences and other undesirable effects. The optical fiber provides the data transmission at a few tens of megabits per second and the distance of data transmission is more than a kilometer. The fiber can also provide the short-distance transmission inside large-scale network, and hence optical networks are widely deployed today [8, 48].

Recent rapid growth of the Internet requires evermore bandwidth due to multimedia applications such as voice over IP (VoIP), video conference, and video-on-demand. Although huge bandwidth can be supported with several optical fibers, it causes high cost to construct the optical networks. Therefore, multiplexing technique is important to transmit data at higher rates over a single fiber.

Currently, wavelength division multiplexing (WDM) is widely utilized as the multiplexing technique in the optical networks. The WDM technique multiplexes several wavelengths into a single optical fiber and can provide huge bandwidth over a single fiber as shown in Fig. 1.1. The devices for wavelength multiplexing and demultiplexing are called multiplexer and demultiplexer, respectively, and array waveguide grating (AWG) is generally used as both devices due to lower loss and flatter passband [11, 48].

In the future, the number of wavelengths in a fiber will be increased to a thousand wavelengths and a wavelength will support more than 40 Gbps trans-

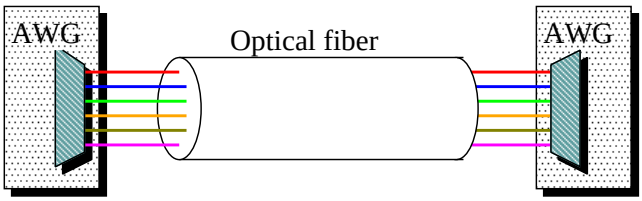

Figure 1.1. Wavelength division multiplexing.

mission. That is, several Tbps transmission will be realized over a single fiber with WDM. Therefore, WDM networks are attractive for the infrastructure of the next generation Internet [5, 7, 9, 18, 19, 37, 45, 50, 52]. In order to transmit the data in the WDM networks efficiently, three network architectures with photonic technologies, such as wavelength routing, optical burst switching (OBS), and optical packet switching (OPS) have been studied and developed [69]. In the following sections, we explain the three architectures in detail.

1.2. Wavelength Routing

1.2.1 Lightpath Configuration

In the wavelength routing network, a connection called *lightpath* is established by a wavelength between end nodes and data is transmitted over the lightpath [3, 15, 36, 47, 49, 51, 53, 54]. Because the lightpaths is routed optically from one link to another link at each node, the data transmission does not require opto-electronic-optic (O/E/O) conversion [32]. Optical add/drop multiplexer (OADM) and optical crossconnect (OXC) are utilized as core devices at node (see Fig. 1.2). The OADM selectively adds and drops wavelengths to establish lightpaths [4]. On the other hand, the OXC establishes lightpaths by switching wavelengths from input ports to output ones in optical domain. The OADMs and OXCs are utilized in ring network and mesh network, respectively.

When the configuration of lightpaths is pre-determined and the lightpaths are permanently established, it is important to design in advance the lightpath configuration depending on network topology and traffic requirements. This is

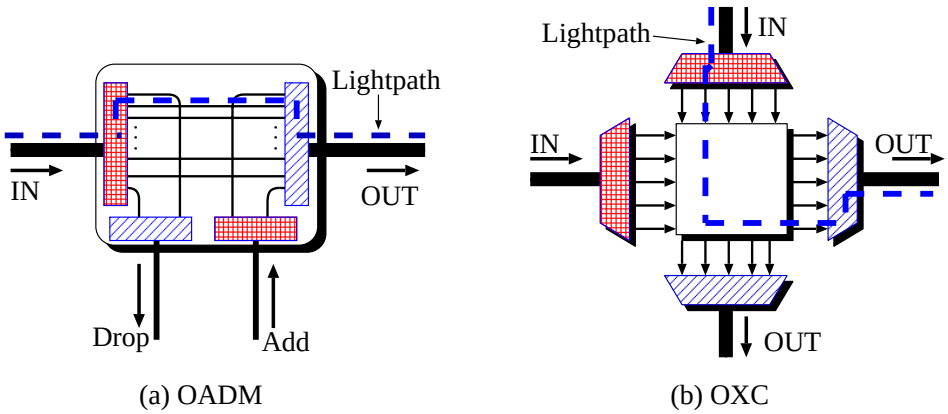

Figure 1.2. Optical devices.

called route and wavelength assignment (RWA) problem and several studies have appeared in the literature [40, 46]. In general, the RWA problem for a general network topology is quite difficult. If the optimal solution for the RWA is obtained, it does not always provide the best performance when traffic demand changes over short time-scales.

On the other hand, the dynamic lightpath configuration have been considered to establish and release the lightpaths dynamically. When a request of lightpath establishment arrives at a node, an available wavelength is allocated to the lightpath. If all wavelength allocations in the nodes along the path succeed, the lightpath is eventually established. When there is no data transmission in the established lightpath, the lightpath is released. Therefore, the lightpath configuration changes depending on the traffic requirement at each node. If there is no available wavelength in any node along the path, the lightpath establishment fails.

1.2.2 Wavelength Continuity Constraint

Generally, whether the lightpath configuration is static or dynamic, the lightpath has to be established with the same wavelength from source node to destination one (*wavelength continuity constraint*). This wavelength continuity constraint increases the connection loss probability and degrades the performance of the

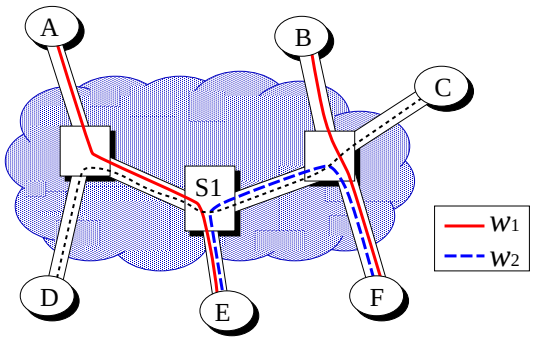

Figure 1.3. Wavelength continuity constraint in wavelength routing.

wavelength routing network [11]. If the nodes have the capability of wavelength conversion, the lightpath can be established with the different wavelengths at each link.

Fig. 1.3 shows the wavelength routing network where only two wavelengths, w_1 and w_2, are multiplexed at each link. In this figure, a lightpath is already established between nodes A (B) and E (F) with the wavelength w_1 (w_2). In this case, a new lightpath can not be established between nodes D and F. This is because there is no available wavelength between the two nodes. However, if the switch S1 has the wavelength conversion capability which can convert w_1 to w_2 and vice versa, the new lightpath can be established. Thus, the wavelength conversion significantly improves the performance of the wavelength routing network.

1.3. Optical Packet Switching

In the OPS, data is transmitted from source node to destination one with optical packets. The OPS can transmit the data from different source nodes over the same wavelength, and hence wavelengths are utilized efficiently. When the OPS network is used in the Internet, an optical packet corresponds to an IP packet.

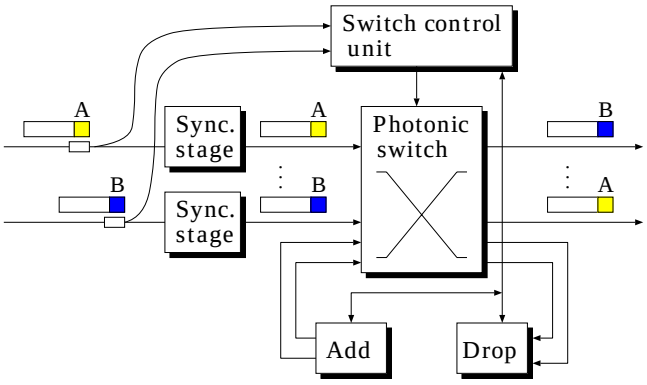

Figure 1.4. Node architecture of the slotted OPS network.

1.3.1 Switching Function

The optical packet consists of a header which contains routing information, and a payload which contains data. When an optical packet arrives at an optical switching node, the node reads its header, and switches it to an appropriate output port. Note that the header is processed in the electronic domain with the O/E/O conversion. The node may also impose a new header on the packet.

If two packets from different input ports are switched to the same output port, one of the packets must be switched to another output port, or be buffered in the node. It is difficult to store data in optical domain because optical random access memory has still been in development phase. With fiber delay line (FDL) which is a length of fiber, optical packets are stored in the node optically.

1.3.2 Slotted and Unslotted Networks

The OPS networks are classified into two categories: slotted (synchronous) networks and unslotted (asynchronous) ones. In the slotted networks, all the optical packets have the same size and a fixed time slot contains both the payload and header [11].

Fig. 1.4 shows a general optical switching node in the slotted networks. In the node, all the arriving packets from the input port are aligned in phase with one another before entering the optical switch. To synchronize all the arriving

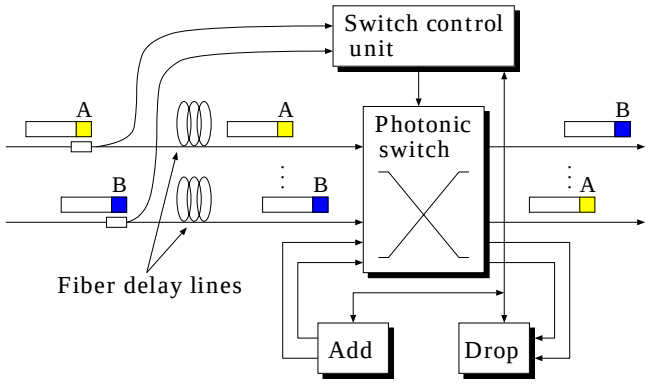

Figure 1.5. Node architecture of the unslotted OPS network.

packets successfully, it is important to design the synchronization stages in the node. Because the packet-synchronization causes insertion loss and crosstalk, optical amplification is required and the signal-to-noise ratio may degrade. The crosstalk is also accumulated due to the synchronization stage and the bit-error rate becomes large. Thus, the synchronization stage may significantly degrade the performance of the OPS.

In the unslotted network, packets may or may not have the same size. All the arriving packets enter the switch without being aligned, and hence the switching of packets is performed at any point in time. Fig. 1.5 shows a general node architecture and packet transmission for the unslotted networks. In the node, the FDLs with fixed length are used to store the packets during the header processing and switch control. Note that there is no packet alignment stage and the synchronization of packets are not required.

Obviously, in the unslotted networks, the contention between multiple packets occurs more frequently than that in the slotted networks and more optical packets are likely to be lost. This is because the behavior of the packet is more unpredictable. On the other hand, the unslotted networks are more flexible than the slotted networks, because the unslotted networks can switch packets of variable sizes.

1.4. Optical Burst Switching

Recently, as a new network architecture for the WDM networks, the OBS has been studied and developed. In the OBS networks, multiple IP packets are assembled into a burst with variable length at an ingress edge node and is transmitted to its destination one [10, 16, 42, 64, 70, 71]. A burst is pure payload and has the associated control packet which contains control information such as burst length and routing information [21, 67]. As is the case with the OPS networks, the control packet is processed electrically with the O/E/O conversion at each node.

1.4.1 Signaling Protocol

In order to reduce signaling delay, a source node starts burst transmission without receiving any acknowledgement from its destination edge node (one-way reservation). For the one-way reservation, several signaling protocols such as Just-Enough-Time (JET) and Just-In-Time (JIT) have been proposed with regard to the reservation period of a wavelength for the burst transmission [12, 43, 44].

In the JET signaling protocol, a source node sends a control packet and then sends the corresponding burst after some offset time [70, 71]. The offset time is preobtained from the number of hops and the processing time of the control packet. Using extra information to better predict the start and end of the burst, a wavelength is reserved efficiently to transmit the burst (see Fig. 1.6 (a)). When there are no available wavelengths at the arrival time of the burst, the control packet fails the wavelength reservation and the burst is lost. Moreover, in the JET protocol, the void between two bursts in a wavelength can be utilized (void filling) and wavelengths are utilized effectively. Therefore, the JET protocol will achieve a better performance than other signaling protocols [43].

On the other hand, in the JIT protocol such as *Explicit Setup and Explicit Release* (ESER) or *Explicit Setup and Implicit Release* (ESIR), an output wavelength is reserved after the arrival of a setup message [2, 58, 62]. When there are no available wavelengths at the arrival time of the setup message, the setup message is rejected and the corresponding burst is lost. In the ESER, the wavelength is released after the arrival of the corresponding release message (see Fig. 1.6 (a)), while in the ESIR, the wavelength is released with a timer just after the burst

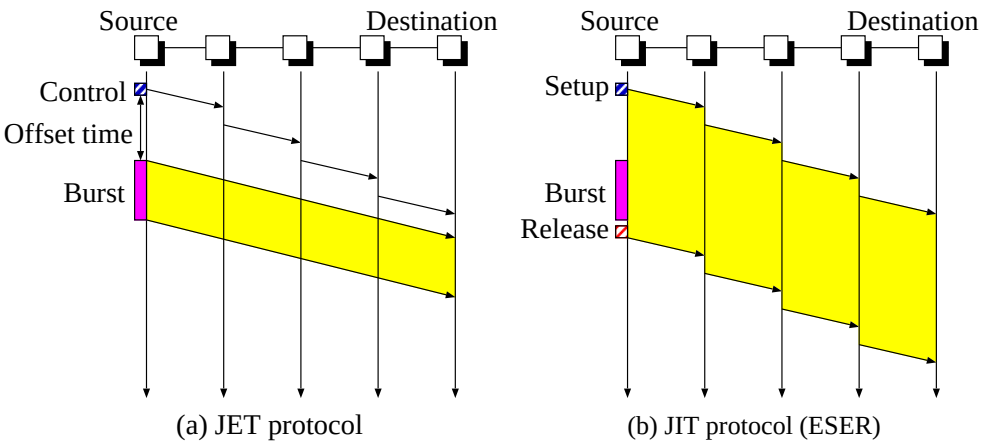

Figure 1.6. Signaling protocol.

transmission. Because a wavelength is reserved immediately after the arrival of setup message, the void filling cannot be utilized in both schemes. Although the JIT protocol can not use wavelengths efficiently, the wavelengths are reserved more simply and more straightforward than the JET protocol.

1.4.2 Burst Assembly Technique

Burst assembly is an important issue for the OBS and several burst assembly techniques have been proposed. Most of the techniques are classified into threshold-based and timer-based burst assemblies. [59] proposed a threshold-based burst assembly technique in which a threshold is used in order to limit the maximum number of packets within a burst. With this burst assembly, bursts with the same length are frequently transmitted over the OBS network.

In [16], a timer-based burst assembly technique called the *Fixed-Time-Min-Length burst assembly algorithm* was proposed. In this technique, a timer is started at the arrival time of the first packet and a burst is assembled when the timer reaches a pre-specified timeout value. If the amount of IP packets for the burst is too small, it is assembled with padding the null data. This burst assembly technique creates bursts with variable length but provides an upper bound on delay due to the timeout value. [72] reported that the distribution of

burst length approaches to a Gaussian distribution with zero variance when the timeout value becomes large.

[67] proposed the timer-based burst assembly in which both the timeout value and the maximum burst size are taken into consideration. [60] developed the [67]'s scheme into the one which provides a Quality-of-Service (QoS) guarantee. [6] proposed a timer-based burst assembly algorithm focusing on the TCP congestion control. In this method, the timeout value and the minimum burst size are adapted to TCP flows. [33] considered the DiffServ-based burst assembly scheme where each burst assembly time is adapted to the actual traffic arrival rate and the QoS requirement.

1.4.3 Burst Transmission Scheduling

The assembled burst is sent into the OBS network after some offset time which is calculated according to burst scheduling [60]. The burst transmission scheduling affects the performance of the OBS networks, and hence several burst transmission schedulings have been studied.

In the first-come first-served (FCFS) scheduling, bursts are transmitted in their assembling order. In the priority queueing (PQ), a burst with low priority is sent to an output port only if there is no burst with high priority. In the weighted round-robin (WRR), each prioritized burst queue is served in a round-robin order and the number of bursts sent in each round depends on the weight assigned by the policy. In the waiting time priority (WTP), a scheduler transmits the burst with the longest waiting time to the OBS network.

1.5. Physical Constraints on WDM Network Development

Physical constraints significantly affects the performances of the three network architectures. In this section, we consider the three physical constraints; wavelength conversion, photonic processing, and optical buffering.

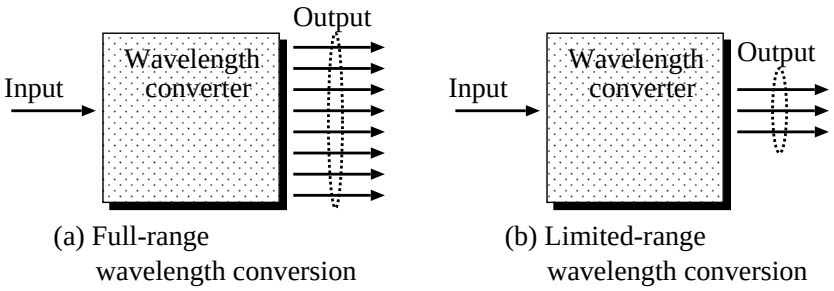

Figure 1.7. Two types of wavelength conversion.

1.5.1 Wavelength Conversion

In the WDM networks, the wavelength conversion is important function to improve network utilization. If the wavelength conversion is available in the wavelength routing networks, a lightpath can be established with the different wavelengths along the path. As for the OPS and OBS networks, optical packets and optical bursts can utilize another wavelength to avoid the packet loss and burst loss due to the contention, respectively. Here, the wavelength conversion is classified into two categories: full-range wavelength conversion and limited-range wavelength conversion [15, 20, 47, 51, 69].

The full-range wavelength conversion can convert any input wavelength to any output wavelength as shown in Fig. 1.7(a). The limited-range wavelength conversion can convert an input wavelength to some wavelength within a limited range (see Fig. 1.7(b)). Although the full-range wavelength conversion is more effective than the limited-range one, it is difficult to realize the full-range wavelength conversion under the current technology [20]. Therefore, the limited-range wavelength conversion is a popular conversion technique. The wavelength conversion capability has to be carefully taken into consideration, no matter which network architecture is focused on.

1.5.2 Photonic Processing

Photonic processing techniques, such as reading a header and routing a packet, are still not practical. Therefore, as denoted previously, the header of an op-

tical packet is processed electrically. The control packet of an optical burst is also processed in the electric domain. This electrical process requires the O/E/O conversion, and the O/E/O conversion causes the overhead in the network architectures. Therefore, the photonic processing is one of the most important constraints to develop the WDM networks.

If the photonic processing will be available in the future, optical packets will be processed in the optical domain just like IP packets in the electric domain. It is expected that the OPS network based on the photonic processing is the most effective for the next-generation Internet.

1.5.3 Optical Buffering

Currently, optical random access memory has still been in development phase, and hence the FDLs are utilized in the OPS and OBS networks to store data in the optical domain. The FDL only provides fixed delay and is completely different from a conventional buffer. For example, the FDL whose length is 200 m can store a packet for 1.0 μs [1] . Hence, the volume of a FDL becomes large in order to store data for a long time.

Several structures of FDLs have been considered. Fig. 1.8 shows a feed-forward FDL structure and a feedback one. The feed-forward FDLs in this figure has two input ports and two output ports with three 2×2 switches. If each delay line can store one optical packet, a node with this FDL structure can store two packets. If two packets with the same output port come from both input ports simultaneously, one of packets will be switched to the FDL and stored for the buffering time.

On the other hand, in the feedback configuration, the FDLs are connected from output ports to input ones. Generally, some ports are utilized for buffering. If multiple packets with the same output port come from multiple input ports, some packets are switched to the FDLs and stored for some buffering time. After the packets are stored in the FDLs, the packets are transmitted to the output ports. However, the buffering time is still limited.

Thus, the optical buffering with the FDL is one of the most important aspects

[1] Optical signal propagates in the optical fiber approximately 200,000 km per second.

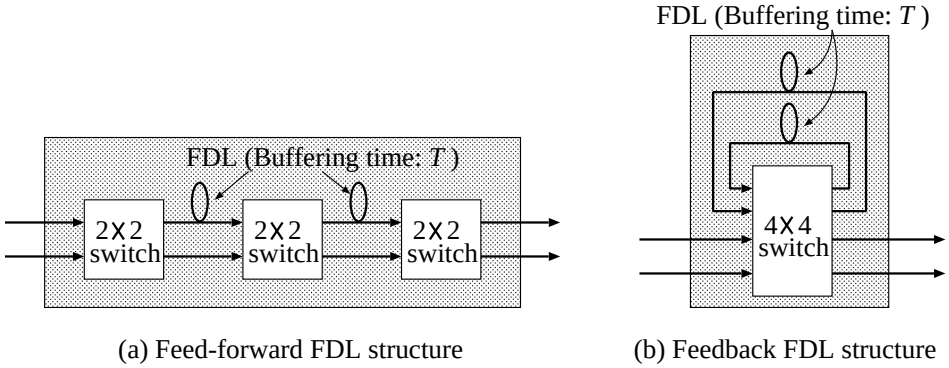

(a) Feed-forward FDL structure (b) Feedback FDL structure

Figure 1.8. Two types of FDL structures.

for the development of the WDM networks.

1.6. Objective and Overview of the Dissertation

The previous section shows that the wavelength conversion, the photonic processing, and the optical buffering are primary constraints to develop the WDM networks. Currently, the WDM networks are deploying world-wide and the research for the realization of all-optical Internet has become more active than ever before. Therefore, it is important to develop the network architectures, such as wavelength routing, OBS, and OPS, under those constraints. The evaluation of performance measures such as loss probability, throughput, and wavelength utilization plays a crucial role for quantitative characterization of the developed network architectures.

In the dissertation, we consider new network architectures for the WDM networks and evaluate their performances with queueing theory and simulation. With the analysis and simulation results, we investigate how the physical constraints affect the proposed methods and discuss the development capability of the architectures.

The organization of the dissertation is as follows. In Chapter 2, we consider the case where a lightpath supports multiple label switched paths (LSPs). An LSP is used to transmit packet flows from an access network to the other ac-

cess network. In order to evaluate the performance of the dynamic lightpath configuration for packet-flow transmission, we consider a symmetric WDM ring network under two traffic conditions: light and heavy ones. In the light traffic case, we model the dynamic lightpath configuration system as a continuous-time Markov chain to take into account the lightpath establishment/release time. In the heavy traffic case, established lightpaths are likely to be held for a while and those are rarely established or released. Therefore, we consider an $M/G/1/K$ and multiple $M/G/c/c$ queues for modeling the system in the heavy traffic case. In both cases, a packet flow which consists of consecutive packets is considered as a customer, and the loss probability of packet flow and wavelength utilization factor are derived.

In Chapter 3, we focus on the connection loss probability as the QoS metric to provide multiple QoS classes for the loss probability. We propose a QoS-guaranteed wavelength allocation for the wavelength routing network with limited-range wavelength conversion. In the proposed allocation, the pre-determined number of wavelengths are allocated to each QoS class depending on the priority of loss probability. Here, a wavelength set for a QoS class is a proper subset of other sets for higher classes. Moreover, the wavelength set for the highest priority class includes all wavelengths multiplexed in an optical fiber so as to decrease the connection loss probability.

We consider two wavelength selection rules according to which idle wavelength is selected from the wavelength set for the requested QoS class. The connection loss probability of each class greatly depends on the combination of the wavelength selection rules. We consider three combinations of wavelength selection rules and compare those in a single link and uni-directional ring network. As for the performance evaluation of the QoS-guaranteed wavelength allocation, we derive the connection loss probability of each QoS class for the single link using a continuous-time Markov chain. With this analytical result, we investigate the impact of three combinations of wavelength selection rules on the connection loss probability of each QoS class. We also investigate the connection loss probability for a uni-directional ring network with limited wavelength conversion by simulation.

In Chapter 4, we propose a shared wavelength allocation method to provide

multiple QoS classes for the connection loss probability. When a connection request arrives at node, one of available wavelengths in the dedicated wavelength set for its priority class is allocated to the connection. If there are no available wavelengths in the dedicated wavelength set, one of wavelengths in the shared wavelength set is allocated to the connection. Since shared wavelengths are utilized by all classes, it is expected that the total connection loss probability decreases. Moreover, we consider how to apply the shared wavelength allocation method to the all-optical wavelength routed network with limited-range wavelength conversion. To be more precise, wavelengths are classified into multiple wavelength subsets in advance, and then the shared wavelength allocation method is applied to each subset. To evaluate the performance of our proposed method for a single link case, we investigate the connection loss probability of each QoS class using approximation analysis and simulation. In the approximation analysis, we model the proposed method as a two-stage queueing model which has multiple primary stations and a single secondary station. Using the equivalent random method (EQRM), the connection loss probability of each QoS class is calculated. We also investigate the performance of the method in uni-directional ring network by simulation.

In Chapter 5, we analyze the performance of the timer-based burst assembly at an edge OBS node without FDLs. A burst is assembled in a round-robin manner, and with the JET signaling protocol, assembled bursts are transmitted into the OBS network at multiples of some fixed interval. We model the edge node as a loss model with geometric and Poisson arrivals, and explicitly derive the burst loss probability, burst throughput, and data throughput. We also investigate those performance measures for uni-directional ring and mesh-torus networks by simulation, and discuss the effectiveness of our analysis in comparison with the Erlang loss model and simulation.

Finally, we conclude the dissertation in Chapter 6.

Chapter 2

Dynamic Lightpath Configuration

2.1. Introduction

OADM selectively adds and drops a wavelength to establish an all-optical connection in WDM ring networks shown in Fig. 2.1. The all-optical connection is called *lightpath* and it is established between any pair of OADMs as shown in Fig. 2.2. The wavelengths to be added and dropped are pre-selected in each OADM [17, 38, 48] and the lightpath configuration is not changed frequently. However, when traffic pattern changes over short time-scales, the static lightpath configuration degrades the performance of the network [63]. If the wavelengths are dynamically added and dropped, the high utilization of wavelengths and small packet loss probability are expected [1].

In [73], a lightpath configuration method for the OADM has been proposed. In the method, a lightpath is dynamically established according to the congestion state of a node, however, the release of the established lightpath is not taken into consideration. In [55], we considered a dynamic lightpath configuration method with which a lightpath is established according to the congestion state of the node and is released when there are no packets to be transmitted with the lightpath. Note that both lightpath establishment and release times are overhead and the lightpath can not be utilized during those times. Therefore, frequent establishment or release of lightpath may decrease the utilization of wavelengths. In

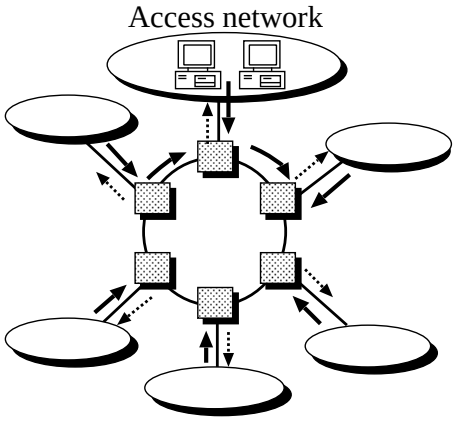

Figure 2.1. Ring network model.

[55], we introduced a design parameter called *extra holding time* and when there are no packets to be transmitted with some lightpath, the lightpath is still held during the extra holding time. The lightpath is released if there are no arriving packets during the extra holding time. Numerical examples in [55] showed that the dynamic lightpath configuration provides smaller loss probability than the static lightpath configuration in asymmetric ring networks.

In [55], a lightpath is established for the transmission of a packet. In general, because the cost of the lightpath establishment and release is high, a lightpath is used for packet flows which consist of consecutive packets with the same destination network address or the same-destination label-switching router (LSR) in some access network connected to the other WDM node. In this chapter, we consider the case where a lightpath supports multiple label switched paths (LSPs) and the LSP is used to transmit the packet flow from an access network to the other access network (see Fig. 2.1).

In order to evaluate the performance of the dynamic lightpath configuration for packet-flow transmission, we consider a symmetric WDM ring network under two traffic conditions: light and heavy ones. In the light traffic case, we model the dynamic lightpath configuration system as a continuous-time Markov chain to take into account the lightpath establishment/release time. In the heavy traf-

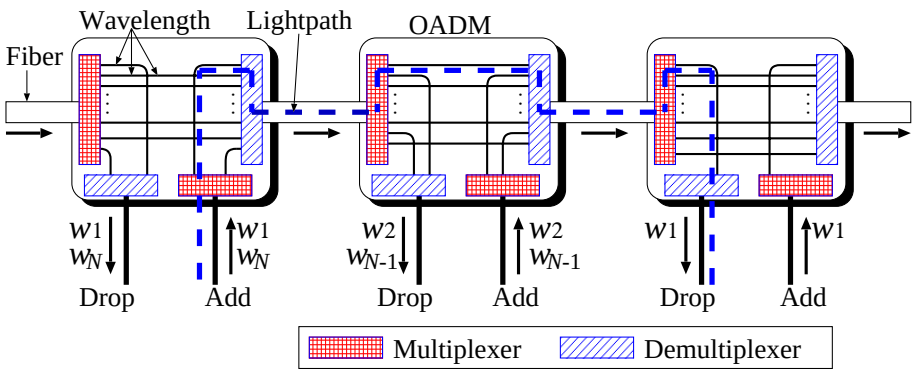

Figure 2.2. Optical add/drop multiplexer.

fic case, established lightpaths are likely to be held for a while and those are rarely established or released. Therefore, we consider an $M/G/1/K$ and multiple $M/G/c/c$ queues for modeling the system in the heavy traffic case. In both cases, a packet flow which consists of consecutive packets is considered as a customer, and derive the loss probability of the packet flow and wavelength utilization factor.

Note that in the dynamic lightpath configuration considered in the chapter, the lightpath establishment and release do not occur frequently in the symmetric ring network. Therefore, our performance analysis for the symmetric ring network provides the worst case analysis and is useful for the asymmetric ring network.

The rest of the chapter is organized as follows. Section 2.2 describes the lightpath configuration method in detail, and in Section 2.3, the ring network model is presented. The performance analysis of the method in the light traffic case is shown in Section 2.4 and the performance analysis in the heavy traffic case is presented in Section 2.5. Numerical examples are given in Section 2.6 and finally, conclusions are presented in Section 2.7.

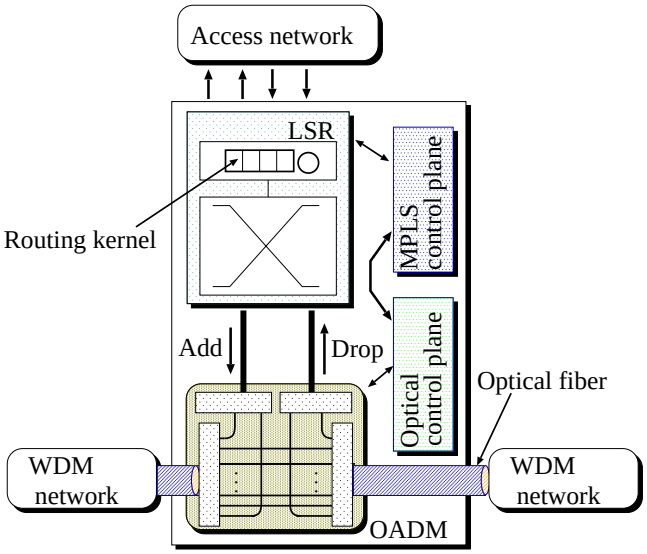

Figure 2.3. Node architecture.

2.2. Proposed Method

In this section, we summarize the dynamic lightpath configuration method where multiple LSPs are supported in a lightpath [55, 73]. Each node in a WDM network consists of an OADM and an LSR as shown in Fig. 2.3, and the nodes are connected with optical fibers as shown in Fig. 2.4. The procedure of lightpath configuration is as follows (see Fig. 2.5).

For simplicity, we consider a tandem network with three nodes, namely, the nodes A, B, and C. Each node is connected to its own access network through the LSR. Suppose $W + 1$ wavelengths are multiplexed into an optical fiber in the WDM network. Among $W + 1$ wavelengths, the W wavelengths are used to transmit data traffic and one is dedicated to distribute control traffic (see Fig. 2.4). Let w_i $(i = 0, \cdots, W - 1)$ denote the ith wavelength for data traffic.

The wavelength w_0 is used for the transmission to adjacent nodes (from A to B and from B to C in Fig. 2.5). We call w_0 the default path in the following. The default path only supports hop by hop transmission. Packets transmitted with the default path arrive at the layer 3 routing kernel in the LSR. At the

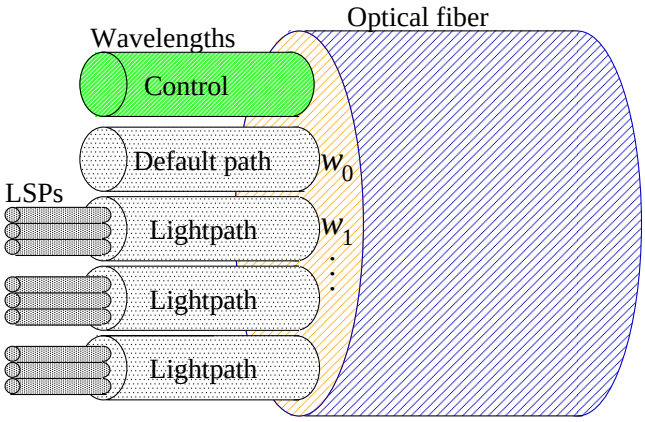

Figure 2.4. Data transmission structure.

routing kernels in the source and intermediate nodes, packets are routed to the next node. At the routing kernel in the destination node, on the other hand, packets are routed to the access network.

Other $W - 1$ wavelengths are used for lightpaths which connect any pair of source and destination nodes. Those lightpaths are dynamically established and released between the source and destination nodes according to congestion states in the source and intermediate nodes along the path. An established lightpath contains multiple cut-through LSPs which have the same source and destination OADMs but have the different pairs of source and destination network addresses or the different pairs of LSRs in the access networks connected to those nodes.

When the first packet in the packet flow whose destination is in the node C's access network arrives at the node A from the A's access network, the LSR of the node A selects a wavelength with which the packet flow is transmitted. If there exists an established lightpath between the two nodes, a new cut-through LSP is established in the lightpath. If the establishment of the cut-through LSP fails due to the shortage of available bandwidth in the lightpath, the packet flow is forwarded to the routing kernel and transmitted to the destination through the default path [41].

In the dynamic lightpath configuration method, a buffer in the routing kernel

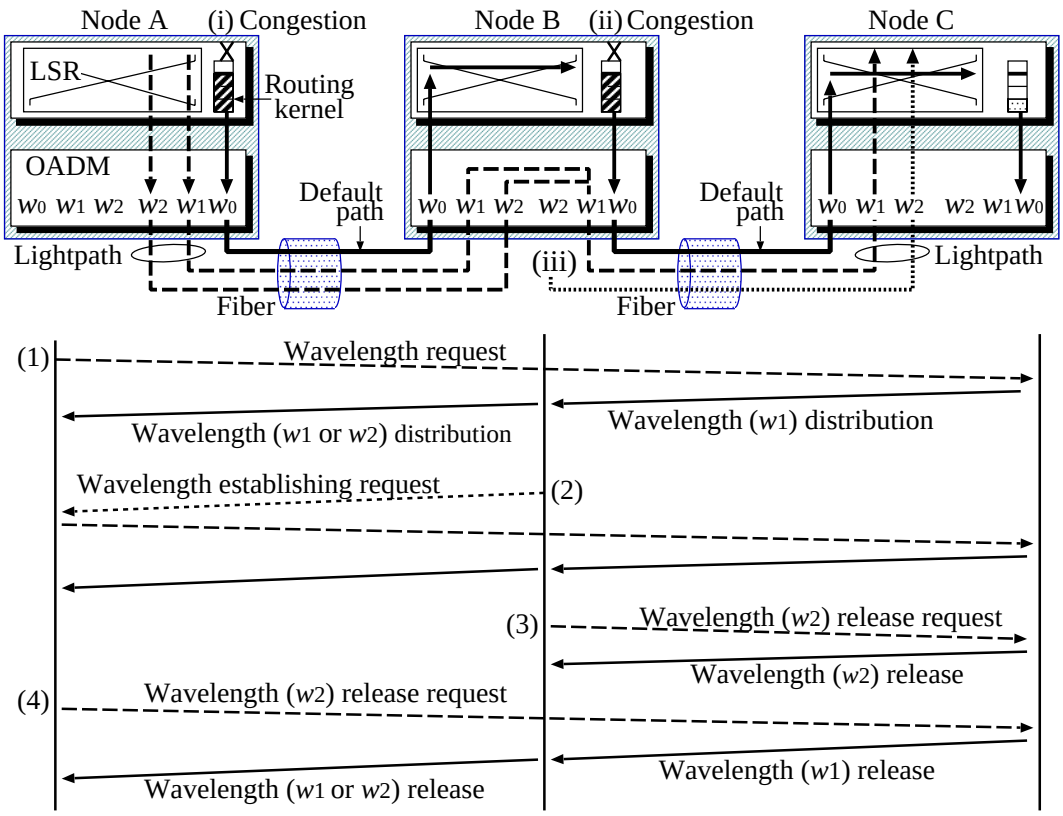

Figure 2.5. Dynamic lightpath configuration.

of the LSR has a pre-specified threshold [73]. If the amount of packets in the buffer becomes equal to or greater than the threshold, the LSR regards the routing kernel as being in congestion and decides to establish a new lightpath between the source and destination nodes for the packet flow. This happens when the packet flow transmitted from the nodes A to C triggers congestion at the node A, or when it triggers congestion at the node B.

In both cases, a lightpath is established as shown in Fig. 2.5 (1) and (2) [73]. Each node has the information of current lightpath configuration and the new lightpath configuration is performed based on the information. If the same wavelength can not be available at consecutive links, the wavelength conversion may be required at the corresponding node [48]. If no wavelengths are available

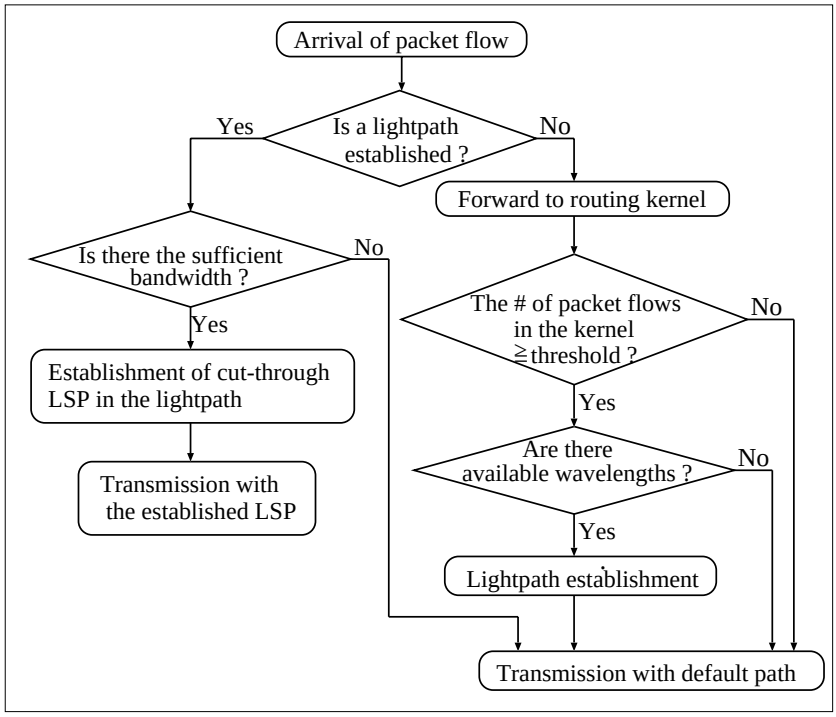

Figure 2.6. Flowchart of lightpath establishment.

at the node, the lightpath configuration fails.

When no IP packets are transmitted with the LSP during a given time interval, the node releases the LSP. When the lightpath established between the nodes B (A) and C (C) becomes idle, the timer for the extra holding time in the source node B (A) starts. The lightpath is released if the extra holding time is over and no LSP is established in the lightpath (Fig. 2.5 (3) ((4))). The procedures of the lightpath establishment and release are shown in Figs. 2.6 and 2.7, respectively.

2.3. Network Model

For the performance analysis of the dynamic lightpath configuration, we consider a symmetric WDM ring network with L_{node} nodes, shown in Fig. 2.1. Each node consists of an OADM and an LSR, and lightpaths are established or released

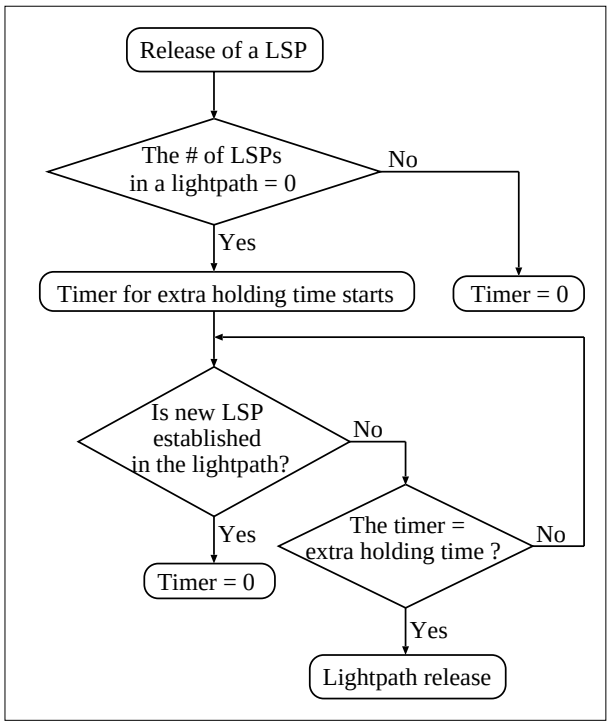

Figure 2.7. Flowchart of lightpath establishment.

according to the dynamic lightpath configuration method. In addition, each node is connected to its own access network through the LSR. For simplicity, we assume that the unit of transmission is a packet flow and that multiple lightpaths between any pair of nodes are not permitted. Moreover, we assume that the LSP is released after all IP packets in a packet flow are transmitted.

The number of wavelengths available at each node is W and all wavelengths can be converted regardless of any wavelength pairs. One of the W wavelengths is for the default path and the others are for the lightpaths which are dynamically established and released. The $W-1$ wavelengths are numbered from 1 to $W-1$ and a lightpath is established with one of the $W-1$ wavelengths according to the first-fit strategy in which the available wavelength with the smallest index number is selected.

Moreover we assume that the size of a packet flow is exponentially distributed

with the mean δ_{flow} bits and that the destination of each packet flow is equally likely. This implies that the destination of packet flow which arrives at node i is node j ($j \neq i$) with probability $1/(L_{node} - 1)$. Packet flows sent to some destination arrive at a node according to a Poisson process with rate λ_{flow}. Since there are $L_{node} - 1$ destinations for each node, packet flows arrive at the node from its access network according to a Poisson process with rate $(L_{node} - 1)\lambda_{flow}$. In this ring network, packet flows are transmitted in clockwise direction. Since the network is symmetric, we focus on a node in the network and consider the performance of the dynamic lightpath configuration method.

We assume that W wavelengths have the same bandwidth E bps, i.e., the bandwidth of an established lightpath also has E bps. In addition, all established cut-through LSPs have the same bandwidth equal to E_l bps. Therefore, a lightpath supports up to $K_l = \lfloor E/E_l \rfloor$ cut-through LSPs where $\lfloor x \rfloor$ is the maximum integer smaller than or equal to x.

Let $K_r\delta_{flow}$ [bits] denote the capacity of the layer 3 routing kernel in the LSR. Here, the capacity consists of a waiting room in which packet flows are stored for transmission, and a server where a packet flow is in transmission. Let $T_h\delta_{flow}$ [bits] denote the pre-specified value of the threshold for the routing kernel. For simplicity of the analysis, we assume that the unit of both K_r and T_h is the number of packet flows.

2.4. Performance Analysis in the Light Traffic Case

In this and the following sections, we analyze the performance of the dynamic configuration for a symmetric WDM ring network. This section is devoted to the analysis in the light traffic case and the next subsection to that in the heavy traffic case.

2.4.1 System Model

In the light traffic case, the establishment and release of lightpaths may greatly affect the performance of the dynamic lightpath configuration method. Thus we

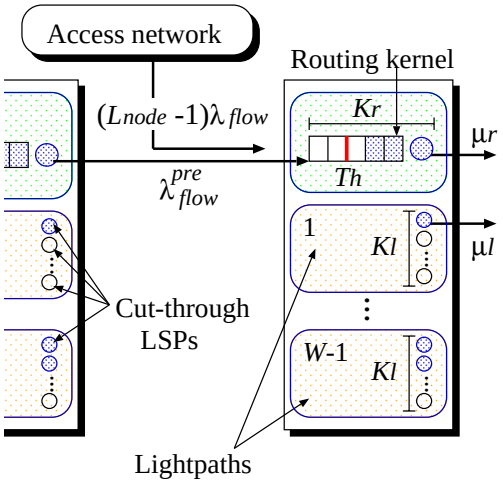

Figure 2.8. Ring node model with light traffic.

consider a multiple queueing system under light traffic as shown in Fig. 2.8. In this network model, there are W queues in a node: one is for layer 3 routing kernel and the other $W-1$ queues are for the lightpaths which are dynamically used according to the congestion of the routing kernel. Here a lightpath supports K_l cut-through LSPs. In the light traffic case, we assume that the transmission times of packet flows for the routing kernel and cut-through LSP are exponentially distributed with rates μ_r and μ_l, respectively. Because the processing speed of the routing kernel is E_r bps and the size of a packet flow is δ_{flow} bits, the mean transmission time of the routing kernel is given by $1/\mu_r = \delta_{flow}/E_r$, and that of the cut-through LSP is given by $1/\mu_l = \delta_{flow}/E_l$. Note that $E_r \leq E$ and $E_l \leq E$ where E is the bandwidth of a lightpath. We also assume that the lightpath establishment/release time and the extra holding time are exponentially distributed with rates p and h, respectively.

We have two kinds of packet flows that arrives at the node: one is from the access network and the other is from the previous node. As shown in the above, we assume that packet flows arrive at the node from the access network according to a Poisson process with rate $(L_{node}-1)\lambda_{flow}$.

Next we consider packet flow traffic from the previous node. Since the packet

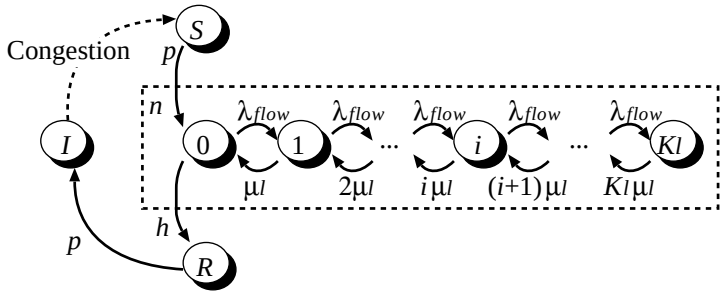

Figure 2.9. State transition diagram for a lightpath.

flow arrives at the routing kernel depending on the congestion state and the queue size of the routing kernel is finite, our ring network is not an open Jackson queueing network. However, due to light traffic, a newly arriving packet flow is hardly lost and is likely to be transmitted through the default path. Therefore we can approximate the arrival process from the previous node with the similar approach to the analysis of open Jackson network [28, 65].

The packet flow transmitted with the default path from the previous node arrives at the routing kernel in the tagged node, and then it is routed to the node's access network or the next node. Let λ_{flow}^{pre} denote the arrival rate at the routing kernel in the tagged node. Considering the transmissions originated from the other $(L_{node} - 1)$ nodes, we obtain

$$\lambda_{flow}^{pre} = \frac{L_{node}(L_{node} - 1)}{2}\lambda_{flow}. \tag{2.1}$$

We assume that the packet flow arrival process from the previous node to the routing kernel is Poisson with rate λ_{flow}^{pre}. Thus the whole arrival rate of packet flows at the node, λ_{flow}^{all}, is given by

$$\lambda_{flow}^{all} = (L_{node} - 1)\lambda_{flow} + \lambda_{flow}^{pre} = \frac{(L_{node} + 2)(L_{node} - 1)}{2}\lambda_{flow}. \tag{2.2}$$

2.4.2 Performance Analysis

Let l_i $(1 \leq i \leq W-1)$ denote the ith lightpath dynamically established and released at the node. We define the state of l_i at t as follows.

$$J_{l_i}(t) = \begin{cases} n, (n = 0, \cdots, K_l), & \text{if } l_i \text{ is busy and } n \text{ cut-through LSPs} \\ & \quad \text{are established,} \\ I, & \text{if } l_i \text{ is idle,} \\ S, & \text{if } l_i \text{ is being established,} \\ R, & \text{if } l_i \text{ is being released.} \end{cases}$$

Let $N_r(t)$ denote the number of packet flows in the routing kernel at t. Then we define the state of the system at t as $(N_r(t),\ \boldsymbol{J}_l(t))$, where

$$\boldsymbol{J}_l(t) = (J_{l_1}(t), \cdots, J_{l_{W-1}}(t)). \tag{2.3}$$

The state transition diagram for l_i is illustrated in Fig. 2.9. Note that in this figure, $1/p$ and $1/h$ denote the mean lightpath establishment/release time and the mean extra holding time, respectively. Let $U_{r,l}$ denote the whole state space of $(N_r(t),\ \boldsymbol{J}_l(t))$ and U_l the space comprised of $\boldsymbol{J}_l(t)$.

Here, we define $M_l^B(\boldsymbol{J}_l(t))$ as the number of busy lightpaths in the state $(N_r(t),\ \boldsymbol{J}_l(t))$. $M_l^B(\boldsymbol{J}_l(t))$ is given by

$$M_l^B(\boldsymbol{J}_l(t)) = \sum_{i=1}^{W-1} \sum_{n=0}^{K_l} 1_{\{J_{l_i}(t)=n\}}, \tag{2.4}$$

where $1_{\{X\}}$ is the indicator function of event X. Similarly, we define $M_l^{K_l}(\boldsymbol{J}_l(t))$ as the number of lightpaths where K_l cut-through LSPs are established. Let $M_l^I(\boldsymbol{J}_l(t))$ denote the number of idle lightpaths. We have

$$M_l^{K_l}(\boldsymbol{J}_l(t)) = \sum_{i=1}^{W-1} 1_{\{J_{l_i}(t)=K_l\}}, \tag{2.5}$$

$$M_l^I(\boldsymbol{J}_l(t)) = \sum_{i=1}^{W-1} 1_{\{J_{l_i}(t)=I\}}. \tag{2.6}$$

In the remainder of this section, the argument t is omitted since we consider the system in equilibrium.

Table 2.1. State transition rate in ring network model.

Number of idle lightpaths	Current state $(N_r,\ \boldsymbol{J}_l)$	Next state	Transition rate
$M_l^I > 0$	$N_r < T_h$	$(N_r+1,\ \boldsymbol{J}_l)$	$\lambda_{flow}^{all} - (M_l^B - M_l^{K_l})\lambda_{flow}$
	$T_h \le N_r < K_r$	$(N_r+1, \boldsymbol{J}_l),\ J_{l_{i_I^{\min}}} = S$	$\lambda_{flow}^{all} - M_l^B \lambda_{flow}$
	$T_h \le N_r < K_r$	$(N_r+1,\ \boldsymbol{J}_l)$	$M_l^{K_l}\lambda_{flow}$
	$N_r = K_r$	$(N_r,\ \boldsymbol{J}_l),\ J_{l_{i_I^{\min}}} = S$	$\lambda_{flow}^{all} - M_l^B \lambda_{flow}$
	$N_r > 0$	$(N_r-1,\ \boldsymbol{J}_l)$	μ_r
$M_l^I = 0$	$N_r < K_r$	$(N_r+1,\ \boldsymbol{J}_l)$	$\lambda_{flow}^{all} - (M_l^B - M_l^{K_l})\lambda_{flow}$
	$N_r > 0$	$(N_r-1,\ \boldsymbol{J}_l)$	μ_r
State of lightpaths	Current state $(N_r,\ \boldsymbol{J}_l)$	Next state	Transition rate
$J_{l_i} = S$	$(N_r,\ \boldsymbol{J}_l)$	$(N_r,\ \boldsymbol{J}_l),\ J_{l_i} = 0$	p
$J_{l_i} = n$	$n < K_l$	$(N_r,\ \boldsymbol{J}_l + \boldsymbol{e}_i)$	λ_{flow}
	$n > 0$	$(N_r,\ \boldsymbol{J}_l - \boldsymbol{e}_i)$	$n\mu_l$
	$n = 0$	$(N_r,\ \boldsymbol{J}_l),\ J_{l_i} = R$	h
$J_{l_i} = R$	$(N_r,\ \boldsymbol{J}_l)$	$(N_r,\ \boldsymbol{J}_l),\ J_{l_i} = I$	p

The transition rate from the state $(N_r,\ \boldsymbol{J}_l)$ is shown in Table 2.1. Here, $\boldsymbol{e}_i$ is a $1 \times (W-1)$ vector whose ith element is one and the others are zero. $i_I^{\min}$ in Table 2.1 is defined as

$$i_I^{\min} = \min\{\, i\ ; J_{l_i} = I,\ 1 \le i \le W-1\}. \tag{2.7}$$

and $(\boldsymbol{J}_l(t))$ is omitted from $M_l^x(\boldsymbol{J}_l(t))$, $(x = B,\ K_l,\ I)$.

Finally, let $\pi(N_r,\ \boldsymbol{J}_l)$ denote the steady state probability of the state $(N_r,\ \boldsymbol{J}_l)$. $\pi(N_r,\ \boldsymbol{J}_l)$ is uniquely determined by equilibrium state equations and the following normalized condition

$$\sum_{(N_r, \boldsymbol{J}_l) \in U_{r,l}} \pi(N_r,\ \boldsymbol{J}_l) = 1. \tag{2.8}$$

In Appendix A, we present the equilibrium state equations in the case of $W = 2$.

With $\pi(K_r,\ \boldsymbol{J}_l)$, the packet-flow loss probability $P_{f,loss}$ is yielded as

$$P_{f,loss} = \sum_{(K_r,\boldsymbol{J}_l)\in U_{r,l}} \left\{1 - M_l^B(\boldsymbol{J}_l)\frac{\lambda_{flow}}{\lambda_{flow}^{all}} + M_l^{K_l}(\boldsymbol{J}_l)\frac{\lambda_{flow}}{\lambda_{flow}^{all}}\right\}\pi(K_r,\ \boldsymbol{J}_l). \tag{2.9}$$

We define $P_{f,light}$ as the lightpath utilization factor and $P_{f,wave}$ as the wavelength utilization factor. With $\pi(N_r,\ \boldsymbol{J}_l)$, $P_{f,light}$ and $P_{f,wave}$ are expressed as

$$P_{f,light} = \sum_{(N_r,\boldsymbol{J}_l)\in U_{r,l}} \sum_{i=1}^{W-1} 1_{\{0<J_{l_i}\le K_l\}}\frac{\pi(N_r,\ \boldsymbol{J}_l)}{W-1}, \tag{2.10}$$

$$P_{f,wave} = \sum_{(N_r,\boldsymbol{J}_l)\in U_{r,l}} \left\{1_{\{N_r>0\}} + \sum_{i=1}^{W-1} 1_{\{0<J_{l_i}\le K_l\}}\right\}\frac{\pi(N_r,\ \boldsymbol{J}_l)}{W}. \tag{2.11}$$

2.5. Performance Analysis in Heavy Traffic Case

In this section, we analyze the performance of our method in the heavy traffic case.

2.5.1 System Model

Since the establishment/release of lightpaths rarely occurs and each node receives the same volume of traffic, we assume that each node maintains γ lightpaths. As a result, we have an $M/G/1/K_r$ queue for the layer 3 routing kernel and γ $M/G/K_l/K_l$ queues for established lightpaths, respectively (see Fig. 2.10). Note that $W-\gamma-1$ wavelengths are used for lightpaths established by the other nodes.

In our approximation under heavy traffic, γ plays an important role to obtain good estimates of performance measures. We give upper and lower bounds of γ by considering the combination of lightpaths between any pairs of nodes in the ring network.

We define the length of lightpath as the number of links between source and destination nodes. γ reaches its maximum when the number of lightpaths in the ring network is the largest and this occurs in the following way as shown in Fig. 2.11. First, establish the lightpaths whose length equals two with two wavelengths [1] . Second, establish the lightpaths whose length equals three with

[1] The lightpath whose length equals one is used for the default path.

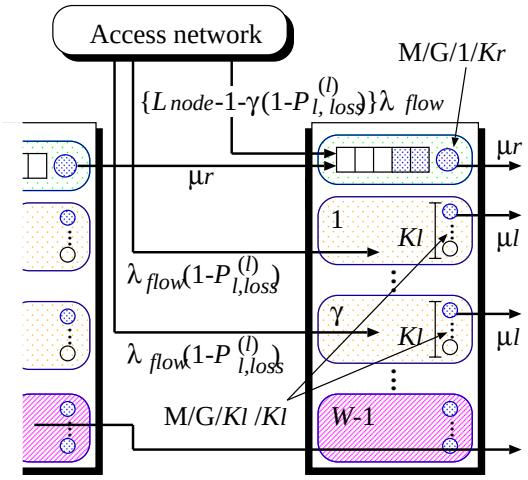

Figure 2.10. Ring node model with heavy traffic.

the least number of available wavelengths, and so on. Note that all the nodes try to establish lightpaths equally in the symmetric ring network. It is easy to see that n wavelengths should be used if all the nodes establish the lightpaths with length equal to n. Since there are $W-1$ wavelengths, the maximum length n is given by

$$n = \max\{\, i : \ \frac{i^2+i-2}{2} \leq W-1\}. \tag{2.12}$$

Each node can establish $n-1$ lightpaths, however, it cannot always establish a lightpath with length equal to $n+1$ due to the shortage of available wavelengths.

Next we estimate the effect of the wavelengths which are not used in the above procedure. In each node, the number of the wavelengths which are not used for lightpaths is

$$W-1-\frac{n^2+n-2}{2} = W-\frac{n(n+1)}{2}.$$

There are L_{node} nodes and hence L_{node} links in the ring network. The number of the lightpaths with length equal to $n+1$ in the network is given by

$$\frac{L_{node}}{n+1}\{W-\frac{n(n+1)}{2}\},$$

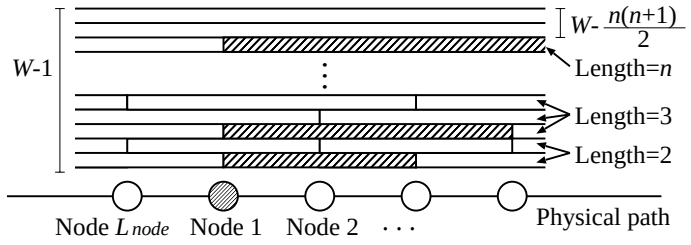

Figure 2.11. Upper bound of the number of established wavelengths.

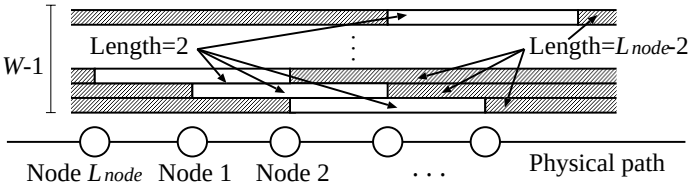

Figure 2.12. Lower bound of the number of established wavelengths.

and hence the effect of the above per node is roughly estimated by

$$\frac{1}{n+1}\{W - \frac{n(n+1)}{2}\}.$$

Combining the above results yields the upper bound of γ as

$$\gamma \leq n - 1 + \frac{1}{n+1}\{W - \frac{n(n+1)}{2}\}. \tag{2.13}$$

To obtain the lower bound of γ, we consider a wasteful use of wavelengths. The most wasteful way is the establishment of the lightpaths with length equal to $L_{node} - 2$. In this case, we have two lightpaths in a wavelength: one is the path with length equal to $L_{node} - 2$ and the other is that with length equal to two (see Fig. 2.12).

Since the number of lightpaths established in the network is $2(W-1)$, the effect per node is given by $2(W-1)/L_{node}$. That is,

$$\gamma \geq \frac{2(W-1)}{L_{node}}. \tag{2.14}$$

From (2.13) and (2.14), we finally obtain the range of γ as follows:

$$\frac{2(W-1)}{L_{node}} \leq r \leq n-1+\frac{1}{n+1}\{W-\frac{n(n+1)}{2}\}. \tag{2.15}$$

As is the case with the light traffic case, we have two kinds of packet flow traffic that arrives at the node: one is from the access network and the other is from the previous node. First we consider packet flow traffic coming from the access network. Since γ lightpaths are established, a packet flow from the access network arrives at the routing kernel or one of the established lightpaths. A packet flow arrives at the routing kernel according to a Poisson process with rate $(L_{node}-1-\gamma)\lambda_{flow}$ while it arrives at the established lightpath according to a Poisson process with rate λ_{flow}.

The packet flow which arrives at the lightpath tries to establish a new cut-through LSP in the lightpath. If a new cut-through LSP is not established due to the shortage of bandwidth, the packet flow is forwarded to the routing kernel for the transmission with the default path. Let $P_{f,loss}^{(l)}$ denote the probability that this cut-through LSP establishment fails at the packet-flow arriving point. With the $M/G/K_l/K_l$ queueing model, $P_{f,loss}^{(l)}$ is given by

$$P_{f,loss}^{(l)} = \frac{(\lambda_{flow}/\mu_l)^{K_l}/K_l!}{\sum_{k=0}^{K_l}(\lambda_{flow}/\mu_l)^k/k!}, \tag{2.16}$$

where $1/\mu_l$ is the mean transmission time of a packet flow for a cut-through LSP.

Since the packet flow which fails in establishing a new cut-through LSP in the lightpath is forwarded to the routing kernel with rate $P_{f,loss}^{(l)}\lambda_{flow}$, we assume that packet flows arrive at the routing kernel from its access network according to a Poisson process with rate $\{L_{node}-1-\gamma(1-P_{f,loss}^{(l)})\}\lambda_{flow}$.

Next we consider packet flow traffic from the previous node. Because the packet flow is transmitted from the previous node to the tagged node with the default path all the time under heavy traffic, we assume that the packet flow leaves the previous node according to a Poisson process with rate μ_r. Thus the whole arrival rate of packet flows at the node, λ_{flow}^{all}, is given by

$$\lambda_{flow}^{all} = (L_{node}-1)\lambda_{flow}+\mu_r. \tag{2.17}$$

Finally, the arrival rate of the packets at the routing kernel in the tagged node, λ^r_{flow}, is given by

$$\lambda^r_{flow} = \{L_{node} - 1 - \gamma(1 - P^{(l)}_{f,loss})\}\lambda_{flow} + \mu_r. \tag{2.18}$$

2.5.2 Performance Analysis

In this subsection, we derive performance measures of the dynamic lightpath configuration method in the case of heavy traffic. As shown in Fig. 2.10, we consider an $M/G/1/K_r$ queue and γ $M/G/K_l/K_l$ queues.

Let ρ_r and ρ'_r denote the offered and carried loads of the routing kernel, respectively. We have

$$\rho_r = \frac{\lambda^r_{flow}}{\mu_r}, \tag{2.19}$$

where λ^r_{flow} is given by (2.18). We define π^r_0 as the steady state probability that there are no packet flows in the routing kernel. Then ρ'_r is expressed as [57]

$$\rho'_r = \frac{\rho_r}{\pi^r_0 + \rho_r}, \tag{2.20}$$

Since a packet flow is lost only at the routing kernel and hence the loss probability $P_{f,loss}$ is given by

$$P_{f,loss} = \left\{1 - \frac{1}{\pi^r_0 + \rho_r}\right\} \frac{\lambda^r_{flow}}{\lambda^{all}_{flow}}. \tag{2.21}$$

Moreover, the wavelength utilization factor $P_{f,wave}$ is expressed as

$$P_{f,wave} = \frac{\rho'_r + \gamma\left\{1 - \frac{1}{\sum_{k=0}^{K_l}(\lambda_{flow}/\mu_l)^k/k!}\right\}}{W}. \tag{2.22}$$

We can calculate π^r_0 in a recursive procedure [57].

Remark. Since γ is defined as the number of established lightpaths at the node, γ should take integer value. However, $P_{f,loss}$ and $P_{f,wave}$ are approximations and it is not clear whether non-integer γ greatly affects $P_{f,loss}$ and $P_{f,wave}$, or not. Therefore, for the calculations of $P_{f,loss}$ and $P_{f,wave}$, we use (2.15) which takes real values.

2.6. Numerical Examples

In this section, we show some numerical results calculated by the approximation analysis and simulation. In the simulation, we assume that the lightpath establishment/release time, $1/p$, and the extra holding time, $1/h$, are constant, while they are exponentially distributed with the means $1/p$ and $1/h$ in the approximation analysis.

We assume that the bandwidth of a wavelength, E, is equal to 10 Gbps and a packet flow contains 10 packets whose sizes are 1,250 bytes on average [2] . Hence the size of a packet flow is exponentially distributed with the mean δ_{flow} =100,000 bits.

2.6.1 Light Traffic Case

In this subsection, we show numerical results in the case of light traffic. Here, performance measures are calculated with the analysis results of Section 2.4.

2.6.1.1 Impact of Processing Speed of the Routing Kernel

First we consider how the processing speed of the routing kernel affects the packet-flow loss probability and wavelength utilization factor. We set $W = 4$, $K_r = 5$, $T_h = 3$, and $L_{node} = 10$. In this network, we assume that each wavelength supports cut-through LSPs with fixed bandwidth $E_l = 2.5$ Gbps. Hence the number of cut-through LSPs in a lightpath, K_l, is equal to 4 and the mean transmission time of a cut-through LSP, $1/\mu_l$, becomes equal to 2.5 μs. In addition, we assume that both the mean lightpath establishment/release time $1/p$ and the mean extra holding time $1/h$ are equal to 10 ms.

Figs. 2.13(a) and (b) show the packet-flow loss probability and wavelength utilization factor, respectively, against the arrival rate of packet flows in the cases of $1/\mu_r = 10$, 20, and 100 μs.

[2] We investigated the case where the average number of packets in a packet flow is 1000 and obtained the tendency similar to those in the case where the number of packets is 10. In this case, however, lightpaths are rarely established and released, and hence the impact of the lightpath establishment/release time becomes small.

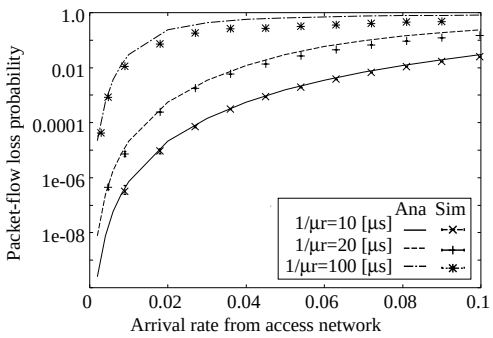

(a) Packet-flow loss probability.

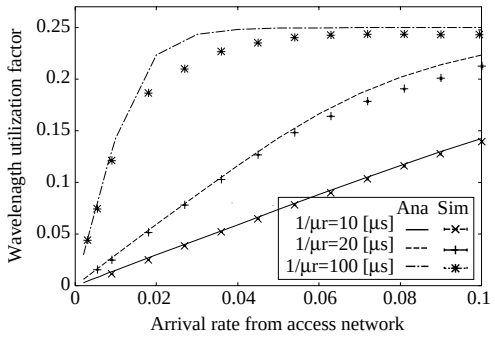

(b) Wavelength utilization factor.

Figure 2.13. Packet-flow loss probability and wavelength utilization factor vs. arrival rate from access network in the light traffic case.

From Fig. 2.13(a), we observe that the loss probability calculated with the approximation analysis is almost the same as that with the simulation when the processing speed of the routing kernel is 10 μs. On the other hand, we can see the discrepancy between the analysis and simulation results when the processing speed of the routing kernel becomes large. This is because a large processing time of the routing kernel causes a large loss probability and our assumption does not hold. However, our approximation analysis is useful for the calculation of the loss probability especially when the loss probability is smaller than 0.05.

In addition, from Fig. 2.13(b), we observe that the analytical model is useful for the calculation of the wavelength utilization factor when the wavelength utilization factor is smaller than 0.15. Therefore, our approximation analysis in the case of light traffic is effective.

From both figures, we observe that the large processing time of the routing kernel gives a large loss probability and a large wavelength utilization factor. This is because the large processing time of the routing kernel causes congestion and this results in the increase of the number of established lightpaths.

In the following subsections for the light traffic case, only analytical results are shown because the analytical and simulation results are almost the same.

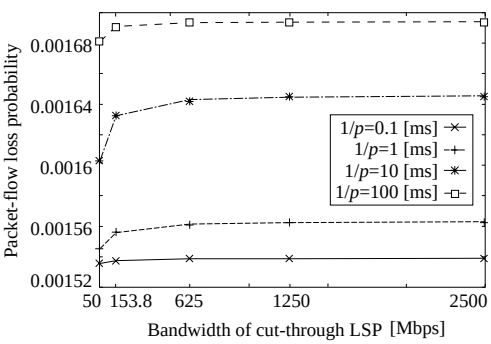

(a) Packet-flow loss probability.

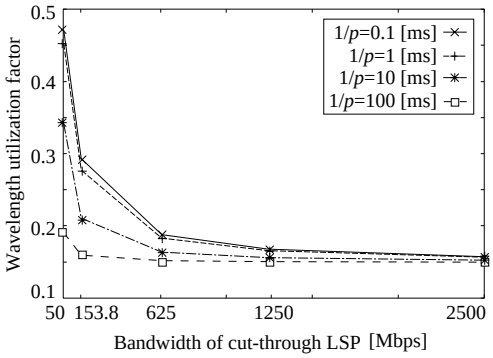

(b) Wavelength utilization factor.

Figure 2.14. Packet-flow loss probability and wavelength utilization factor vs. bandwidth of cut-through LSP in the light traffic case.

2.6.1.2 Impact of the Bandwidth of Cut-Through LSPs

Next we investigate how the bandwidth of cut-through LSPs in a lightpath affects the packet-flow loss probability and the wavelength utilization factor. We assume that $W = 2$, $K_r = 5$, $T_h = 1$, $L_{node} = 10$, $1/\mu_r = 10$ μs, and $1/h = 10$ ms. In terms of the arrival rate of packet flows from access network, we set $(L_{node} - 1)\lambda_{flow} = 0.05$.

Figs. 2.14(a) and (b) show the packet-flow loss probability and wavelength utilization factor, respectively, against the bandwidth of cut-through LSPs in the cases of $1/p = 0.1$, 1, 10, and 100 ms. Here, the bandwidths of cut-through LSPs, E_l, are set to 50, 153.8, 625, 1250, and 2500 Mbps, i.e., the numbers of cut-through LSPs in a lightpath, K_l, are 200, 65, 16, 8, and 4.

From these figures, we observe that smaller bandwidth of a cut-through LSP gives a smaller loss probability and a larger wavelength utilization factor. In particular, from Fig. 2.14(b), we observe that the small bandwidth of LSPs in a lightpath gives a large wavelength utilization factor as the lightpath establishment/release time becomes small. This implies that multiple LSPs with small bandwidth effectively utilize the large bandwidth of a lightpath

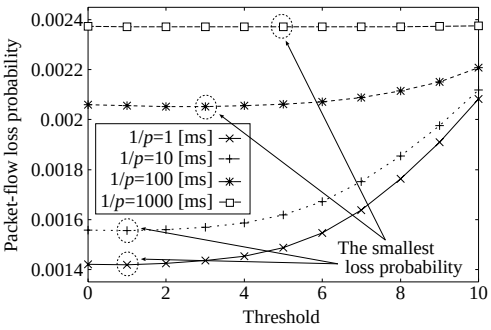

(a) Packet-flow loss probability.

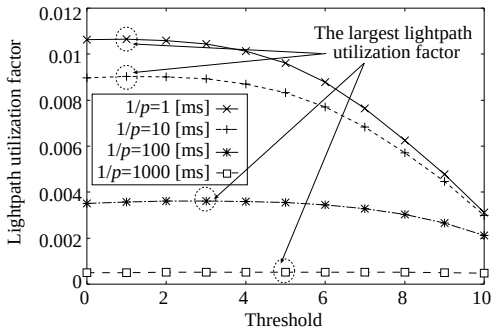

(b) Lightpath utilization factor.

Figure 2.15. Packet-flow loss probability and lightpath utilization factor vs. threshold in the light traffic case.

2.6.1.3 Impact of Congestion Threshold

Next, we investigate how the congestion threshold affects the packet-flow loss probability and lightpath utilization factor. We assume that $W = 4$, $K_r = 10$, $L_{node} = 10$, $1/\mu_r = 10$, and $1/h = 10$ ms. In addition, we assume that $E_l = 10$ Gbps and $(L_{node} - 1)\lambda_{flow} = 0.1$.

Figs. 2.15(a) and (b) show the packet-flow loss probability and lightpath utilization factor, respectively, against the threshold in the cases of $1/p$ set to 1, 10, 100, and 1000 ms. In addition, we indicate the optimal thresholds which achieve the smallest loss probability and the largest lightpath utilization factor in both figures.

From Fig. 2.15(a), we find that the values of T_h equal to 1, 1, 3, and 5 give the smallest loss probability in the cases of $1/p = 1$, 10, 100 and 1000 ms, respectively. Moreover, in Fig. 2.15(b), the same thresholds also give the largest lightpath utilization factor. That is, the optimal thresholds in terms of both performance measures are the same.

When the threshold is smaller than the optimal threshold, congestion occurs frequently and this results in frequent lightpath establishment and release. Note that both the loss probability and the lightpath utilization factor do not degrade so much even though the wavelength can not be used during the lightpath establishment/release time.

On the other hand, as the threshold becomes larger than the optimal thresh-

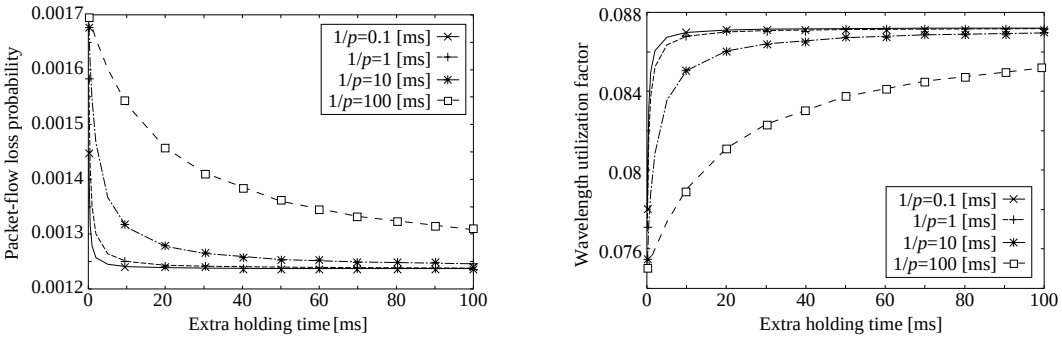

(a) Packet-flow loss probability. (b) Wavelength utilization factor.

Figure 2.16. Packet-flow loss probability and wavelength utilization factor vs. extra holding time in the light traffic case.

old, the congestion rarely occurs. If the congestion does not occur, most of arriving packet flows are transmitted with the default path. This causes a large loss probability and a small lightpath utilization factor.

Moreover, as the lightpath establishment/release time becomes large, the impact of the threshold on both performance measures becomes large. Therefore, it is important to design the threshold carefully in order to achieve a small loss probability and a large lightpath utilization factor.

2.6.1.4 Impact of Extra Holding Time

In this subsection, we consider how the extra holding time affect the packet-flow loss probability and wavelength utilization factor. We assume that $W = 4$, $K_r = 5$, $T_h = 1$, $L_{node} = 10$, and $1/\mu_r = 10$ μs. We also assume that $E_l = 2.5$ Gbps and $(L_{node} - 1)\lambda_{flow} = 0.05$.

Figs. 2.16(a) and (b) show the loss probability and wavelength utilization factor, respectively, against the extra holding time in the cases of $1/p = 0.1$, 1, 10, and 100 ms.

From Fig. 2.16(a), we observe that the packet-flow loss probability decreases as the extra holding time becomes large. In addition, the loss probability becomes large when the lightpath establishment/release time is large. This is because a wavelength can not be used during the lightpath establishment/release time and frequent establishment and release of lightpaths waste the time.

However, a small extra holding time becomes efficient for the loss probability when the lightpath establishment/release time is in the order of 10 ms. If the lightpath establishment/release time is 10 ms, the extra holding time of 20 ms is enough for providing a small loss probability.

From Fig. 2.16(b), we observe that the wavelength utilization factor increases as the extra holding time becomes large. In addition, we find that the wavelength utilization factor is large when the lightpath establishment/release time is large. A small extra holding time becomes efficient for the wavelength utilization factor when the lightpath establishment/release time is in the order of 10 ms. If the lightpath establishment/release time is 10 ms, the extra holding time of 20 ms is also enough for providing a large wavelength utilization factor.

From the above observations, a small extra holding time can provide a small loss probability and a large wavelength utilization factor when the lightpath establishment/release time is in the order of 10 ms. The extra holding time should be set to 20 ms rather than 100 ms in the case of $1/p = 10$ ms, because the small extra holding time is effective for an asymmetric ring network.

2.6.2 Heavy Traffic Case

In this subsection, we present numerical examples of the packet-flow loss probability and wavelength utilization factor for the heavy traffic case. We assume that $W = 4$, $K_r = 5$, $T_h = 3$, $L_{node} = 10$, and $1/\mu_r = 10$ μs. We also set $E_l = 2.5$ Gbps.

2.6.2.1 Impact of Lightpath Establishment/Release Time

We investigate how the lightpath establishment/release time affects the packet-flow loss probability and wavelength utilization factor.

Figs. 2.17(a) and (b) illustrate the packet-flow loss probability and wavelength utilization factor, respectively, against the arrival rate from the access network with $1/h = 10$ ms and $1/p = 0.1$, 1, 10, and 100 ms. From Figs. 2.17(a) and (b), we observe that the results of simulation lie between the curves of the upper and lower bounds. Note that in Fig. 2.17(a), the upper bound value of γ gives the lower bound of the packet-flow loss probability, while the lower bound of γ

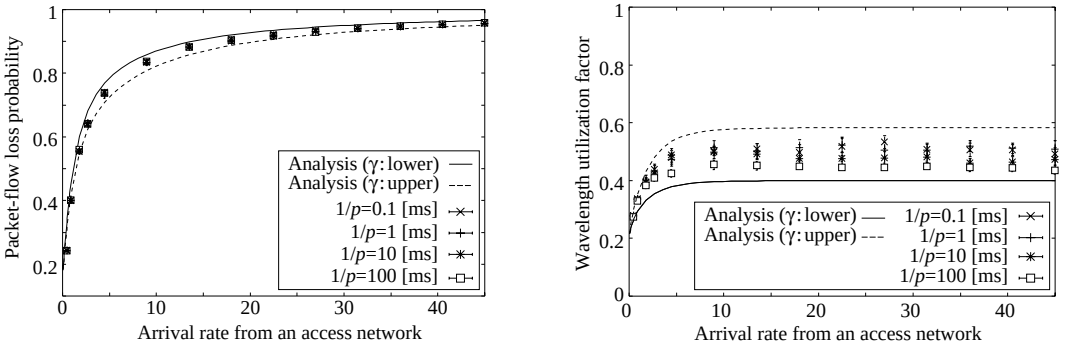

(a) Packet-flow loss probability.

(b) Wavelength utilization factor.

Figure 2.17. Packet-flow loss probability and wavelength utilization factor vs. arrival rate in the heavy traffic case, $1/h = 10$ ms.

gives the upper bound of the packet-flow loss probability. On the other hand, in Fig. 2.17(b), the upper bound value of γ gives the upper bound of the wavelength utilization factors and vice versa.

In Fig. 2.17(a), the simulation results close to the upper bound regardless of the establishment/release time. Note that the upper bound of the packet-flow loss probability is calculated with the lower bound of γ equal to $2(W-1)/L_{node}$. That is, the lower bound of γ succeeds in the prediction of loss behavior at packet-flow level under heavy traffic.

On the other hand, we observe in Fig. 2.17(b) that the simulation results become close to the lower bound when the establishment/release time becomes large. However, the discrepancy between the upper and lower bounds is relatively large.

Figs. 2.17(a) and (b) show that the packet-flow loss probability and the wavelength utilization factor do not change so much when the lightpath establishment/release time becomes large. This is because the established lightpaths are not released frequently due to the heavy traffic.

2.6.2.2 Impact of Extra Holding Time

Finally, we investigate how the extra holding time affects the packet-flow loss probability and the wavelength utilization factor. Figs. 2.18(a) and (b) show the packet-flow loss probability and the wavelength utilization factor, respectively,

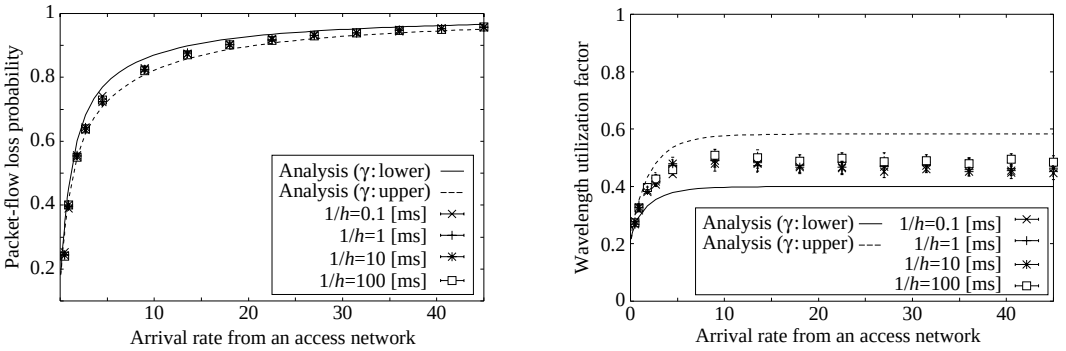

(a) Packet-flow loss probability.

(b) Wavelength utilization factor.

Figure 2.18. Packet-flow loss probability and wavelength utilization factor vs. arrival rate in the heavy traffic case, $1/p = 10$ ms.

against the arrival rate with $1/p = 10$ ms and $1/h = 0.1$, 1, 10, and 100 ms.

From Fig. 2.18(a), simulation results lie between the upper and lower bounds. As is the case with Fig. 2.17(a), the upper bound gives the good estimate of the packet-flow loss probability. From Fig. 2.18(b), we also observe the same tendency as Fig. 2.17(b). As a result, the upper and lower bounds for the packet-flow loss probability gives good estimates, while those for the wavelength utilization factor fails in providing accurate estimates. Further improvement is needed for the accurate estimation of the wavelength utilization factor.

2.7. Conclusions

In this chapter, we considered the dynamic lightpath configuration method where a lightpath supports multiple LSPs, and analyzed the loss probability of packet flows and the wavelength utilization factor under light and heavy traffic conditions for symmetric WDM ring networks.

Numerical results in the light traffic case showed that our approximation analysis gives good estimates for the packet-flow loss probability and wavelength utilization factor. With multiple LSPs in a lightpath, the dynamic lightpath configuration method becomes effective when the lightpath establishment/release time becomes small. As for the design of the threshold in the method, the optimal thresholds which give the smallest loss probability and the largest lightpath uti-

lization factor can be obtained from the light traffic analysis. It is important to design the threshold carefully in order to achieve a small loss probability and a large lightpath utilization factor. We also observed in the light traffic case that a small extra holding time is effective when the lightpath establishment/release time is in the order of 10 ms.

In the heavy traffic case, we showed that our approximation analysis with the lower bound of γ is useful to estimate the packet-flow loss probability. On the other hand, the resulting estimates of the wavelength utilization factor are not accurate. Further improvement of the approximation is needed for the well estimation of the wavelength utilization factor.

Chapter 3

QoS-Guaranteed Wavelength Allocation

3.1. Introduction

With the recent increase of Internet users and the diversity of network applications, QoS provisioning becomes increasingly important in all-optical wavelength routing networks. In [23, 24, 25, 26, 27], the general approach for service-specific routing and wavelength allocation has been proposed. With the approach, a connection is established according to twofold metrics, i.e., QoS metrics (service requirements) and resource metrics (quality constraints). In this approach, wavelengths are classified into multiple groups which can support different services according to the quality attributes. As for QoS metrics, transmission quality, restoration, network management, and policies have been considered. Given that connections are established according to the above QoS metrics, the connection loss probability of each QoS class has been evaluated.

On the other hand, when wavelengths are transparent to bit rate, protocol, and modulation formats, a connection with any service requirements is established with any idle wavelength [23, 48]. In such a network, QoS guarantee for the connection loss probability is also important.

Moreover, under the current wavelength conversion technology, one of the popular conversion techniques is limited-range wavelength conversion which can convert input wavelength to some wavelength within a limited range. [74] has

shown that four wavelength mixing (FWM) can convert an input wavelength into any output wavelength within 65nm which is the difference between the output and input wavelengths. In this chapter, we focus on the connection loss probability as the QoS metric and consider a QoS-guaranteed wavelength allocation for the wavelength routing network with the limited-range wavelength conversion.

In the proposed allocation, the pre-determined number of wavelengths are allocated to each QoS class depending on the priority of loss probability. Here, a wavelength set for a QoS class is a proper subset of other sets for higher classes. Moreover, the wavelength set for the highest priority class includes all wavelengths multiplexed in an optical fiber so as to decrease the connection loss probability. When a connection of a QoS class is established along several links, an idle wavelength in the wavelength set of the class is allocated at each link. Here, we consider two wavelength selection rules according to which idle wavelength is selected from the wavelength set for requested QoS class. The connection loss probability of each class greatly depends on the combination of the wavelength selection rules. We consider three combinations of wavelength selection rules and compare those in a single link and in a uni-directional ring network.

As for the performance evaluation of the QoS-guaranteed wavelength allocation, we derive connection loss probability of each QoS class on a single link in wavelength routing network using continuous-time Markov chain. With this analytical result, we investigate the impact of three combinations of wavelength selection rules on connection loss probability of each QoS class. We also investigate the connection loss probability for a uni-directional ring network with the limited wavelength conversion by simulation.

The rest of the chapter is organized as follows. Section 3.2 represents the QoS-guaranteed wavelength allocation method. In Section 3.3, we present our analytical model on a single link in the wavelength routing network and derive the connection loss probability of each QoS class. Numerical examples are shown in Section 3.4 and conclusions are presented in Section 3.5.

3.2. Proposed Method

In this section, we present our QoS-guaranteed wavelength allocation method in detail. We consider an all-optical wavelength routing network where each node has FWM wavelength conversion, because FWM does not depend on the modulation format and the bit rate [48]. Let W denote the number of wavelengths multiplexed into an optical fiber. According to the threshold model in [20] and [69], we assume that the range of FWM wavelength conversion for wavelength w_i $(1 \leq i \leq W)$ is from $w_{\max(1,i-\theta)}$ to $w_{\min(i+\theta,W)}$ where θ is a non-negative integer and called threshold in the following. Note that the FWM wavelength conversions with $\theta = 0$ and $W-1$ are corresponding to no wavelength conversion and full-range wavelength conversion, respectively.

In this wavelength routing network, M QoS classes require different acceptable loss probabilities. M QoS classes are numbered from 1 to M and class i has high priority over class j when $i < j$ and the class i requires smaller connection loss probability than class j. Therefore, the connections of class 1 have the highest priority and require the smallest loss probability.

In our QoS-guaranteed wavelength allocation, W wavelengths $\{w_1, \cdots, w_W\}$ are classified into M wavelength sets $D_q^{(i)}$ $(i = 1, \cdots, M)$. Let $W_q^{(i)}$ denote the number of wavelengths in $D_q^{(i)}$. Connection of class i is established with wavelength in $D_q^{(i)}$. Each $D_q^{(i)}$ and $W_q^{(i)}$ satisfy the followings.

$$D_q^{(M)} \subset \cdots \subset D_q^{(i)} \subset \cdots \subset D_q^{(1)}, \tag{3.1}$$

$$D_q^{(i)} = \{w_1, \cdots, w_{W_q^{(i)}}\}, \ 1 \leq i \leq M, \tag{3.2}$$

$$0 < W_q^{(M)} < \cdots < W_q^{(i)} < \cdots < W_q^{(1)} = W. \tag{3.3}$$

(3.3) implies that higher priority class can use more wavelengths and it is expected that the resulting connection loss probability of high priority class is small. Figure 3.1 shows how W wavelengths are classified into M QoS classes in the proposed method.

In the QoS-guaranteed wavelength allocation, the following two different rules of wavelength selection are considered.

Rule 1: The wavelength with the *minimum* index number in $D_q^{(i)}$ is selected.

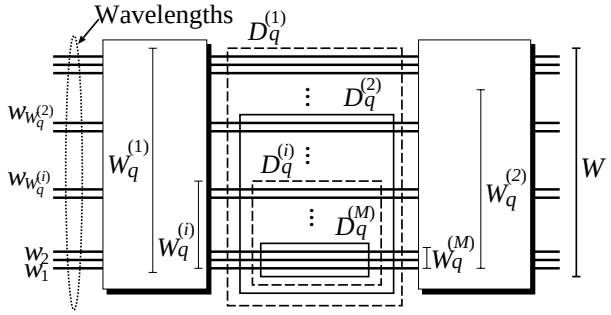

Figure 3.1. QoS-guaranteed wavelength allocation.

Rule 2: The wavelength with the *maximum* index number in $D_q^{(i)}$ is selected.

A connection of class i is established with an idle wavelength in $D_q^{(i)}$ at each link. Each QoS class follows either Rule 1 or Rule 2. The wavelength selection rule of each QoS class affects the performance of the proposed method. Note that the number of available wavelengths for class i under Rule 1 is likely to be larger than that under Rule 2. In other words, the connection loss probability of the class i under Rule 1 is likely to be smaller than that under Rule 2. However, the connection establishment of the class i under Rule 1 directly affects the number of available wavelengths for lower priority classes than i. This implies that the traffic intensity of the class i under Rule 1 greatly affects the connection loss probabilities for lower priority classes.

When the class i follows Rule 2, on the other hand, the connection establishment of the class i does not significantly affect the number of available wavelengths for lower priority classes and this means that the connection loss probabilities of lower priority classes are less affected by the traffic intensity of the class i. Note that the connection establishment under Rule 2 hardly has a large impact on higher priority classes.

Because the number of classes is M, there are 2^M combinations of the wavelength selection rules. In this chapter, however, we consider three combinations shown in Table 3.1.

In Method 1, all classes follow Rule 1 and, in Method 2, class 1 follows Rule 2 and the other classes follow Rule 1. Classes 1 and 2 follow Rule 2 and other

Table 3.1. Three combinations of wavelength selection rules.

	class 1	class 2	other classes
Method 1	Rule 1	Rule 1	Rule 1
Method 2	Rule 2	Rule 1	Rule 1
Method 3	Rule 2	Rule 2	Rule 1

classes follow Rule 1 in Method 3. Note that the number of available wavelengths for lower priority classes than classes 1 and 2 for Method 1 is likely to be the smallest while that for Method 3 the largest.

Here, we explain how a connection of each class is established between end nodes. As mentioned the above, W wavelengths $\{w_1, \cdots, w_W\}$ are multiplexed into a fiber at every link and each node has an FWM wavelength converter with threshold θ. At each link, W wavelengths are classified into M wavelength sets and wavelength set $D_q^{(i)}$ $(i = 1, \cdots, M)$ is allocated to class i. When $w_j \in D_q^{(i)}$ is selected for the class i connection at some link, the conversion range for wavelength at the next link is from $w_{\max(1,j-\theta)}$ to $w_{\min(j+\theta, W_q^{(i)})}$. In this case, an available wavelength for the next link is selected according to either of the following two procedures based on first-fit algorithm [20].

Procedure 1: If the class i $(i = 1, \cdots, M)$ follows Rule 1, an idle wavelength with the *minimum* index number in the set $\{w_{\max(1,j-\theta)}, \cdots, w_{\min(j+\theta, W_q^{(i)})}\}$ is selected.

Procedure 2: If the class i $(i = 1, \cdots, M)$ follows Rule 2, an idle wavelength with the *maximum* index number in the set $\{w_{\max(1,j-\theta)}, \cdots, w_{\min(j+\theta, W_q^{(i)})}\}$ is selected.

If wavelength allocations in all links along the path succeed, lightpath connection is eventually established.

3.3. Performance Analysis

In this section, we derive the connection loss probability of each QoS class for a single link in the wavelength routing network. We use the following assumptions.

1. W wavelengths are multiplexed into a fiber at a single link.
2. The number of QoS classes is M and the class i ($i = 1, \cdots, M$) has priority over the class j if $i < j$.
3. Connections of the class i arrive at the single link according to a Poisson process with rate $\lambda_{conn}^{(i)}$ and total arrival rate is $\lambda_{conn} = \sum_{i=1}^{M} \lambda_{conn}^{(i)}$.
4. Connection holding times of all classes are exponentially distributed with rate μ_{conn}.
5. No queueing for connection request is permitted, that is, the connection is lost immediately after the connection establishment fails.

Let $\bar{D}_q^{(i)}$ ($i = 1, \cdots, M$) denote the wavelength set given by

$$\bar{D}_q^{(i)} = \begin{cases} D_q^{(i)} - D_q^{(i+1)}, & i < M, \\ D_q^{(M)}, & i = M, \end{cases} \tag{3.4}$$

where $D_q^{(i)}$ is a wavelength set of the class i. In addition, we define $\bar{W}_q^{(i)}$ ($i = 1, \cdots, M$) as the number of wavelengths in $\bar{D}_q^{(i)}$. We have

$$\bar{W}_q^{(i)} = \begin{cases} W_q^{(i)} - W_q^{(i+1)}, & i < M, \\ W_q^{(M)}, & i = M. \end{cases} \tag{3.5}$$

Let $N_q^{(i)}(t)$ ($i = 1, \cdots, M$) denote the number of wavelengths which are utilized in $\bar{D}_q^{(i)}$ at time t. Note that

$$0 \le N_q^{(i)}(t) \le \bar{W}_q^{(i)}, \quad i = 1, \cdots, M. \tag{3.6}$$

We define the state of the link at time t as

$$(N_q^{(1)}(t), \cdots, N_q^{(i)}(t), \cdots, N_q^{(M)}(t)). \tag{3.7}$$

Table 3.2. State transition rate in Method 1.

Current state: $(N_q^{(1)}, \cdots, N_q^{(i)}, \cdots, N_q^{(M)})$	Next state	Transition rate
$N_q^{(M)} < \bar{W}_q^{(M)}$	$(N_q^{(1)}, \cdots, N_q^{(M)} + 1)$	λ_{conn}
$N_q^{(i)} < \bar{W}_q^{(i)}$for $\exists i \in \{1, \cdots, M-1\}$, $N_q^{(k)} = \bar{W}_q^{(k)}$ for $\forall k \in \{i+1, \cdots, M\}$	$(N_q^{(1)}, \cdots, N_q^{(i)} + 1, \cdots, N_q^{(M)})$	$\sum_{m=1}^{i} \lambda_{conn}^{(m)}$
$N_q^{(i)} > 0$	$(N_q^{(1)}, \cdots, N_q^{(i)} - 1, N_q^{(M)})$	$N_q^{(i)} \mu_{conn}$

Table 3.3. State transition rate in Method 2.

Current state: $(N_q^{(1)}, \cdots, N_q^{(i)}, \cdots, N_q^{(M)})$	Next state	Transition rate
$N_q^{(1)} < \bar{W}_q^{(1)}$	$(N_q^{(1)} + 1, \cdots, N_q^{(M)})$	$\lambda_{conn}^{(1)}$
$N_q^{(i)} < \bar{W}_q^{(i)}$ for $\exists i \in \{2, \cdots, M-1\}$, $N_q^{(j)} = \bar{W}_q^{(j)}$ for $\forall j \in \{1, \cdots, i-1\}$, $N_q^{(k)} < \bar{W}_q^{(k)}$ for $\exists k \in \{i+1, \cdots, M\}$	$(N_q^{(1)}, \cdots, N_q^{(i)} + 1, \cdots, N_q^{(M)})$	$\lambda_{conn}^{(1)}$
$N_q^{(M)} < \bar{W}_q^{(M)}$, $N_q^{(i)} < \bar{W}_q^{(i)}$ for $\exists i \in \{1, \cdots, M-1\}$	$(N_q^{(1)}, \cdots, N_q^{(M)} + 1)$	$\sum_{m=2}^{M} \lambda_{conn}^{(m)}$
$N_q^{(i)} < \bar{W}_q^{(i)}$ for $\exists i \in \{2, \cdots, M-1\}$, $N_q^{(j)} < \bar{W}_q^{(j)}$ for $\exists j \in \{1, \cdots, i-1\}$, $N_q^{(k)} = \bar{W}_q^{(k)}$ for $\forall k \in \{i+1, \cdots, M\}$	$(N_q^{(1)}, \cdots, N_q^{(i)} + 1, \cdots, N_q^{(M)})$	$\sum_{m=2}^{i} \lambda_{conn}^{(m)}$
$N_q^{(M)} < \bar{W}_q^{(M)}$, $N_q^{(i)} = \bar{W}_q^{(i)}$ for $\forall i \in \{1, \cdots, M-1\}$	$(N_q^{(1)}, \cdots, N_q^{(M)} + 1)$	λ_{conn}
$N_q^{(i)} < \bar{W}_q^{(i)}$ for $\exists i \in \{2, \cdots, M-1\}$, $N_q^{(j)} = \bar{W}_q^{(j)}$ for $\forall j \in \{1, \cdots, i-1\}$ $N_q^{(k)} = \bar{W}_q^{(k)}$ for $\forall k \in \{i+1, \cdots, M\}$	$(N_q^{(1)}, \cdots, N_q^{(i)} + 1, \cdots, N_q^{(M)})$	$\sum_{m=1}^{i} \lambda_{conn}^{(m)}$
$N_q^{(i)} > 0$	$(N_q^{(1)}, \cdots, N_q^{(i)} - 1, \cdots, N_q^{(M)})$	$N_q^{(i)} \mu_{conn}$

Let U_q denote the state space of $(N_q^{(1)}(t), \cdots, N_q^{(M)}(t))$. From the above assumptions, $(N_q^{(1)}(t), \cdots, N_q^{(M)}(t))$ is a continuous-time Markov chain [31]. Since we consider the queueing behavior in equilibrium, we omit t in the following. In Tables 3.2, 3.3 and 3.4, we show transition rates from the state $(N_q^{(1)}, \cdots, N_q^{(i)}, \cdots, N_q^{(M)})$ in Methods 1, 2 and 3, respectively.

Let $\pi(N_q^{(1)}, \cdots, N_q^{(M)})$ denote the steady state probability of $(N_q^{(1)}, \cdots, N_q^{(M)})$. $\pi(N_q^{(1)}, \cdots, N_q^{(M)})$ is uniquely determined by equilibrium state equations and following normalized condition

$$\sum_{(N_q^{(1)}, \cdots, N_q^{(M)}) \in U_q} \pi(N_q^{(1)}, \cdots, N_q^{(M)}) = 1. \tag{3.8}$$

Table 3.4. State transition rate in Method 3.

Current state: $(N_q^{(1)}, \cdots, N_q^{(i)}, \cdots, N_q^{(M)})$	Next state	Transition rate
$N_q^{(1)} < \bar{W}_q^{(1)}$	$(N_q^{(1)}+1, \cdots, N_q^{(M)})$	$\lambda_{conn}^{(1)}$
$N_q^{(1)} < \bar{W}_q^{(1)}$, $N_q^{(2)} < \bar{W}_q^{(2)}$	$(N_q^{(1)}, N_q^{(2)}+1, \cdots, N_q^{(M)})$	$\lambda_{conn}^{(2)}$
$N_q^{(1)} < \bar{W}_q^{(1)}$, $N_q^{(i)} < \bar{W}_q^{(i)}$ for $\exists i \in \{3, \cdots, M-1\}$, $N_q^{(j)} = \bar{W}_q^{(j)}$ for $\forall j \in \{2, \cdots, i-1\}$, $N_q^{(k)} < \bar{W}_q^{(k)}$ for $\exists k \in \{i+1, \cdots, M\}$	$(N_q^{(1)}, \cdots, N_q^{(i)}+1, \cdots, N_q^{(M)})$	$\lambda_{conn}^{(2)}$
$N_q^{(M)} < \bar{W}_q^{(M)}$, $N_q^{(i)} < \bar{W}_q^{(i)}$ for $\exists i \in \{2, \cdots, M-1\}$	$(N_q^{(1)}, \cdots, N_q^{(M)}+1)$	$\sum_{m=3}^{M} \lambda_{conn}^{(m)}$
$N_q^{(i)} < \bar{W}_q^{(i)}$ for $\exists i \in \{3, \cdots, M-1\}$, $N_q^{(j)} < \bar{W}_q^{(j)}$ for $\exists j \in \{2, \cdots, i-1\}$, $N_q^{(k)} = \bar{W}_q^{(k)}$ for $\forall k \in \{i+1, \cdots, M\}$	$(N_q^{(1)}, \cdots, N_q^{(i)}+1, \cdots, N_q^{(M)})$	$\sum_{m=3}^{i} \lambda_{conn}^{(m)}$
$N_q^{(i)} < \bar{W}_q^{(i)}$ for $\exists i \in \{2, \cdots, M-1\}$, $N_q^{(j)} = \bar{W}_q^{(j)}$ for $\forall j \in \{1, \cdots, i-1\}$, $N_q^{(k)} < \bar{W}_q^{(k)}$ for $\exists k \in \{i+1, \cdots, M\}$	$(N_q^{(1)}, \cdots, N_q^{(i)}+1, \cdots, N_q^{(M)})$	$\lambda_{conn}^{(1)} + \lambda_{conn}^{(2)}$
$N_q^{(M)} < \bar{W}_q^{(M)}$, $N_q^{(1)} < \bar{W}_q^{(1)}$ $N_q^{(j)} = \bar{W}_q^{(j)}$ for $\forall j \in \{2, \cdots, M-1\}$	$(N_q^{(1)}, \cdots, N_q^{(M)}+1)$	$\sum_{m=2}^{M} \lambda_{conn}^{(m)}$
$N_q^{(i)} < \bar{W}_q^{(i)}$ for $\exists i \in \{2, \cdots, M-1\}$, $N_q^{(1)} < \bar{W}_q^{(1)}$, $N_q^{(j)} = \bar{W}_q^{(j)}$ for $\forall j \in \{2, \cdots, i-1\}$ $N_q^{(k)} = \bar{W}_q^{(k)}$ for $\forall k \in \{i+1, \cdots, M\}$	$(N_q^{(1)}, \cdots, N_q^{(i)}+1, \cdots, N_q^{(M)})$	$\sum_{m=2}^{i} \lambda_{conn}^{(m)}$
$N_q^{(M)} < \bar{W}_q^{(M)}$ $N_q^{(j)} = \bar{W}_q^{(j)}$ for $\forall j \in \{1, \cdots, M-1\}$	$(N_q^{(1)}, \cdots, N_q^{(M)}+1)$	λ_{conn}
$N_q^{(i)} < \bar{W}_q^{(i)}$ for $\exists i \in \{3, \cdots, M-1\}$, $N_q^{(j)} = \bar{W}_q^{(j)}$ for $\forall j \in \{1, \cdots, i-1\}$ $N_q^{(k)} = \bar{W}_q^{(k)}$ for $\forall k \in \{i+1, \cdots, M\}$	$(N_q^{(1)}, \cdots, N_q^{(i)}+1, \cdots, N_q^{(M)})$	$\sum_{m=1}^{i} \lambda_{conn}^{(m)}$
$N_q^{(i)} > 0$	$(N_q^{(1)}, \cdots, N_q^{(i)}-1, \cdots, N_q^{(M)})$	$N_q^{(i)} \mu_{conn}$

Equilibrium state equations for Method 2 are shown in Appendix B. Similarly, those for other methods can be obtained from Tables 2 and 4.

With $\pi(N_q^{(1)}, \cdots, N_q^{(M)})$, the connection loss probability of the class i, $P_{q,loss}^{(i)}$, is given by

$$P_{q,loss}^{(i)} = \sum_{(N_q^{(1)}, \cdots, N_q^{(i-1)}) \in U_q^{(i-1)}} \pi(N_q^{(1)}, \cdots, N_q^{(i-2)}, N_q^{(i-1)}, \bar{W}_q^{(i)}, \bar{W}_q^{(i+1)}, \cdots, \bar{W}_q^{(M)}). \tag{3.9}$$

Here, $U_q^{(i)}$ denotes the state space of $(N_q^{(1)}, \cdots, N_q^{(i)})$.

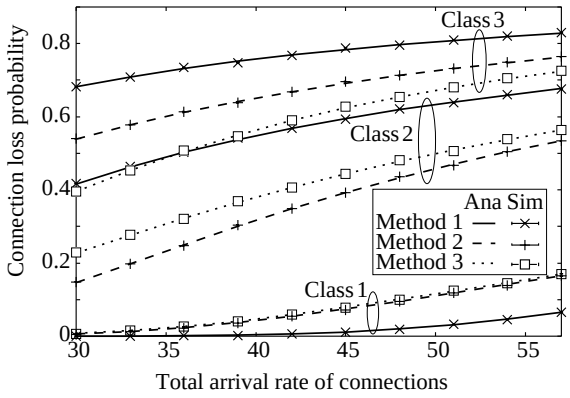

Figure 3.2. Connection loss probability vs. total connection arrival rate for a single link.

3.4. Numerical Examples

In this section, we show some numerical examples for the QoS-guaranteed wavelength allocation in cases of Methods 1, 2 and 3. First we consider a single link in the wavelength routing network, and then we consider a uni-directional ring network. In both cases, we assume that the number of QoS classes is three. Moreover, we assume that the connection holding time is exponentially distributed with rate $\mu_{conn} = 1$.

3.4.1 Single Link in Wavelength Routing Network

In this subsection, we consider a single link in the wavelength routing network. The connection loss probabilities of three QoS classes, $P^{(1)}_{q,loss}$, $P^{(2)}_{q,loss}$, and $P^{(3)}_{q,loss}$, are calculated by the analysis in the previous section and by simulation.

3.4.1.1 Impact of Total Connection Arrival Rate

First, we consider how the total arrival rate of connections affects the connection loss probability for each QoS class. Here we assume that the number of wavelengths is $W = 32$. 32 wavelengths are classified into $D^{(1)}_q$, $D^{(2)}_q$ and $D^{(3)}_q$ and the numbers of wavelengths in these sets are given by $W^{(1)}_q = 32$, $W^{(2)}_q = 16$ and

$W_q^{(3)} = 10$, respectively. In addition, we set $\lambda_{conn}^{(1)} = \lambda_{conn}^{(2)} = \lambda_{conn}^{(3)} = \lambda_{conn}/3$.

In Fig. 3.2, lines and dots denote the results of the analysis and simulation, respectively. From this figure, we observe that analytical and simulation results are almost the same regardless of the increase of total arrival rate. Therefore the analytical results are effective for the evaluation of the three methods under the above setting.

We also see that the QoS-guaranteed wavelength allocation method provides multiple QoS classes in terms of the connection loss probability. The connection loss probability of the class 1 for any method is the smallest among three priority classes because the connections of the class 1 can utilize more wavelengths than those of the other classes. However, this results in the large loss probabilities of the classes 2 and 3.

As for the effect of the combination of wavelength selection rules, the loss probability of the class 1 for Method 1 is the smallest among three Methods. This is because for Method 1, the connections of the class 1 are likely to utilize the largest number of wavelengths in $D_q^{(2)}$ and $D_q^{(3)}$ among three methods.

We also observe from this figure that the connection loss probability for any method increases as the total connection arrival rate becomes large. Nevertheless, for each QoS class, the above tendency of connection loss probabilities for the three methods does not change.

3.4.1.2 Impact of the Loss Probability Required for Each QoS Class

Next, we consider how the connection loss probability required for each QoS class affects the performances of Methods 1, 2, and 3. Here we assume that the number of wavelengths $W = 32$ and that $\lambda_{conn}^{(1)} = \lambda_{conn}^{(2)} = \lambda_{conn}^{(3)} = 7$. In addition, it is required that $P_{q,loss}^{(3)}$ is smaller than or equal to the constant α. When α is given, the number of wavelengths for each QoS class is determined so as to satisfy $P_{q,loss}^{(3)} \leq \alpha$. Note that as α becomes small, the number of wavelengths for each QoS class is restricted to a small set.

Connection loss probabilities $P_{q,loss}^{(1)}$, $P_{q,loss}^{(2)}$ and $P_{q,loss}^{(3)}$ are calculated with (3.9) for all $(W_q^{(2)}, W_q^{(3)})$'s such that $0 < W_q^{(3)} < W_q^{(2)} < 32$, and $P_{q,loss}^{(1)}$ and $P_{q,loss}^{(2)}$ with which $P_{q,loss}^{(3)} \leq \alpha$ holds are plotted in Fig. 3.3. We also calculate with $M/M/c/c$ the connection loss probability for single QoS class where no QoS is guaranteed

Table 3.5. Comparison of analytical results with simulation ones (with 95% confidence interval) in the case of $W_q^{(2)} = 25$ and $W_q^{(3)} = 23$.

(a) Method 1.

	Analysis	Simulation
$P_{q,loss}^{(1)}$	7.418504e-05	7.289973e-05±1.067724e-05
$P_{q,loss}^{(2)}$	5.388198e-02	5.413990e-02±0.042510e-02
$P_{q,loss}^{(3)}$	1.055443e-01	1.057769e-01±0.005052e-01

(b) Method 2.

	Analysis	Simulation
$P_{q,loss}^{(1)}$	3.852461e-03	3.802187e-03±0.113577e-03
$P_{q,loss}^{(2)}$	8.275647e-03	8.224171e-03±0.166026e-03
$P_{q,loss}^{(3)}$	1.400443e-02	1.400785e-02±0.023819e-01

(c) Method 3.

	Analysis	Simulation
$P_{q,loss}^{(1)}$	4.095847e-03	4.045786e-03±0.113599e-03
$P_{q,loss}^{(2)}$	9.383536e-03	9.346767e-03±0.179258e-03
$P_{q,loss}^{(3)}$	1.040093e-02	1.034486e-02±0.019668e-02

(no QoS in Fig. 3.3).

Table 3.5 shows the comparison of analytical results with simulation ones (with 95% confidence interval). From this table, we find that those results are almost the same regardless of QoS class and method in the case of $W_q^{(1)} = 32$, $W_q^{(2)} = 25$ and $W_q^{(3)} = 23$. We have investigated other cases of $(W_q^{(2)}, W_q^{(3)})$'s and observed that analytical results are almost the same as simulation ones. Therefore, our analytical results under the traffic condition $\lambda_{conn}^{(i)} = 7$ for $i = 1, 2$ and 3 are efficient enough to discuss the performance of the proposed method.

Figs. 3.3(a), (b), and (c) show $P_{q,loss}^{(1)}$ and $P_{q,loss}^{(2)}$ for Methods 1, 2, and 3 in the case of $\alpha = 1.0$, respectively. Note that, in the case with $\alpha = 1.0$, any combination

of $(W_q^{(2)}, W_q^{(3)})$ satisfies $P_{q,loss}^{(3)} \leq \alpha$. From these figures, we observe that Method 1 can provide the smallest loss probability for the class 1 among three methods. This is because, in Method 1, all QoS classes follow the wavelength selection rule 1 and the class 1 connections can use more wavelengths in $D_q^{(2)}$ and $D_q^{(3)}$. However, Method 1 tends to provide larger loss probability for the class 2 than Methods 2 and 3. On the other hand, in Method 2, the class 1 follows the rule 1 and the classes 2 and 3 follow the rule 2. Because the class 2 connections can use more wavelengths in $D_q^{(2)}$ and $D_q^{(3)}$, Method 2 can provide the smallest loss probability for the class 2 among three methods.

Figs. 3.3(d), (e), and (f) show $P_{q,loss}^{(1)}$ and $P_{q,loss}^{(2)}$ in the case of $\alpha = 0.5$. As is the case with $\alpha = 1.0$, we observe from Figs. 3.3(d) and (e) that Method 1 can provide the smallest connection loss probability for the class 1, and that Method 2 can provide the smallest connection loss probability for the class 2. With Method 2, both loss probabilities of the classes 1 and 2 can be smaller than the connection loss probability provided in no QoS-guaranteed network. Because, in Method 1, the classes 1 and 2 adopt Rule 1, the number of wavelengths which the class 2 can use becomes slightly large and this results in the slight decrease of $P_{q,loss}^{(2)}$. That is, in Method 1, increasing $W_q^{(2)}$ does not improve $P_{q,loss}^{(2)}$ so much. On the other hand, in Method 2, $P_{q,loss}^{(2)}$ is greatly improved by the increase of $W_q^{(2)}$. This implies that the improvement of $P_{q,loss}^{(2)}$ depends on not only $W_q^{(2)}$ but also the rule adopted by individual QoS class.

Figs. 3.3(g), (h), and (i) show the case of $\alpha = 0.05$. As α becomes small, connection loss probabilities for the classes 1 and 2 become large and the number of pairs of $P_{q,loss}^{(1)}$ and $P_{q,loss}^{(2)}$ which satisfy $P_{q,loss}^{(3)} \leq \alpha$ becomes small. This is because the number of wavelengths allocated for the class 3 increases and thus causes the decrease of wavelengths available for the classes 1 and 2.

Figs. 3.3(j), (k) and (l) show $P_{q,loss}^{(1)}$ and $P_{q,loss}^{(2)}$ in the case of $\alpha = 0.01$. We observe that Methods 2 and 3 can provide a small number of pairs of $P_{q,loss}^{(1)}$ and $P_{q,loss}^{(2)}$ while no wavelength combination exists for Method 1. In Method 1, all QoS classes follow Rule 1 and the resulting number of wavelengths utilized by the class 3 decreases. On the other hand, Rule 2 is adopted for the class 1 in Method 2 and the classes 1 and 2 in Method 3, and this causes the increase of the number of wavelengths utilized by the class 3.

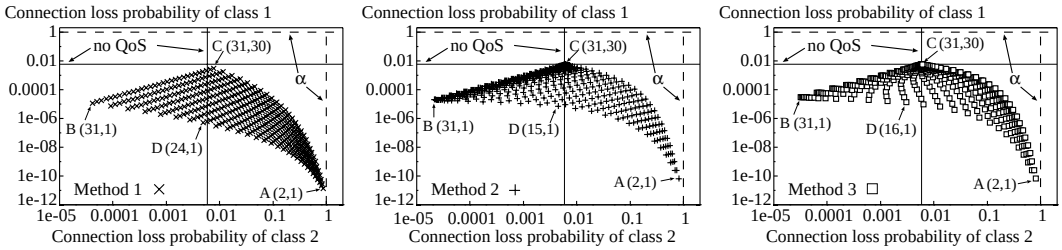

(a) Method 1, $\alpha = 1.0$.

(b) Method 2, $\alpha = 1.0$.

(c) Method 3, $\alpha = 1.0$.

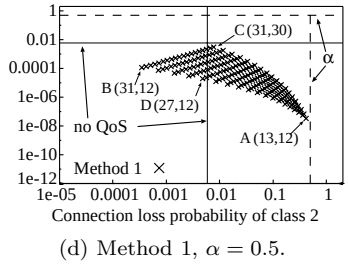

(d) Method 1, $\alpha = 0.5$.

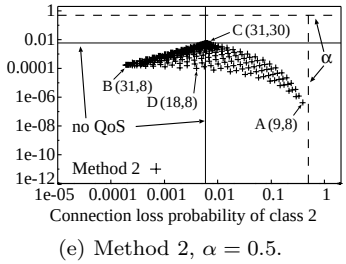

(e) Method 2, $\alpha = 0.5$.

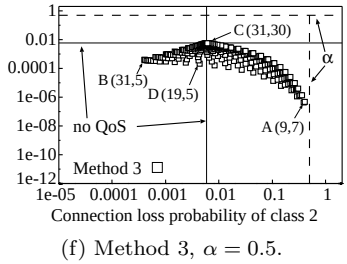

(f) Method 3, $\alpha = 0.5$.

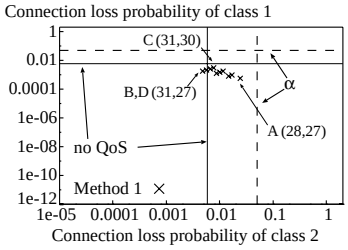

(g) Method 1, $\alpha = 0.05$.

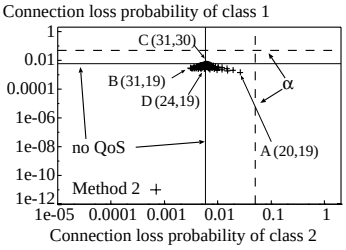

(h) Method 2, $\alpha = 0.05$.

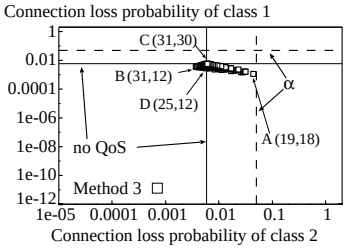

(i) Method 3, $\alpha = 0.05$.

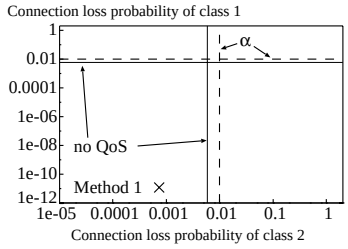

(j) Method 1, $\alpha = 0.01$.

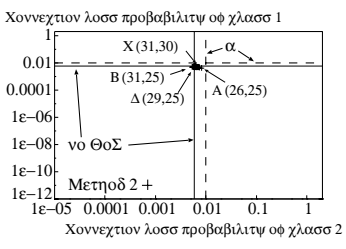

(k) Method 2, $\alpha = 0.01$.

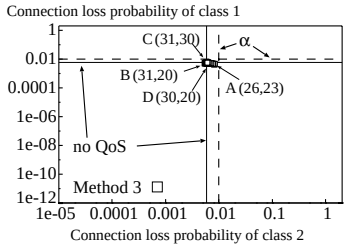

(l) Method 3, $\alpha = 0.01$.

Figure 3.3. Impact of required loss probability for each QoS class.

Furthermore, Method 3 can provide 46 pairs of $P_{q,loss}^{(1)}$ and $P_{q,loss}^{(2)}$ whereas Method 2 provides 26 pairs. In Method 3, only the class 3 follows the Rule 1. Hence, with Method 3, the connections of the class 3 can use more wavelengths in $D_q^{(3)}$ and Method 3 can provide the smallest loss probability for the lowest priority class 3 among three methods. Therefore, Method 3 is effective when low priority class requires small connection loss probability.

In Fig. 3.3, the following four points are defined.

A: $P_{q,loss}^{(1)}$ is the smallest.
B: $P_{q,loss}^{(2)}$ is the smallest.
C: $P_{q,loss}^{(3)}$ is the smallest.
D: $P_{q,loss}^{(1)}$ is the smallest among the points such that both $P_{q,loss}^{(1)}$ and $P_{q,loss}^{(2)}$ are smaller than the connection loss probability in the no QoS guaranteed case.

We also present $(W_q^{(2)}, W_q^{(3)})$ at each point.

When α is one, regardless of methods, $(W_q^{(2)}, W_q^{(3)}) = (2, 1)$, $(31, 1)$, and $(31, 30)$ provide the smallest loss probability for the classes 1, 2 and 3, respectively. As α decreases, larger $W_q^{(3)}$ is required to provide the smaller connection loss probability of the class 3. In particular, Method 1 requires the largest $W_q^{(3)}$ among three methods.

In Methods 1 and 2, the point A is given by $(W_q^{(2)}, W_q^{(3)}) = (W_q^{(3)} + 1, W_q^{(3)})$, as expected. However, A in Method 3 does not always satisfy $(W_q^{(3)} + 1, W_q^{(3)})$ (see Figs. 3.3(f) and (l)). This is because $P_{q,loss}^{(3)}$ for Method 3 is largely affected by $\bar{W}_q^{(2)}$. When $\bar{W}_q^{(2)}$ is small, the class 2 is likely to use wavelength in $D_q^{(3)}$ and this causes large $P_{q,loss}^{(3)}$. As a result, $P_{q,loss}^{(3)} \leq \alpha$ does not hold with $(W_q^{(2)}, W_q^{(3)}) = (W_q^{(3)} + 1, W_q^{(3)})$. As for the points B and C, we always have $W_q^{(2)} = W - 1$ for B and $(W_q^{(2)}, W_q^{(3)}) = (W - 1, W - 2)$ for C.

From Fig. 3.3, we can obtain the best wavelength allocation according to a given QoS policy. For example, if we have a QoS policy in which $P_{q,loss}^{(1)}$ and $P_{q,loss}^{(2)}$ are smaller than the connection loss probability and $P_{q,loss}^{(3)} \leq \alpha$, the point D provides the best combination of $(W_q^{(2)}, W_q^{(3)})$.

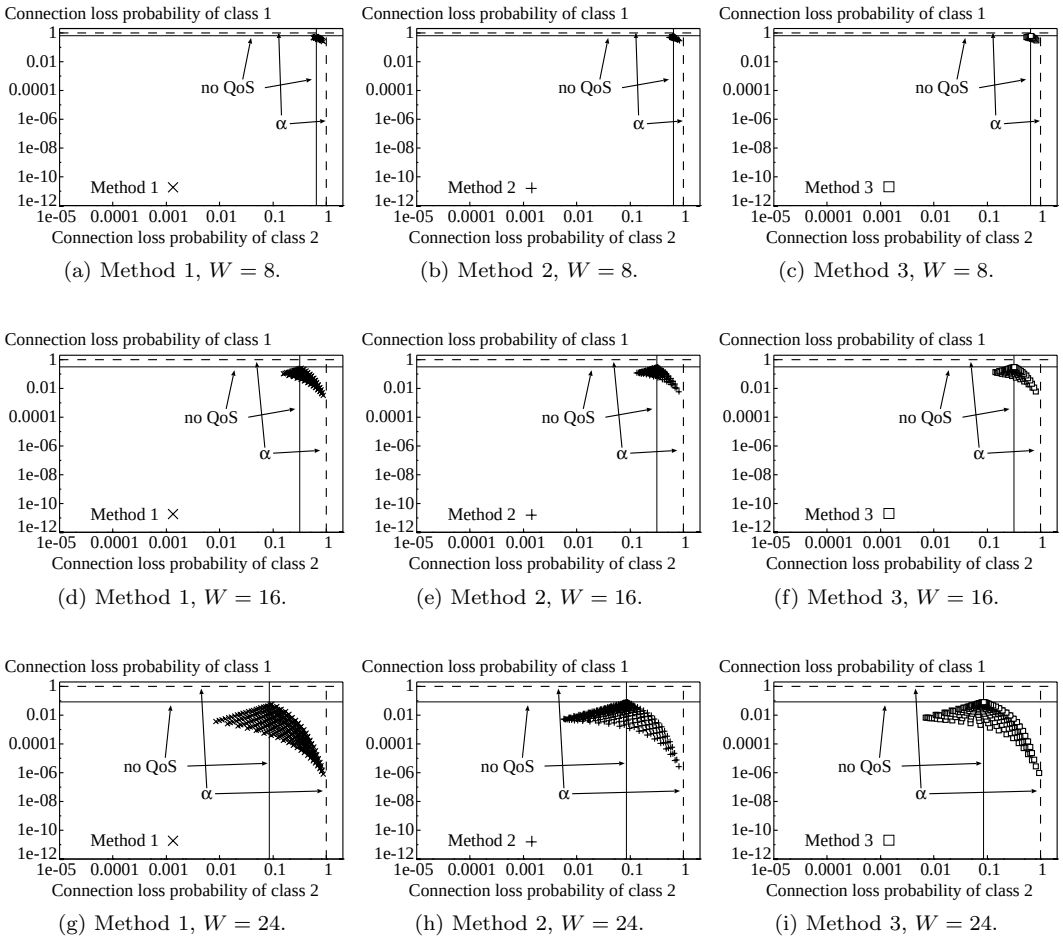

(a) Method 1, $W = 8$. (b) Method 2, $W = 8$. (c) Method 3, $W = 8$.

(d) Method 1, $W = 16$. (e) Method 2, $W = 16$. (f) Method 3, $W = 16$.

(g) Method 1, $W = 24$. (h) Method 2, $W = 24$. (i) Method 3, $W = 24$.

Figure 3.4. Impact of the number of wavelengths.

3.4.1.3 Impact of the Number of Wavelengths

We consider how the number of wavelengths affects the performance of QoS-guaranteed wavelength allocation. Here we assume that $\lambda_{conn}^{(1)} = \lambda_{conn}^{(2)} = \lambda_{conn}^{(3)} = 7$.

Fig. 3.4 shows $P_{q,loss}^{(1)}$ and $P_{q,loss}^{(2)}$ when $P_{q,loss}^{(3)} \leq \alpha = 1.0$. Figs. 3.4(a), (b), and (c), Figs. 3.4(d), (e), and (f), and Figs. 3.4(g), (h), and (i) show the results in the cases of $W = 8$, 16, and 24, respectively. Note that Figs. 3.3(a), (b) and (c) correspond to the results in the case of $W = 32$.

From Figs. 3.4(a), (b), and (c), we observe that Methods 1, 2, and 3 have almost the same performance when the number of wavelengths is eight. This is because $\bar{W}_q^{(1)}$, $\bar{W}_q^{(2)}$ and $\bar{W}_q^{(3)}$ are small and the wavelength selection rules do not affect the connection loss probability of each class. Even if the number of wavelengths becomes 16, we can see the same tendency from Figs. 3.4(d), (e), and (f).

When the number of wavelengths becomes 24 (see Figs. 3.4(g), (h), and (i)), the connection loss probability of each class comes to depend on wavelength selection rule. Method 1 can provide the smallest connection loss probability for class 1 among three method because the connection of the class 1 can use more wavelengths in $D_q^{(3)}$. Methods 2 and 3 can provide smaller connection loss probability for the class 2 than Method 1 because the class 2 connection can use more wavelengths in $D_q^{(3)}$. However, Method 2 can provide smaller connection loss probability for the class 1 than Method 3 because the class 1 can use more wavelengths in $\bar{D}_q^{(2)}$. From the above, when the number of wavelengths is large, it is important to adopt a suitable method for QoS provisioning policy.

3.4.2 Ring Network

In this subsection, we investigate the performance of the proposed method in a uni-directional ring network. Here, in the uni-directional ring network, the benefit of wavelength conversion is limited due to load correlation [29]. If θ becomes large, the performances of three methods do not change so much. Therefore, the results similar to those in the ring network are obtained in other network topologies where the benefit of wavelength conversion is large [1] .

In the ring network, in addition to the assumptions in Section 3.3, we assume that the number of nodes L_{node} is equal to 10 and that the number of wavelengths W equals 32. Moreover, we assume that all nodes have the capability of the FWM wavelength conversion with threshold θ. The pair of source and destination nodes of a connection is distributed uniformly, i.e., any pair is selected with the same probability. The connection loss probability for the ring network is calculated by simulation. We also evaluate the connection loss probability in no

[1] We investigated the performance of the proposed method in a random mesh network and obtained the tendency similar to those in the ring network.

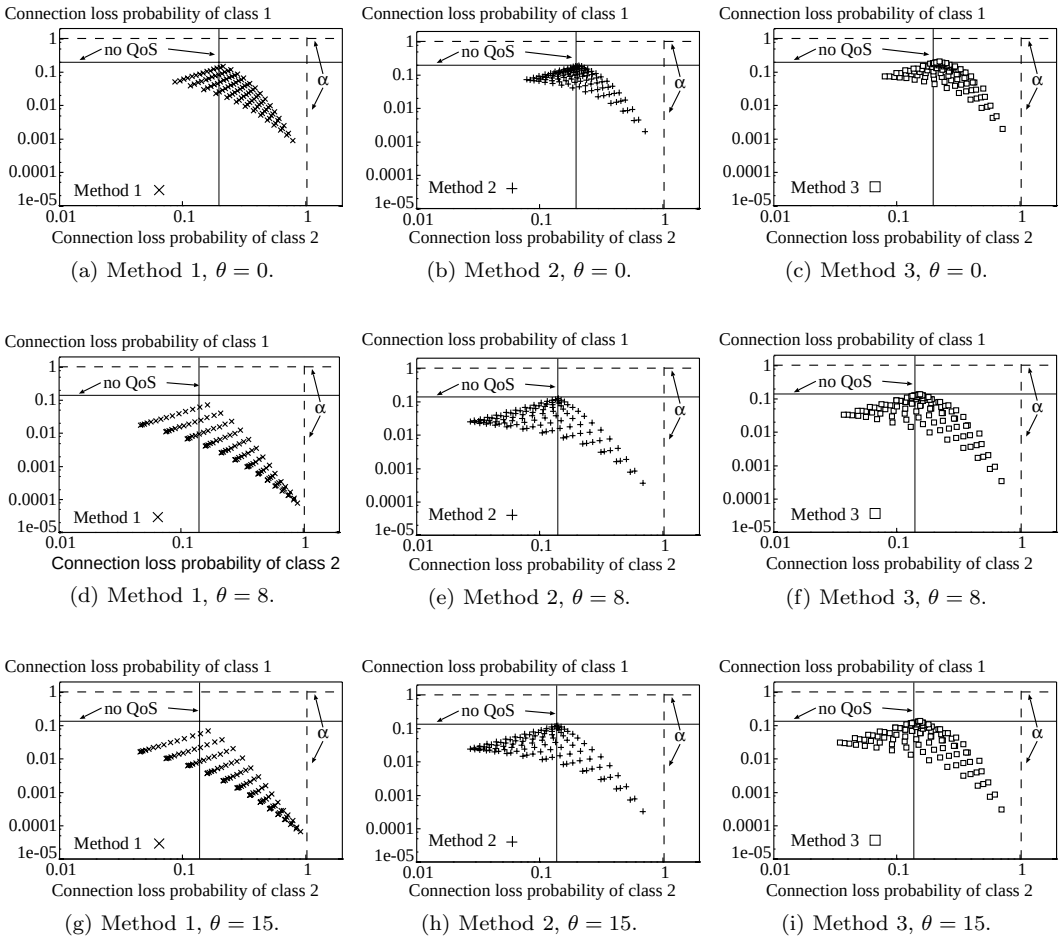

(a) Method 1, $\theta = 0$. (b) Method 2, $\theta = 0$. (c) Method 3, $\theta = 0$.

(d) Method 1, $\theta = 8$. (e) Method 2, $\theta = 8$. (f) Method 3, $\theta = 8$.

(g) Method 1, $\theta = 15$. (h) Method 2, $\theta = 15$. (i) Method 3, $\theta = 15$.

Figure 3.5. Impact of threshold.

QoS-guaranteed network with FWM wavelength conversion by simulation.

3.4.2.1 Impact of Threshold

In this subsection, we consider how the threshold of FWM wavelength conversion affects the performances of Methods 1, 2, and 3. Here we assume that the number of wavelengths $W = 16$ and that $\lambda_{conn}^{(1)} = \lambda_{conn}^{(2)} = \lambda_{conn}^{(3)} = 9$.

As is the case with Fig. 3.4, Fig. 3.5 shows $P_{q,loss}^{(1)}$ and $P_{q,loss}^{(2)}$ when $P_{q,loss}^{(3)} \leq \alpha = 1.0$. Figs. 3.5(a), (b), and (c), Figs. 3.5(d), (e), and (f), and Figs. 3.5(g), (h), and (i) show the simulation results in the cases of $\theta = 0$, 8, and 15, respectively.

From Figs. 3.5(a), (b), and (c), we can find that the performances of three methods are almost the same. Note that $\theta = 0$ corresponds to no wavelength conversion and this causes the large connection loss probability of each QoS class. In this case, no matter what method is adopted, the connection loss probability of each QoS class does not change so much.

When θ is 8 (see Figs. 3.5(d), (e), and (f)), Method 1 provides the smallest connection loss probability for the class 1 and Method 2 provides the smallest connection loss probability for the class 2, as expected. On the other hand, Method 3 can not provide the smallest connection loss probability for both the classes 1 and 2.

We also observe the tendency in Figs. 3.5(g), (h), and (i), those are the case of $\theta = 15$. Comparing the case of $\theta = 8$ with that of $\theta = 15$, we observe that the results are almost the same in each method. Note that $\theta = 15$ corresponds to full-range wavelength conversion for each wavelength set. These figures show that large conversion capability does not always improve the connection loss probability remarkably.

We have also investigated the effect of the wavelength conversion capability on the connection loss probability. Fig. 3.6 shows how the threshold affects the connection loss probability for three methods. We assume that $W = 32$ and $\lambda_{conn}^{(1)} = \lambda_{conn}^{(2)} = \lambda_{conn}^{(3)} = 20$. We set $W_q^{(1)} = 32$, $W_q^{(2)} = 19$, and $W_q^{(3)} = 7$ for Method 1, $W_q^{(1)} = 32$, $W_q^{(2)} = 10$, and $W_q^{(3)} = 3$ for Method 2, and $W_q^{(1)} = 32$, $W_q^{(2)} = 10$, and $W_q^{(3)} = 5$ for Method 3 so that connections of class 1 for three Methods have almost the same loss probability when the threshold is equal to zero.

From Fig. 3.6, we observe that large θ is effective for the connection loss probability of the class 1 while it does not improve those of the classes 2 and 3. In addition, the connection loss probability of the class 1 in Method 1 is greatly improved by θ. Note that the connection loss probability of the class 1 in any Method is less improved when $\theta > 15$. This suggests that large capability of wavelength conversion is not needed for the improvement of the connection loss probability.

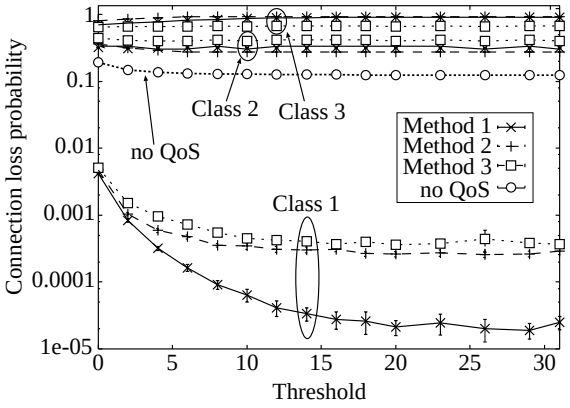

Figure 3.6. Connection loss probability vs. threshold for ring network.

3.4.2.2 Impact of Arrival Rate of Each QoS Class

Finally, we investigate how the arrival rate of each class affects the loss probability of class 1 in ring network. Figs. 3.7(a), (b) and (c), Figs. 3.7(d), (e) and (f), Figs. 3.7(g), (h) and (i), and Figs. 3.7(j), (k) and (l) are the cases of $\theta = 31$, 15, 10, and 0, respectively. When $\lambda_{conn}^{(i)}$ ($i = 1, 2,$ and 3) is a variable parameter, $\lambda_{conn}^{(j)}$'s ($j \neq i$) are constant and equal to 20. We set $W_q^{(1)} = 32$, $W_q^{(2)} = 20$ and $W_q^{(3)} = 10$ for Method 1, $W_q^{(1)} = 32$, $W_q^{(2)} = 8$ and $W_q^{(3)} = 4$ for Method 2, and $W_q^{(1)} = 32$, $W_q^{(2)} = 9$ and $W_q^{(3)} = 3$ for Method 3. In the above setting, when the arrival rates of all classes are 20 and the threshold is equal to zero, the loss probabilities of the classes 2 and 3 for three methods become almost the same.

From Fig. 3.7(a), we observe that the connection loss probabilities of the class 1 for three methods show the same tendency in the case of $\theta = 31$. On the other hand, in Fig. 3.7(b), the connection loss probability for Method 1 increases as the arrival rate of the class 2 becomes large. However, loss probabilities for Methods 2 and 3 are almost constant when the arrival rate of the class 2 is larger than 10.

Because Method 1 adopts the wavelength selection rule 1 for all classes, the class 1 connections can use more wavelengths in $D_q^{(2)}$ and $D_q^{(3)}$ than the classes 2 and 3. On the other hand, since Methods 2 and 3 adopt the wavelength rule 2 for the class 1, the class 1 connections use less wavelengths in $D_q^{(2)}$ and $D_q^{(3)}$.

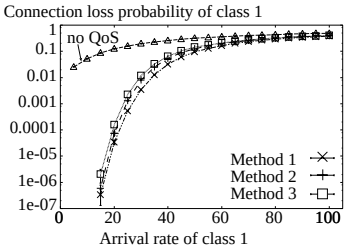

(a) Loss prob. of class 1 vs arrival rate of class 1, $\theta = 31$.

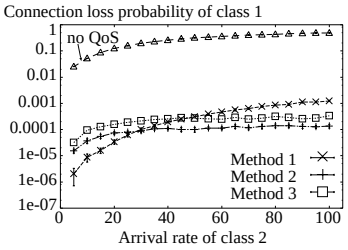

(b) Loss prob. of class 1 vs arrival rate of class 2, $\theta = 31$.

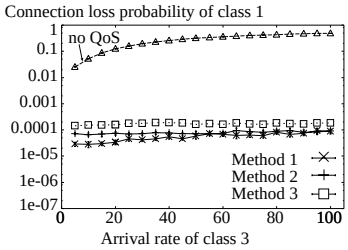

(c) Loss prob. of class 1 vs arrival rate of class 3, $\theta = 31$.

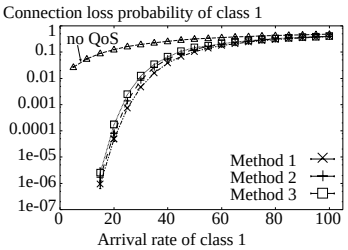

(d) Loss prob. of class 1 vs arrival rate of class 1, $\theta = 15$.

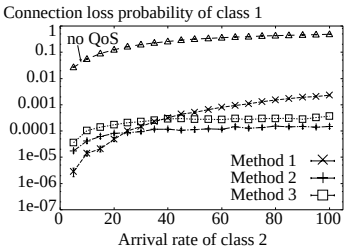

(e) Loss prob. of class 1 vs arrival rate of class 2, $\theta = 15$.

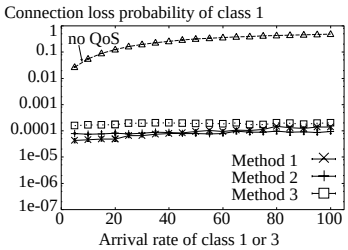

(f) Loss prob. of class 1 vs arrival rate of class 3, $\theta = 15$.

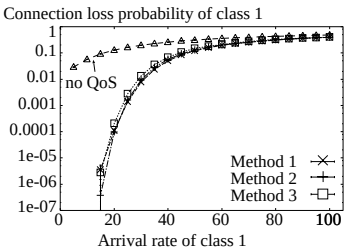

(g) Loss prob. of class 1 vs arrival rate of class 1, $\theta = 10$.

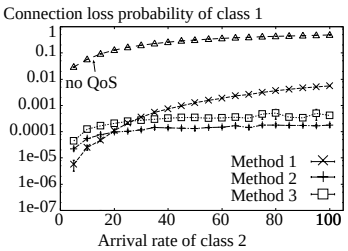

(h) Loss prob. of class 1 vs arrival rate of class 2, $\theta = 10$.

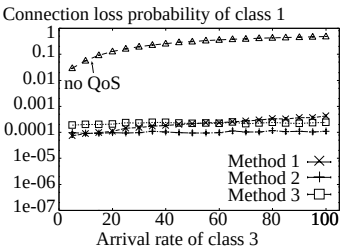

(i) Loss prob. of class 1 vs arrival rate of class 3, $\theta = 10$.

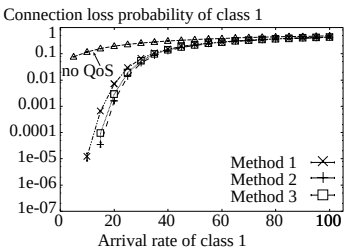

(j) Loss prob. of class 1 vs arrival rate of class 1, $\theta = 0$.

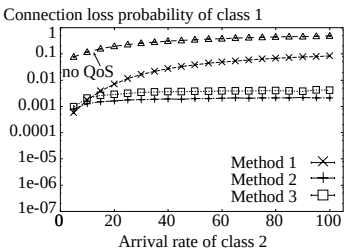

(k) Loss prob. of class 1 vs arrival rate of class 2, $\theta = 0$.

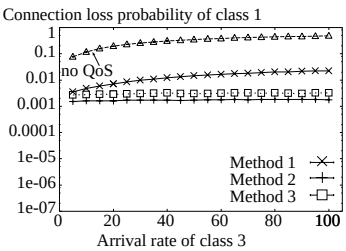

(l) Loss prob. of class 1 vs arrival rate of class 3, $\theta = 0$.

Figure 3.7. Impact of threshold θ for FWM wavelength conversion.

Note that $W_q^{(2)}$ and $W_q^{(3)}$ for Method 1 is larger than those for Methods 2 and 3. That is, the number of wavelengths which only the class 1 can use for Method 1 is smaller than those for Methods 2 and 3. When $\lambda_{conn}^{(i)}$ $(i = 2, 3)$ is larger than 20, wavelengths in $D_q^{(2)}$ and $D_q^{(3)}$ are likely to be utilized by the classes 2 and 3. In this situation, the class 1 is likely to use $\bar{W}_q^{(1)}$ wavelengths and this results in the increase of the connection loss probability of the class 1 for Method 1.

From Fig. 3.7(c), we observe that the connection loss probability of the class 1 for each method is not affected by the arrival rate of the class 3. Note that in each method, $W_q^{(3)}$ is smaller than $W_q^{(1)} - W_q^{(3)}$, that is, $W_q^{(3)} : W_q^{(1)} - W_q^{(3)} = 10 : 22$ for Method 1, $4 : 28$ for Method 2 and $3 : 29$ for Method 3. The class 3 can not use $W_q^{(1)} - W_q^{(3)}$ wavelengths and this results in small connection loss probability of the class 1 against the increase of the class 3 arrivals. Therefore, Methods 2 and 3 are robust in the sense of keeping the connection loss probability of the class 1 constant despite the increase of arrival rate of the other classes.

When θ decreases from 31 to 15, connection loss probabilities of all classes become large as shown in Figs. 3.7(d), (e) and (f). This is because the number of available wavelengths on the next link is restricted. From these figures, we also find that the connection loss probability for Method 1 increases as the arrival rate of the class 2 becomes large. The connection loss probability of the class 1 for Method 1 becomes larger than one for Method 2 when $\lambda_{conn}^{(2)}$ is larger than 25.

Figs. 3.7(g), (h) and (i) show the case of $\theta = 10$. The connection loss probability of the class 1 for Method 1 becomes larger than that for Method 2 when $\lambda_{conn}^{(2)}$ is larger than 20. In addition, from Fig. 3.7(i), we can find that the connection loss probability of the class 1 increases as the connection arrival rate of the class 3 increases.

Figs. 3.7(j), (k), and (l) show the connection loss probability in the ring network without wavelength conversion capability. In these figures, the connection loss probabilities of the class 1 for three methods have the same tendency regardless of the connection arrival rate of the class 1. However, the connection loss probability of the class 1 for Method 1 becomes large as the arrival rate of the class 2 or class 3 increases.

From Figs. 3.7(b), (e), (h), and (k), we find that the advantage of Method 1 decreases as θ becomes small. When θ is small, idle wavelengths are not used

efficiently due to the restriction of wavelength conversion. To decrease the connection loss probability in this case, more wavelengths are required. In Methods 2 and 3, the class 1 can use $W_q^{(1)} - W_q^{(2)} = 24$ and 23 wavelengths, respectively. However, in Method 1, the class 1 uses only $W_q^{(1)} - W_q^{(2)} = 12$ wavelengths. Therefore, connection loss probability of the class 1 for Method 1 increases as θ becomes small.

Hence, in the uni-directional ring network, the connection loss probability of the class 1 for Method 1 is greatly affected by the arrival rates of lower priority classes. When the wavelength conversion capability in the ring network is small, Methods 2 and 3 are more robust and effective than Method 1.

3.5. Conclusions

In this chapter, we proposed a QoS-guaranteed wavelength allocation method which provides multiple QoS classes for the connection loss probability. We considered three combinations of wavelength selection rules and have compared those performances for a single link and a uni-directional ring network. Numerical results showed that our analysis is useful for both the optimal allocation of wavelengths and the best selection of Method.

In numerical examples, we found that Method 1 is effective to the highest priority class. However, the connection loss probabilities of low priority classes becomes large. When a low priority class requires a small connection loss probability, Method 1 is not effective. On the other hand, Method 2 is effective when several priority classes require small loss probabilities. Method 3 is effective when the low priority class requires a small loss probability.

The number of wavelengths and the wavelength conversion capability are also important factors for the connection loss probability. When both the number of wavelengths and the wavelength conversion capability are large, Method 1 can provide the smallest connection loss probability for the class 1 while Method 2 can provide the smallest one for the class 2. Moreover, Method 3 can provide the smallest connection loss probability for the class 3.

When the wavelength conversion capability is small, the robustness should be considered, too. Method 1 is affected by the arrival rates of low priority classes

while Methods 2 and 3 are not affected so much. This robustness of Methods 2 and 3 are attractive for QoS provisioning in terms of the connection loss probability.

Chapter 4

Shared Wavelength Allocation

4.1. Introduction

In the previous section, we proposed the QoS-guaranteed wavelength allocation to provide multiple QoS classes for the connection loss probability. In this proposed allocation, the pre-determined number of wavelengths are allocated to each QoS class depending on the priority of loss probability. Note that a wavelength set for a QoS class is a proper subset of other sets for higher classes. If some wavelengths are shared by all QoS classes and the other wavelengths are exclusively classified into dedicated sets for QoS classes, it is expected that the total connection loss probability becomes smaller than the exclusive wavelength allocation and that the connection loss probability of each QoS class is less affected by the traffic condition of other QoS classes.

In this chapter, we propose a shared wavelength allocation method to provide multiple QoS classes in terms of the connection loss probability. In the shared wavelength allocation, wavelengths are classified into multiple dedicated wavelength sets and a shared wavelength set. Each QoS class can utilize wavelengths within its dedicated wavelength set. To provide multiple QoS classes for the connection loss probability, the dedicated wavelength set of high priority class includes more wavelengths than that of low priority class. When a connection request arrives at node, one of available wavelengths in the dedicated wavelength set for its priority class is allocated to the connection. If there are no available wavelengths in the dedicated wavelength set, one of wavelengths in the

shared wavelength set is allocated to the connection. Since shared wavelengths are utilized by all classes, it is expected that the total connection loss probability decreases.

Since a connection may utilize dedicated and shared wavelengths along its route, wavelength conversion is required at intermediate nodes. With limited-range wavelength conversion, our proposed method is not directly applicable due to the restriction of wavelength conversion capability. In this chapter, we also consider how to apply the shared wavelength allocation method to the all-optical wavelength routed network with the limited-range wavelength conversion. To be more precise, wavelengths are classified into multiple wavelength subsets in advance, and then the shared wavelength allocation method is applied to each subset.

To evaluate the performance of our proposed method on a single link in wavelength routed network, we investigate the connection loss probability of each QoS class using approximation analysis and simulation. In the approximation analysis, we model the proposed method on the single link as a two-stage queueing model which has multiple primary stations and a single secondary station. Using the equivalent random method (EQRM), the connection loss probability of each QoS class is calculated. We also investigate the performance of the method in a uni-directional ring network by simulation. In numerical examples, we show how the shared wavelength allocation affects the connection loss probability in the wavelength routed network with the limited-range wavelength conversion.

The rest of the chapter is organized as follows. Section 4.2 explains the shared wavelength allocation and how to apply the proposed method to the wavelength routed network with the limited-range wavelength conversion. In Section 4.3, to investigate the performance of the shared wavelength allocation method in the single link, we present our analytical model for a node in the wavelength routed network and evaluate the connection loss probability with the EQRM. Numerical examples are shown in Section 4.4 and conclusions are presented in Section 4.5.

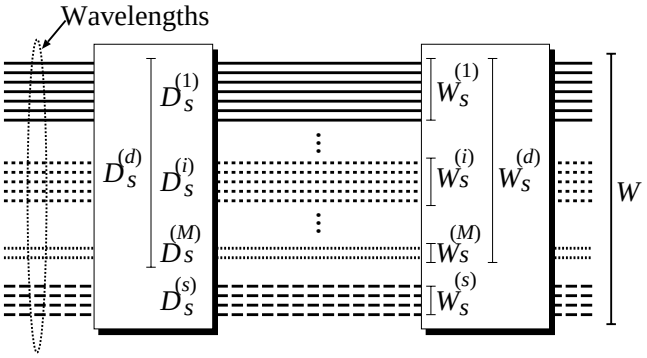

Figure 4.1. Shared wavelength allocation.

4.2. Proposed Method

4.2.1 Full-Range Wavelength Conversion Case

In this section, we explain the shared wavelength allocation. First, we consider an all-optical wavelength routed network where each node has full-range wavelength conversion capability and W wavelengths are multiplexed into an optical fiber. M QoS classes in terms of connection loss probability are provided and they require different acceptable loss probabilities. M QoS classes are numbered from 1 to M and class i has high priority over class j when $i < j$. That is, the class 1 connections have the highest priority and require the smallest loss probability. For simplicity, we call a connection of the class i i-connection.

In the shared wavelength allocation, W wavelengths are classified into two wavelength sets: one is the dedicated wavelength set $D_s^{(d)}$ which includes $W_s^{(d)}$ wavelengths and the other is the shared wavelength set $D_s^{(s)}$ which includes $W_s^{(s)}$ wavelengths (see Fig. 4.1). Here $W_s^{(d)} + W_s^{(s)} = W$, $W_s^{(d)} > 0$ and $W_s^{(s)} > 0$. In the following, we call wavelengths in the dedicated wavelength set the dedicated wavelengths and wavelengths in the shared wavelength set the shared wavelengths.

The dedicated wavelength set $D_s^{(d)}$ is further classified into M dedicated wavelength subsets $D_s^{(i)}$ $(i = 1, 2, \cdots, M)$ and the i-connection can use dedicated wavelengths in the subset $D_s^{(i)}$. There are $W_s^{(i)}$ wavelengths in the dedicated

wavelength subset $D_s^{(i)}$ and we assume that $W_s^{(i)}$ satisfies

$$0 < W_s^{(M)} < \cdots < W_s^{(i)} < \cdots < W_s^{(1)} < W, \tag{4.1}$$

and

$$\sum_{i=1}^{M} W_s^{(i)} = W_s^{(d)}. \tag{4.2}$$

The inequalities of (4.1) imply that higher priority class can use more wavelengths and it is expected that the resulting connection loss probability of high priority class is small. Note that the actual connection loss probability of each class is affected by the traffic load of each class.

On the other hand, all shared wavelength in $D_s^{(s)}$ are available for any class. A shared wavelength is utilized by the i-connection when there is no idle dedicated wavelength in $D_s^{(i)}$. The shared wavelength for the i-connection is chosen according to the following procedure.

step 1: If there is at lease one idle wavelength in $D_s^{(i)}$, an idle wavelength in $D_s^{(i)}$ is chosen to establish the i-connection.

step 2: If there is no available wavelength in $D_s^{(i)}$ and there is at least one idle wavelength in $D_s^{(s)}$, an idle shared wavelength in $D_s^{(s)}$ is chosen to establish the i-connection.

step 3: If there is no available wavelength in both $D_s^{(i)}$ and $D_s^{(s)}$, the i-connection is lost.

If wavelength allocations in all links along the path succeed, the i-connection is eventually established.

Note that in Step 2, our proposed method requires the full-range wavelength conversion in order that any wavelength allocated for the previous link can be converted to any shared wavelength. In the case of the limited-range wavelength conversion, however, any wavelength allocated for the previous link cannot necessarily be converted to a shared wavelength and we cannot directly apply the shared wavelength allocation. In the next subsection, we develop our proposed method under the limited-range wavelength conversion.

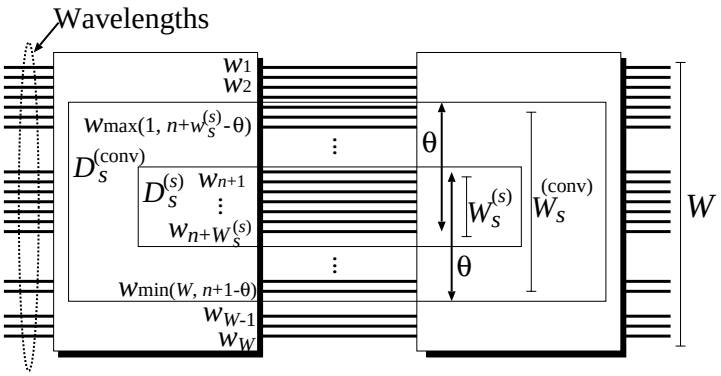

Figure 4.2. Relation of $W_s^{(s)}$, $W_s^{(conv)}$, and θ.

4.2.2 Limited-Range Wavelength Conversion Case

As is the case with the subsection 3.2, we consider the FWM wavelength conversion as the limited-range wavelength conversion. Since the FWM wavelength conversion is restricted to the threshold θ, whether any wavelength in $D_s^{(i)}$ is converted to shared wavelength in $D_s^{(s)}$ or not depends on how to choose wavelengths for the shared wavelength set $D_s^{(s)}$. To understand the relation of W, $W_s^{(s)}$ and θ, we first consider the case where the whole wavelength set $\{w_1, \cdots, w_W\}$ consists of one dedicated wavelength set and one shared wavelength set. In the following, we assume that the shared wavelength set $D_s^{(s)}$ contains successive wavelengths w_{n+1}, w_{n+2},$\cdots$, and $w_{n+W_s^{(s)}}$ for some n (see Fig. 4.2). From the constraint of wavelength conversion due to θ, the minimum index number of the wavelength which can be converted to any wavelength in $D_s^{(s)}$ is $\max(1, n + W_s^{(s)} - \theta)$ and the maximum one is $\min(W, n + 1 + \theta)$. That is, any wavelength in the set

$$D_s^{(conv)} = \Big\{ w_{\max(1,n+W_s^{(s)}-\theta)}, w_{\max(2,n+W_s^{(s)}-\theta+1)}, \cdots, w_{n+1}, \cdots, w_{n+W_s^{(s)}}, \cdots, w_{\min(W-1,n+\theta)}, w_{\min(W,n+1+\theta)} \Big\},$$

can be converted to any wavelength in $D_s^{(s)}$. If $D_s^{(conv)}$ is a subset of $\{w_1, \cdots, w_W\}$, the minimum and maximum indices are given by $n + W_s^{(s)} - \theta$ and $n + 1 + \theta$, respectively. In this case, the number of wavelengths in $D_s^{(conv)}$ is equal to

$$2(\theta + 1) - W_s^{(s)} \equiv W_s^{(conv)}. \tag{4.3}$$

Note that $W_s^{(conv)}$ decreases as $W_s^{(s)}$ increases.

When $W \leq W_s^{(conv)}$, any wavelength in $\{w_1, \cdots, w_W\}$ can be converted to a shared wavelength in $D_s^{(s)}$ and this is equivalent to the full-range wavelength conversion. Therefore it is easy to apply the shared wavelength allocation to this case.

If $W > W_s^{(conv)}$, there are some wavelengths which cannot be converted to a shared wavelength in $D_s^{(s)}$ due to the restriction of θ and we cannot directly apply the shared wavelength allocation. Now consider the classification of the whole wavelength set into the subsets in which the shared wavelength conversion can be applied. Suppose that the whole wavelength set is classified into β subsets $(D_{s,1}, \cdots, D_{s,\beta})$. We introduce the following notations.

$W_{s,n}$: The number of wavelengths in $D_{s,n}$ $(1 \leq n \leq \beta)$.
$D_{s,n}^{(i)}$: The dedicated wavelength set of class i $(1 \leq i \leq M)$ in $D_{s,n}$.
$W_{s,n}^{(i)}$:The number of wavelengths in $D_{s,n}^{(i)}$.
$D_{s,n}^{(s)}$: The shared wavelength set in $D_{s,n}$.
$W_{s,n}^{(s)}$: The number of wavelengths in $D_{s,n}^{(s)}$.

Note that

$$\sum_{n=1}^{\beta} W_{s,n} = W, \quad 1 \leq n \leq \beta,$$
$$\sum_{i=1}^{M} W_{s,n}^{(i)} + W_{s,n}^{(s)} = W_{s,n}, \quad 1 \leq n \leq \beta,$$
$$\sum_{n=1}^{\beta} W_{s,n}^{(i)} = W_s^{(i)}, \quad 1 \leq i \leq M,$$

and

$$\sum_{n=1}^{\beta} W_{s,n}^{(s)} = W_s^{(s)}.$$

For simplicity, we assume that for all m and n $(m \neq n)$,

$$|W_{s,m} - W_{s,n}| \leq 1, \tag{4.4}$$
$$|W_{s,m}^{(s)} - W_{s,n}^{(s)}| \leq 1. \tag{4.5}$$

The inequality (4.4) (resp. (4.5)) implies that the number of wavelengths (resp. shared wavelengths) in $D_{s,n}$ is almost the same as others. Note that, in the case

of $W_{s,n}^{(s)} = 0$, the shared wavelength allocation for the $D_{s,n}$ is identical with the exclusive wavelength allocation. We further assume that for all m and n ($m \neq n$),

$$|(W_{s,m} + W_{s,m}^{(s)}) - (W_{s,n} + W_{s,n}^{(s)})| \leq 1. \tag{4.6}$$

From the inequality (4.6), $W_{s,n} + W_{s,n}^{(s)}$ is given by $\lceil (W + W_s^{(s)})/\beta \rceil$ or $\lfloor (W + W_s^{(s)})/\beta \rfloor$ where $\lceil x \rceil$ ($\lfloor x \rfloor$) is the ceil (floor) function of x.

Now we consider the range of θ when W, $W_s^{(s)}$ and β are given. From (4.3), any wavelength in $D_{s,n}$ is converted to some wavelength in $D_{s,n}^{(s)}$ if $W_{s,n}$ and $W_{s,n}^{(s)}$ satisfy

$$W_{s,n} + W_{s,n}^{(s)} \leq 2(\theta + 1), \quad 1 \leq n \leq \beta. \tag{4.7}$$

Since $W_{s,n} + W_{s,n}^{(s)} \leq \lceil (W + W_s^{(s)})/\beta \rceil$, the shared wavelength allocation can be applied if the following inequality holds.

$$\left\lceil \frac{W + W_s^{(s)}}{\beta} \right\rceil \leq 2(\theta + 1). \tag{4.8}$$

A similar argument yields the upper bound $2(\theta + 1)$ and we finally have

$$\begin{cases} \theta \geq \frac{1}{2}\left(W + W_s^{(s)}\right) - 1, & \beta = 1, \\ \\ \frac{1}{2}\left\lceil \frac{W + W_s^{(s)}}{\beta} \right\rceil - 1 \leq \theta < \frac{1}{2}\left\lceil \frac{W + W_s^{(s)}}{\beta - 1} \right\rceil - 1, & \beta \geq 2. \end{cases} \tag{4.9}$$

Practically, we have to determine β when W, $W_s^{(s)}$ and θ are given. Let $\theta_{\min}$ denote the real value such that

$$\left\lceil \frac{W + W_s^{(s)}}{\beta} \right\rceil = 2(\theta_{\min} + 1). \tag{4.10}$$

Then, we have

$$\frac{W + W_s^{(s)}}{2(\theta_{\min} + 1)} \leq \beta. \tag{4.11}$$

From $\theta \geq \theta_{\min}$, we obtain

$$\frac{W + W_s^{(s)}}{2(\theta + 1)} \leq \beta. \tag{4.12}$$

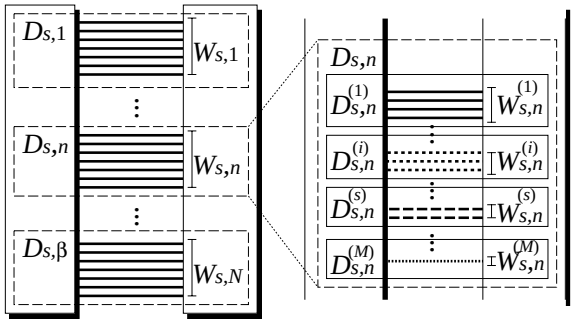

Figure 4.3. Application to limited-wavelength conversion.

Therefore, given W, $W_s^{(s)}$ and θ, β is determined by

$$\beta = \left\lceil \frac{W + W_s^{(s)}}{2(\theta + 1)} \right\rceil . \tag{4.13}$$

To apply the shared wavelength allocation method, each subset $D_{s,n}$ is further classified into $D_{s,n}^{(i)}$ $(1 \leq i \leq M)$ and $D_{s,n}^{(s)}$ (see Fig. 4.3).

A newly arriving i-connection selects an available wavelength subset $D_{s,n}$ according to first-fit strategy. Consider an i-connection which consists of F links between source and destination node. Let l_k denote the kth link $(1 \leq k \leq F)$. The i-connection is established according to the following procedure.

step 1: $n := 1$.

step 2: nth subset $D_{s,n}$ is chosen at l_1 if there exist idle wavelengths in $D_{s,n}^{(i)}$. An available wavelength is chosen according to first-fit strategy and go to step 5. Otherwise, go to step 3.

step 3: nth subset $D_{s,n}$ is chosen at l_1 if there exist idle wavelengths in $D_{s,n}^{(s)}$. An available wavelength is chosen according to first-fit strategy and go to step 5. Otherwise, go to step 4.

step 4: If $n = \beta$, the i-connection is lost. Otherwise, $n := n+1$ and go to step 2.

step 5: Search available wavelength in $D_{s,n}^{(i)}$ or $D_{s,n}^{(s)}$ at each link [1] according to first-fit strategy. If the search succeeds, the i-connection is eventually established. Otherwise, go to step 4.

4.3. Performance Analysis

In this section, we consider the connection loss probability of each QoS class for a single link in the wavelength routed network with the limited-range wavelength conversion. We assume the followings.

1. Connections of the class i arrive at the node according to a Poisson process with parameter $\lambda_{conn}^{(i)}$ and total arrival rate at node is $\lambda_{conn} = \sum_{i=1}^{M} \lambda_{conn}^{(i)}$.

2. Connection holding times of the class i are exponentially distributed with rate $\mu_{conn}^{(i)}$.

3. No queueing for connection request is permitted, that is, the connection is lost immediately after the connection establishment fails.

4. All nodes in the network have FWM wavelength converter with threshold θ.

5. W wavelengths are classified into β subsets where β is determined by (4.13).

Now we consider the wavelength subset $D_{s,n}$ among β wavelength subsets. The $D_{s,n}$ consists of $D_{s,n}^{(i)}$'s, the dedicated wavelength sets for i-connections ($1 \leq i \leq M$), and $D_{s,n}^{(s)}$, the shared wavelength set. A shared wavelength in $D_{s,n}^{(s)}$ is allocated to newly arriving i-connection when there are no available wavelengths in $D_{s,n}^{(i)}$. We model this as a two-stage queueing system illustrated in Fig. 4.4.

The two-stage queueing system has M primary service stations and one secondary service station. The ith primary station is corresponding to $D_{s,n}^{(i)}$, the dedicated wavelength set of the i-connection, and the number of servers of the ith primary station is $W_{s,n}^{(i)}$ which is the number of dedicated wavelengths in $D_{s,n}^{(i)}$.

[1] Note that under the limited-range wavelength conversion, the dedicated wavelength chosen from $D_{s,n}^{(i)}$ at the previous link l_{k-1} ($k = 2, 3, \cdots, F$) can not be always converted to some dedicated wavelength in $D_{s,n}^{(i)}$ at the link l_k.

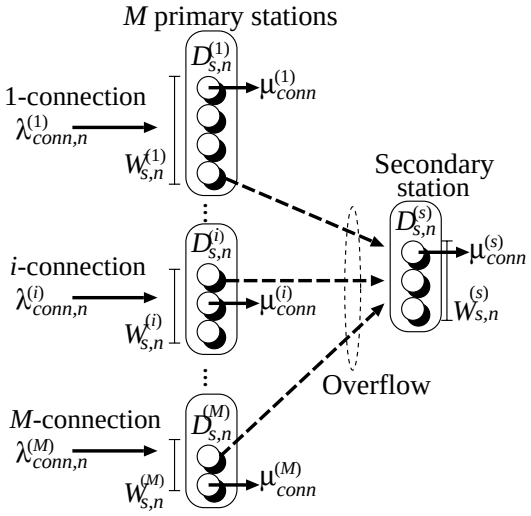

Figure 4.4. Two-stage queueing model for $D_{s,n}$.

Note that all primary stations have no waiting rooms and hence these are loss systems.

On the other hand, the secondary station corresponds to the shared wavelength set $D_{s,n}^{(s)}$ and has $W_{s,n}^{(s)}$ servers. In the following, $D_{s,n}^{(i)}$ implies the ith primary station and $D_{s,n}^{(s)}$ the secondary station.

We assume that i-connection arrives at the node according to a Poisson process with rate $\lambda_{conn}^{(i)}$. Moreover, we assume that the arriving i-connection chooses the wavelength subset $D_{s,n}$ with probability $P_{s,n}^{(i)}$. Hence i-connections arrive at $D_{s,n}$ according to a Poisson process with rate $\lambda_{conn,n}^{(i)} = P_{s,n}^{(i)}\lambda_{conn}^{(i)}$. The connection holding time of the i-connection is exponentially distributed with rate $\mu_{conn}^{(i)}$.

An i-connection arrives at the primary station $D_{s,n}^{(i)}$ and enters one of idle servers in $D_{s,n}^{(i)}$ if those exist. After the completion of holding time of the i-connection, the connection leaves the system. If there are no idle servers in $D_{s,n}^{(i)}$, the i-connection becomes overflow and it goes to the secondary station $D_{s,n}^{(s)}$. If there are also no idle servers in $D_{s,n}^{(s)}$, the i-connection is lost.

In general, a two-stage queueing model with one primary station is analyzable and we can recursively calculate the probability that an arriving connection is eventually lost. First we summarize the recursive calculation of the loss probabil-

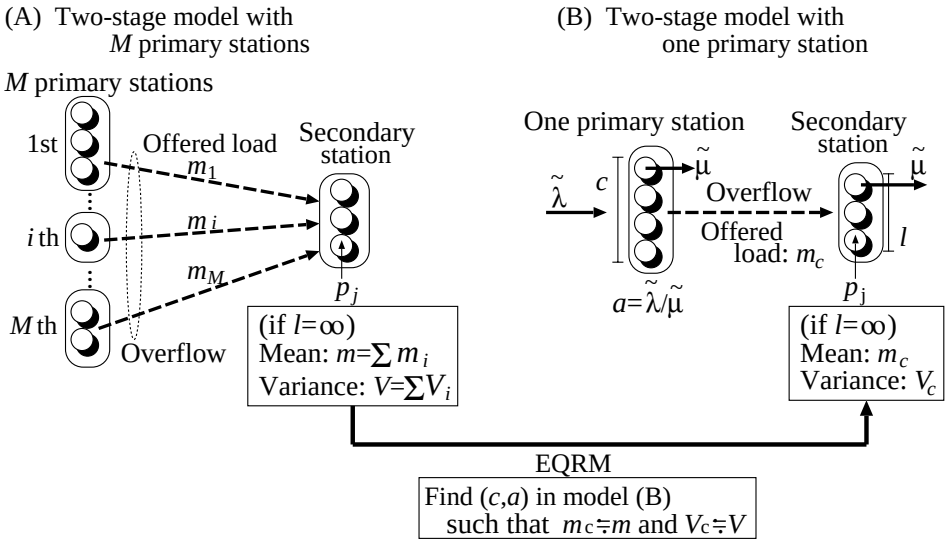

Figure 4.5. Equivalent random method.

ity for the two-stage queueing model with one primary station [65]. The readers are referred to [65] for details.

We assume the followings. The system has one primary station and one secondary station. The numbers of servers in primary and secondary stations are c and l, respectively (see (B) in Fig. 4.5). The customer arrives at the primary station according to a Poisson process with rate λ. The service time of servers in both primary and secondary stations is exponentially distributed with rate μ.

Let $\tilde{B}_c$ denote the blocking probability at the primary station with the number of servers in the primary station equal to c. Then $\tilde{B}_c$ is calculated by the following recursion as a function of c [65].

$$\tilde{B}_{c+1} = \frac{a\tilde{B}_c}{a\tilde{B}_c + c + 1}, \quad c = 0, 1, 2, \cdots, \tag{4.14}$$

$$\tilde{B}_0 = 1, \tag{4.15}$$

where a is the offered load at the primary station and given by $a = \tilde{\lambda}/\tilde{\mu}$.

Let m_c denote the offered load to the secondary station. Then m_c is given by

$$m_c = a\tilde{B}_c, \tag{4.16}$$

and from (4.14), we obtain

$$m_{c+1} = \frac{am_c}{m_c + c + 1}, \quad c = 0, 1, 2, \cdots, \tag{4.17}$$

where $m_0 = a$.

We define p_j as the proportion of time that there are j overflowed customers in the secondary station. Note that if $l = \infty$, that is, the secondary station has infinite servers, the distribution $\{p_j\}$ has mean m_c and variance

$$V_c \equiv \left\{1 - m_c + \frac{a}{m_c + c + 1 - a}\right\} m_c. \tag{4.18}$$

We also define π_j as the proportion of overflowed arrivals who find j overflowed customers in the secondary station. The loss probability of overflowed customers at secondary station is given by

$$\pi_l = \frac{m_{c+l}}{m_c}. \tag{4.19}$$

If there are M primary stations, the loss probability of the overflowed customers at the secondary station cannot be calculated using (4.19). Hence we use the EQRM to calculate the loss probability [65, 66]. The EQRM provides the approximation of the loss probability in this case (see Fig. 4.5).

In the EQRM, the two-stage queueing model with multiple primary stations is identified with the two-stage one with an *equivalent* single primary station. Here, *equivalent* implies that a secondary station with infinite servers has the same mean and variance of the number of customers in the secondary station for this single primary station as it had for the original collection of multiple primary stations [65].

Let m_i and V_i $(1 \leq i \leq M)$ denote the mean and variance of the number of customers in the secondary station generated by ith primary station, and m and V be the corresponding quantities generated by the collection of M primary stations. Then we obtain

$$m = \sum_{i=1}^{M} m_i, \quad V = \sum_{i=1}^{M} V_i. \tag{4.20}$$

The equivalent primary station is expressed with (c, a) such that m and V in (4.20) are equal to m_c in (4.17) and V_c in (4.18), respectively. We can obtain

(c, a) from Rapp's approximation (RA) [65] or graphs in [66] and once (c, a) is determined, the loss probability at the secondary station is approximated by (4.19).

Now we apply the EQRM to our case. Our goal is to calculate the probability that an arriving i-connection at node is eventually lost. First, we focus on the two-stage queueing system in D_n. Let $\tilde{B}_k^{(D_{s,n}^{(i)})}$ denote the blocking probability at the dedicated wavelength set $D_{s,n}^{(i)}$ with k dedicated wavelengths. Since $D_n^{(i)}$ has $W_{s,n}^{(i)}$ dedicated wavelengths, $\tilde{B}_{W_{s,n}^{(i)}}^{(D_{s,n}^{(i)})}$ is required and this can be calculated recursively with (4.14) and (4.15) where the offered load a is given by

$$a = \frac{P_{s,n}^{(i)} \lambda_{conn}^{(i)}}{\mu_{conn}^{(i)}} \quad (\equiv a_n^{(i)}). \tag{4.21}$$

Let $m_k^{(D_{s,n}^{(i)})}$ denote the offered load to the shared wavelength set $D_{s,n}^{(s)}$ generated from $D_{s,n}^{(i)}$. We can calculate $m_{W_{s,n}^{(i)}}^{(D_{s,n}^{(i)})}$ from (4.17) with $a_{s,n}^{(i)}$ in (4.21).

We define $V_k^{(D_{s,n}^{(i)})}$ denote the variance of the number of used wavelengths in the shared wavelength set $D_{s,n}^{(s)}$ given that $D_{s,n}^{(s)}$ has infinite wavelengths and that $D_{s,n}^{(i)}$ has k dedicated wavelengths for the i-connection. Then, from (4.18), $V_{W_{s,n}^{(i)}}^{(D_{s,n}^{(i)})}$ is calculated by

$$V_{W_{s,n}^{(i)}}^{(D_{s,n}^{(i)})} = \left\{ 1 - m_{W_{s,n}^{(i)}}^{(D_{s,n}^{(i)})} + \frac{a_{s,n}^{(i)}}{m_{W_{s,n}^{(i)}}^{(D_{s,n}^{(i)})} + W_{s,n}^{(i)} + 1 - a_{s,n}^{(i)}} \right\} m_{W_{s,n}^{(i)}}^{(D_{s,n}^{(i)})}. \tag{4.22}$$

Let $(W_{s,n}^p, a_{s,n}^p)$ denote the equivalent single primary station. We can find $(W_{s,n}^p, a_{s,n}^p)$ numerically such that

$$m_{W_{s,n}^p} \simeq \sum_{i=1}^{M} m_{W_{s,n}^{(i)}}^{(D_{s,n}^{(i)})}, \tag{4.23}$$

$$V_{W_{s,n}^p} \simeq \sum_{i=1}^{M} V_{W_{s,n}^{(i)}}^{(D_{s,n}^{(i)})}, \tag{4.24}$$

where $m_{W_{s,n}^p}$ and $V_{W_{s,n}^p}$ are calculated by (4.17) and (4.18), respectively.

Once $(W_{s,n}^p, a_{s,n}^p)$ is obtained, the probability that an arriving connection is eventually lost is given by

$$P_{s,loss}^{(D_{s,n})} = \frac{m_{W_{s,n}^p + W_{s,n}^{(s)}}}{m_{W_{s,n}^p}}. \tag{4.25}$$

The loss probability of the i-connection at $D_{s,n}$ is given by

$$P_{s,loss}^{(i)(D_{s,n})} = \frac{m_{W_{s,n}^{(i)}}^{(D_{s,n}^{(i)})}}{m_{W_{s,n}^{p}}} P_{s,loss}^{(D_{s,n})}, \tag{4.26}$$

where $m_{W_{s,n}^{(i)}}^{(D_{s,n}^{(i)})}/m_{W_{s,n}^{p}}$ is the proportion that the overflowed connection to the shared wavelength set in $D_{s,n}$ is the class i. Finally, the loss probability of the i-connection at node level is given by

$$P_{s,loss}^{(i)} = \sum_{n=1}^{\beta} P_{s,n}^{(i)} P_{s,loss}^{(i)(D_{s,n})}. \tag{4.27}$$

4.4. Numerical Examples

In this section, we show some numerical examples for the shared wavelength allocation under limited-range wavelength conversion. First we consider a single link in the wavelength routed network, and then we consider a uni-directional ring network. In both cases, we assume that the number of QoS classes is three and that the connection holding time is exponentially distributed with rate $\mu_{conn}^{(i)} = 1$ $(i = 1, 2, 3)$.

4.4.1 Single Link in Wavelength Routing Network

In this subsection, we consider a single link in wavelength routed network. The connection loss probabilities of three QoS classes, $P_{s,loss}^{(1)}$, $P_{s,loss}^{(2)}$, and $P_{s,loss}^{(3)}$, are calculated by the analysis in the previous section and by simulation.

4.4.1.1 Impact of Total Arrival Rate

First, we consider how the total arrival rate of connections affects the connection loss probability for each QoS class. Here we assume that the number of wavelengths is $W = 32$, and that θ is large enough to convert any wavelength in $D_s^{(i)}$ $(i = 1, 2, \cdots, 3)$ to a shared wavelength in $D_s^{(s)}$. That is, the number of wavelength subsets β is equal to 1 and hence $P_{s,1}^{(i)} = 1.0$. 32 wavelengths are classified into $D_s^{(1)}$, $D_s^{(2)}$, $D_s^{(3)}$ and $D_s^{(s)}$, and in Figs. 4.6(a), (b), and (c), we set

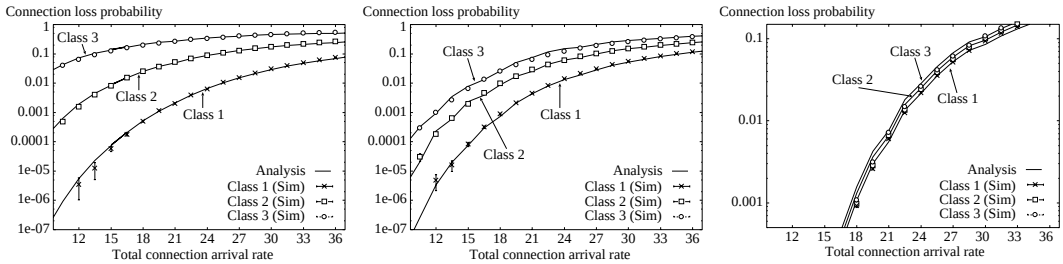

(a) Case of $(W_s^{(1)}, W_s^{(2)}, W_s^{(3)}, W_s^{(s)}) = (15, 10, 5, 2)$.

(b) Case of $(W_s^{(1)}, W_s^{(2)}, W_s^{(3)}, W_s^{(s)}) = (12, 8, 4, 8)$.

(c) Case of $(W_s^{(1)}, W_s^{(2)}, W_s^{(3)}, W_s^{(s)}) = (3, 2, 1, 26)$.

Figure 4.6. Connection loss probability vs. total connection arrival rate for single link.

$(W_s^{(1)}, W_s^{(2)}, W_s^{(3)}, W_s^{(s)}) = (15, 10, 5, 2)$, $(12, 8, 4, 8)$ and $(3, 2, 1, 26)$, respectively. In addition, we set $\lambda_{conn}^{(1)} = \lambda_{conn}^{(2)} = \lambda_{conn}^{(3)} = \lambda_{conn}/3$.

From these figures, we observe that analytical results are almost the same as simulation ones regardless of the increase of total arrival rate and $(W_s^{(1)}, W_s^{(2)}, W_s^{(3)}, W_s^{(s)})$'s. We also observe that the discrepancy between QoS classes increases as $W_s^{(s)}$ becomes small. This is because the small $W_s^{(s)}$ results in a large number of dedicated wavelengths. If the large differentiation in terms of the connection loss probability is required, $W_s^{(s)}$ should be small.

4.4.1.2 Impact of the Loss Probability Required for the Lowest QoS Class

Next, we consider how the connection loss probability required for the lowest QoS class affects the performances of the shared wavelength allocation and exclusive wavelength allocation shown in Introduction. We assume that the number of wavelengths is $W = 32$ and that the number of wavelength subsets is $\beta = 1$. Moreover, we set $\lambda_{conn}^{(1)} = \lambda_{conn}^{(2)} = \lambda_{conn}^{(3)} = 7$. In terms of the shared wavelength allocation, it is required that $P_{s,loss}^{(3)}$ is smaller than or equal to the constant α. Connection loss probabilities $P_{s,loss}^{(1)}$, $P_{s,loss}^{(2)}$ and $P_{s,loss}^{(3)}$ are calculated with (4.27) for all $(W_s^{(1)}, W_s^{(2)}, W_s^{(3)}, W_s^{(s)})$'s such that $0 < W_s^{(3)} < W_s^{(2)} < W_s^{(1)} < 32$ and $W_s^{(1)} + W_s^{(2)} + W_s^{(3)} + W_s^{(s)} = 32$. $P_{s,loss}^{(1)}$ and $P_{s,loss}^{(2)}$ with which $P_{s,loss}^{(3)} \leq \alpha$ holds are plotted in Fig. 4.7.

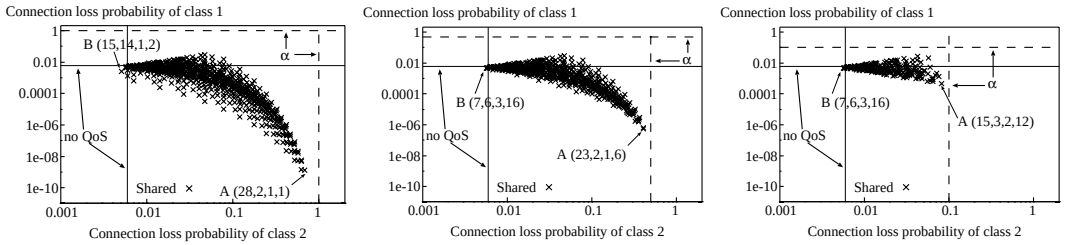

(a) Shared wavelength allocation, $\alpha = 1.0$.

(b) Shared wavelength allocation, $\alpha = 0.5$.

(c) Shared wavelength allocation, $\alpha = 0.1$.

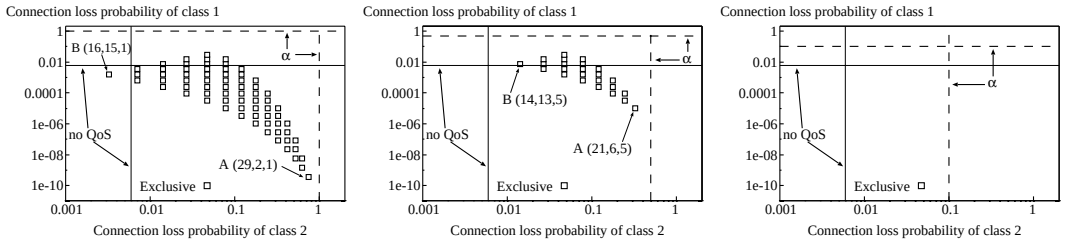

(d) Exclusive wavelength allocation, $\alpha = 1.0$.

(e) Exclusive wavelength allocation, $\alpha = 0.5$.

(f) Exclusive wavelength allocation, $\alpha = 0.1$.

Figure 4.7. Impact of the loss probability required for the lowest QoS class.

Fig. 4.7 also shows $P_{s,loss}^{(1)}$ and $P_{s,loss}^{(2)}$ with which $P_{s,loss}^{(3)} \leq \alpha$ for the exclusive wavelength allocation. Here, $P_{s,loss}^{(1)}$, $P_{s,loss}^{(2)}$ and $P_{s,loss}^{(3)}$ were calculated with $M/M/c/c$ for all $(W_s^{(1)}, W_s^{(2)}, W_s^{(3)})$'s such that $0 < W_s^{(3)} < W_s^{(2)} < W_s^{(1)} < 32$ and $W_s^{(1)} + W_s^{(2)} + W_s^{(3)} = 32$. We also calculated with $M/M/c/c$ the connection loss probability for single QoS class where no QoS is guaranteed (no QoS in Fig. 4.7).

In Fig. 4.7, A is the point at which $P_{s,loss}^{(1)}$ is the smallest and B is the point such that $P_{s,loss}^{(2)}$ is the smallest. We also present the values of $(W_s^{(1)}, W_s^{(2)}, W_s^{(3)}, W_s^{(s)})$ for the shared wavelength allocation and those of $(W_s^{(1)}, W_s^{(2)}, W_s^{(3)})$ for the exclusive one.

Table 4.1 shows the comparison of analytical results with simulation ones (with 95% confidence interval). From this table, we find that analytical results are almost the same as simulation ones in the case of $(W_s^{(1)}, W_s^{(2)}, W_s^{(3)}, W_s^{(s)}) = (12, 7, 4, 9)$. We have investigated other cases of $(W_s^{(1)}, W_s^{(2)}, W_s^{(3)}, W_s^{(s)})$'s and observed that analytical results are almost the same as simulation ones. Therefore,

Table 4.1. Comparison of analysis and simulation (with 95% confidence interval) in the case of $(W_s^{(1)}, W_s^{(2)}, W_s^{(3)}, W_s^{(s)}) = (12, 7, 4, 9)$.

	Analysis	Simulation
$P_{s,loss}^{(1)}$	3.102878e-03	3.105994e-03±0.008722e-03
$P_{s,loss}^{(2)}$	2.851508e-02	2.828295e-02±0.025813e-02
$P_{s,loss}^{(3)}$	6.042185e-02	6.008691e-02±0.040192e-02

our analytical results under the traffic condition $\lambda_{conn}^{(i)} = 7$ for $i = 1, 2$ and 3 are efficient enough to discuss the performance of the shared wavelength allocation.

Figs. 4.7(a) and (d) show $P_{s,loss}^{(1)}$ and $P_{s,loss}^{(2)}$ for the shared and exclusive wavelength allocations in the case of $\alpha = 1.0$, respectively. From these two figures, we observe that the shared wavelength allocation can provide more pairs of $P_{s,loss}^{(1)}$ and $P_{s,loss}^{(2)}$ than the exclusive one. Figs. 4.7(b) and (e) show $P_{s,loss}^{(1)}$ and $P_{s,loss}^{(2)}$ in the case of $\alpha = 0.5$. As is the case with $\alpha = 1.0$, we observe that the shared wavelength allocation can provide more pairs of $P_{s,loss}^{(1)}$ and $P_{s,loss}^{(2)}$ for the classes 1 and 2 than the exclusive one. Furthermore, in this case, the shared wavelength allocation can provide smaller connection loss probabilities than the exclusive one. Figs. 4.7(c) and (f) show the case of $\alpha = 0.1$. In this case, the shared wavelength allocation provides some pairs of $P_{s,loss}^{(1)}$ and $P_{s,loss}^{(2)}$ while no pairs exist in the exclusive one.

As α becomes small, connection loss probabilities for the classes 1 and 2 become large and the number of pairs of $P_{s,loss}^{(1)}$ and $P_{s,loss}^{(2)}$ which satisfy $P_{s,loss}^{(3)} \leq \alpha$ becomes small. In the exclusive wavelength allocation, the class 3 can use only $W_s^{(3)}$ wavelengths and this causes large $P_{s,loss}^{(3)}$. However, in the shared wavelength allocation, the class 3 can use up to $W_s^{(3)} + W_s^{(s)}$ wavelengths. Therefore, the shared wavelength allocation can provide some pairs of $P_{s,loss}^{(1)}$ and $P_{s,loss}^{(2)}$ when the exclusive wavelength allocation can not provide them.

When α is one, for the shared wavelength allocation, $(W_s^{(1)}, W_s^{(2)}, W_s^{(3)}, W_s^{(s)})$ $= (28, 2, 1, 1)$ and $(15, 14, 1, 2)$ provide the smallest loss probability for the classes 1 and 2, respectively. On the other hand, for the exclusive wavelength allocation, $(W_s^{(1)}, W_s^{(2)}, W_s^{(3)}) = (29, 2, 1)$ and $(16, 15, 1)$ provide the smallest loss probability

for the classes 1 and 2, respectively.

As α decreases, large $W_s^{(3)}$ is required to provide the corresponding connection loss probability of the class 3. However, in the shared wavelength allocation, the class 3 connections can use $W_s^{(s)}$ wavelengths in addition to $W_s^{(3)}$. Note that large $W_s^{(s)}$ is also effective for both the classes 1 and 2 and this results in the existence of pairs of $P_{s,loss}^{(1)}$ and $P_{s,loss}^{(2)}$ even when α is small. Thus, if a small connection loss probability is required for low priority class, the shared wavelength allocation is more effective than the exclusive one.

4.4.1.3 Impact of Arrival Rate of Each QoS Class

Next, we investigate how the arrival rate of each class affects the connection loss probabilities. When $\lambda_{conn}^{(i)}$ ($i = 1, 2,$ and 3) is a variable parameter, $\lambda_{conn}^{(j)}$'s ($j \neq i$) are constant and equal to 6. Here, we assume that the number of wavelengths $W = 32$.

We assume that for the shared wavelength allocation, $(W_s^{(1)}, W_s^{(2)}, W_s^{(3)}, W_s^{(s)})$ $= (12, 8, 4, 8)$ in Figs. 4.8(a), (b) and (c), and $(6, 4, 2, 20)$ in Figs. 4.8(d), (e) and (f). On the other hand, for the exclusive wavelength allocation, we set $(W_s^{(1)}, W_s^{(2)}, W_s^{(3)}) = (15, 11, 6)$ in these six figures. In the above setting, when the arrival rates of all QoS classes are 6, the connection loss probabilities of the classes 1 and 2 for the shared wavelength allocation are close to those for the exclusive one.

From Figs. 4.8(a), (b) and (c), we observe that the analytical and simulation results are almost the same. However, in Figs. 4.8(d), (e) and (f), analytical results are somewhat different from simulation ones. Note that large $W_s^{(s)}$ causes large variance of the number of customers in the secondary station and this makes the EQRM approximation less accurate. In addition, each QoS class has its own connection arrival rate and this contributes the variance of the overflow to secondary station. In (4.26), we do not consider the variance of each QoS class in the secondary station and this also causes the discrepancy between analytical and simulation results.

From Figs. 4.8(a), (b) and (c), we observe that in the shared wavelength allocation, the connection loss probabilities of all QoS classes are affected by the arrival rate of each QoS class. This is because shared wavelengths are utilized by

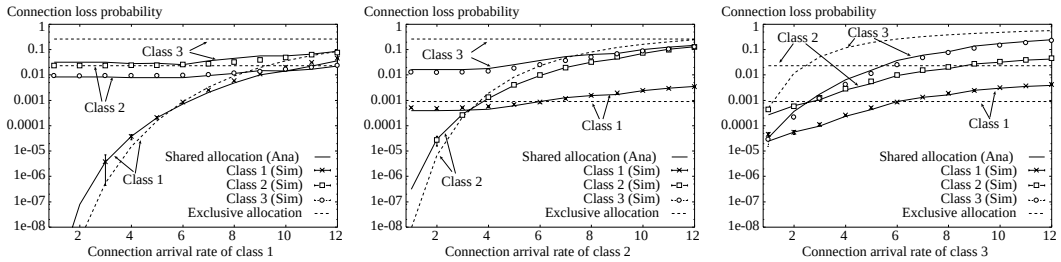

(a) Impact of arrival rate of class 1, $(W_s^{(1)}, W_s^{(2)}, W_s^{(3)}, W_s^{(s)}) = (12, 8, 4, 8)$.

(b) Impact of arrival rate of class 2, $(W_s^{(1)}, W_s^{(2)}, W_s^{(3)}, W_s^{(s)}) = (12, 8, 4, 8)$.

(c) Impact of arrival rate of class 3, $(W_s^{(1)}, W_s^{(2)}, W_s^{(3)}, W_s^{(s)}) = (12, 8, 4, 8)$.

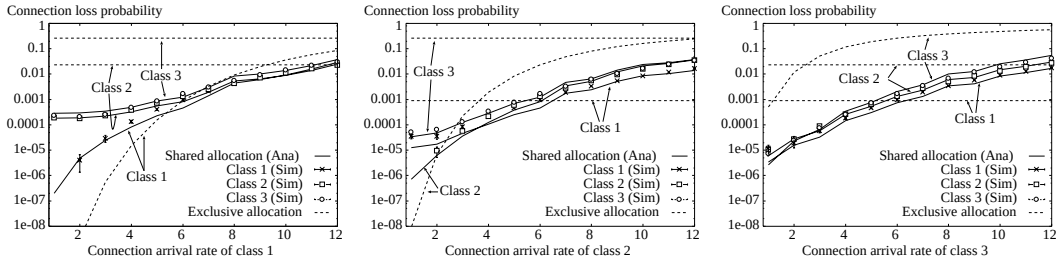

(d) Impact of arrival rate of class 1, $(W_s^{(1)}, W_s^{(2)}, W_s^{(3)}, W_s^{(s)}) = (6, 4, 2, 20)$.

(e) Impact of arrival rate of class 2, $(W_s^{(1)}, W_s^{(2)}, W_s^{(3)}, W_s^{(s)}) = (6, 4, 2, 20)$.

(f) Impact of arrival rate of class 3, $(W_s^{(1)}, W_s^{(2)}, W_s^{(3)}, W_s^{(s)}) = (6, 4, 2, 20)$.

Figure 4.8. Impact of arrival rate of each QoS class.

all QoS classes and the class with large (small) arrival rate uses more (less) shared wavelengths. As the number of shared wavelengths increases, this tendency becomes large. In Figs. 4.8(d), (e) and (f), when the arrival rate of each QoS class becomes large, the connection loss probabilities of all QoS classes increases in the same way.

On the other hand, in the exclusive wavelength allocation, the arrival rate of individual QoS class does not affect the connection loss probabilities of other QoS classes, as expected. Therefore, the exclusive wavelength allocation is robust in the sense of keeping the connection loss probability constant despite the increase of arrival rate of the other classes. To realize the robustness in the shared

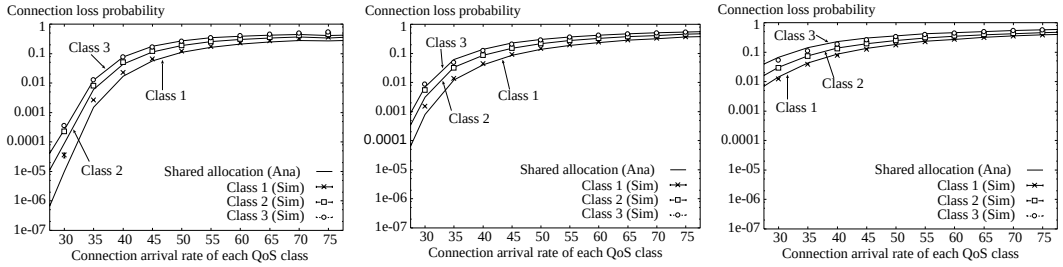

(a) $82 \leq \theta$ and $\beta = 1$. (b) $41 \leq \theta < 82$ and $\beta = 2$. (c) $20 \leq \theta < 27$ and $\beta = 4$.

Figure 4.9. Impact of threshold.

wavelength allocation, a small number of shared wavelengths is required.

4.4.1.4 Impact of Threshold

In this subsection, we consider how the threshold of the FWM wavelength conversion affects the performances of the shared and exclusive wavelength allocations. In the shared wavelength allocation, the number of wavelength subsets β is determined from (4.13) with W, θ and $W_s^{(s)}$.

In Fig. 4.9, we assume that $W = 128$ and $(W_s^{(1)}, W_s^{(2)}, W_s^{(3)}, W_s^{(s)}) = (40, 30, 20, 38)$. In addition, we set $\lambda_{conn}^{(i)} = \lambda_{conn}/3$ $(i = 1, 2, 3)$. From (4.9), we set $\theta \geq 82$ in Fig. 4.9(a), $41 \leq \theta < 82$ in Fig. 4.9(b) and $20 \leq \theta < 27$ in Fig. 4.9(c) and those correspond to $\beta = 1$, $\beta = 2$ and $\beta = 4$, respectively. When β equals 2, we classify 128 wavelengths into two wavelength subsets $D_{s,1}$ and $D_{s,2}$ such that $(W_{s,1}^{(1)}, W_{s,1}^{(2)}, W_{s,1}^{(3)}, W_{s,1}^{(s)}) = (W_{s,2}^{(1)}, W_{s,2}^{(2)}, W_{s,2}^{(3)}, W_{s,2}^{(s)}) = (24, 16, 8, 16)$ according to (4.4), (4.6) and (4.8). On the other hand, in the case of $\beta = 4$, $(W_{s,1}^{(1)}, W_{s,1}^{(2)}, W_{s,1}^{(3)}, W_{s,1}^{(s)}) = (W_{s,2}^{(1)}, W_{s,2}^{(2)}, W_{s,2}^{(3)}, W_{s,2}^{(s)}) = (10, 7, 5, 10)$ and $(W_{s,3}^{(1)}, W_{s,3}^{(2)}, W_{s,3}^{(3)}, W_{s,3}^{(s)}) = (W_{s,4}^{(1)}, W_{s,4}^{(2)}, W_{s,4}^{(3)}, W_{s,4}^{(s)}) = (10, 8, 5, 9)$. Moreover, we assume that each class selects an available wavelength subset equally likely.

From Fig. 4.9, we observe that the connection loss probability for each QoS class becomes large as θ decreases (the number of wavelength subsets increases). Note that the increase of β decreases the number of available wavelengths and this causes the large connection loss probability.

From the above, to provide the small connection loss probability for each QoS class, $W_s^{(s)}$ should be determined so as to satisfy $\beta = 1$ in (4.12).

4.4.2 Ring Network

In this subsection, we investigate the performance of the shared wavelength allocation for a uni-directional ring network by simulation. In our simulation, we assume that the followings in addition to the assumptions in Section 4.3.

1. The number of nodes in the network is L_{node}.
2. The pair of source and destination nodes of arriving connection is distributed uniformly, i.e., each pair is selected with the same probability.

In the following, we set $L_{node} = 10$, $W = 32$ and $\lambda_{conn}^{(1)} = \lambda_{conn}^{(2)} = \lambda_{conn}^{(3)} = 20$.

4.4.2.1 Impact of the Loss Probability Required for the Lowest QoS Class

We consider how the connection loss probability required for the lowest QoS class affects the performances of the shared and exclusive wavelength allocations.

As is the case with Fig. 4.7, Fig. 4.10 shows $P_{s,loss}^{(1)}$ and $P_{s,loss}^{(2)}$ when $P_{s,loss}^{(3)} \leq \alpha$. Figs. 4.10(a), (b), and (c) show the simulation results for the shared wavelength allocation in the cases of $\alpha = 1.0$, 0.5 and 0.3, respectively. Figs. 4.10(d), (e), and (f) show those for the exclusive wavelength allocation in the cases of $\alpha = 1.0$, 0.5 and 0.3, respectively. In these figures, we set $\theta = 31$ and this means that the ring network has the full-range wavelength conversion. We also calculate with simulation the connection loss probability for the case of single QoS class where no QoS is guaranteed (no QoS in Fig. 4.10).

As is the case with single link, we observe from Fig. 4.10 that the shared wavelength allocation can provide more pairs of $P_{s,loss}^{(1)}$ and $P_{s,loss}^{(2)}$ than the exclusive one. Furthermore, even in the case of $\alpha = 0.3$, the shared wavelength allocation can provide some pairs of $P_{s,loss}^{(1)}$ and $P_{s,loss}^{(2)}$ for the classes 1 and 2. With the shared wavelength allocation, $P_{s,loss}^{(1)}$ and $P_{s,loss}^{(2)}$ can be smaller than the connection loss probability provided in no QoS-guaranteed network. Therefore, for the ring network, the shared wavelength allocation is also more effective than the exclusive wavelength allocation for QoS provisioning in the case of full-range wavelength conversion.

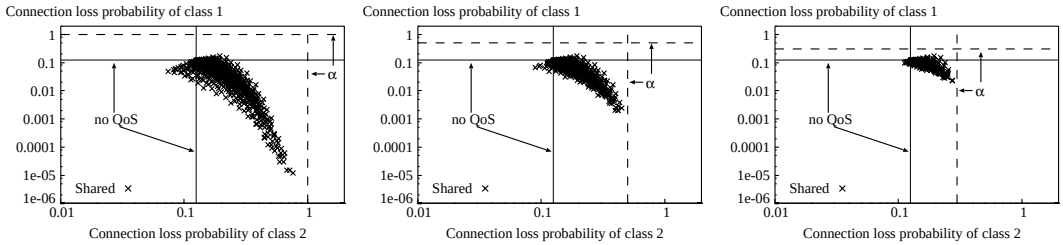

(a) Shared wavelength allocation, $\theta = 31$ and $\alpha = 1.0$.

(b) Shared wavelength allocation, $\theta = 31$ and $\alpha = 0.5$.

(c) Shared wavelength allocation, $\theta = 31$ and $\alpha = 0.3$.

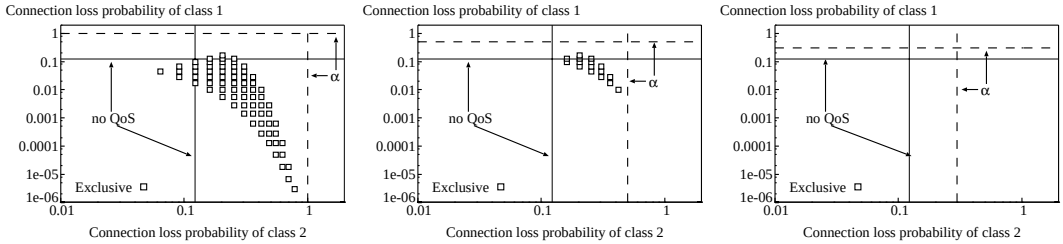

(d) Exclusive wavelength allocation, $\theta = 31$ and $\alpha = 1.0$.

(e) Exclusive wavelength allocation, $\theta = 31$ and $\alpha = 0.5$.

(f) Exclusive wavelength allocation, $\theta = 31$ and $\alpha = 0.3$.

Figure 4.10. Impact of the loss probability required for the lowest QoS class for ring network.

4.4.2.2 Impact of Threshold

Finally, we consider how the capability of FWM wavelength conversion affects the performances of the shared and exclusive wavelength allocations for the ring network.

Figs. 4.11(a), (b) and (c) show $P_{s,loss}^{(1)}$ and $P_{s,loss}^{(2)}$ for the shared wavelength allocation in the cases of $P_{s,loss}^{(3)} \leq \alpha = 1.0$, 0.5 and 0.3, respectively. We also show the number of subsets β. On the other hand, Figs. 4.11(d), (e) and (f) show those for the exclusive wavelength allocation in the cases of $P_{s,loss}^{(3)} \leq \alpha = 1.0$, 0.5 and 0.3, respectively. In these figures, we assume that $\theta = 8$. The connection loss probability for single QoS class is also plotted (no QoS in Fig. 4.11).

From Figs. 4.11(a) and (d), we observe that the number of pairs of $P_{s,loss}^{(1)}$ and $P_{s,loss}^{(2)}$ for the shared wavelength allocation is still larger than that for the exclusive one. Therefore, the shared wavelength allocation is effective even in the case of small threshold. Compared with Fig. 4.10(a), the number of pairs

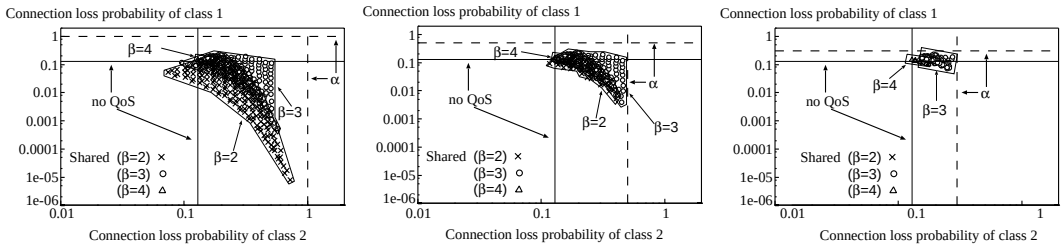

(a) Shared wavelength allocation, $\theta = 8$ and $\alpha = 1.0$.

(b) Shared wavelength allocation, $\theta = 8$ and $\alpha = 0.5$.

(c) Shared wavelength allocation, $\theta = 8$ and $\alpha = 0.3$.

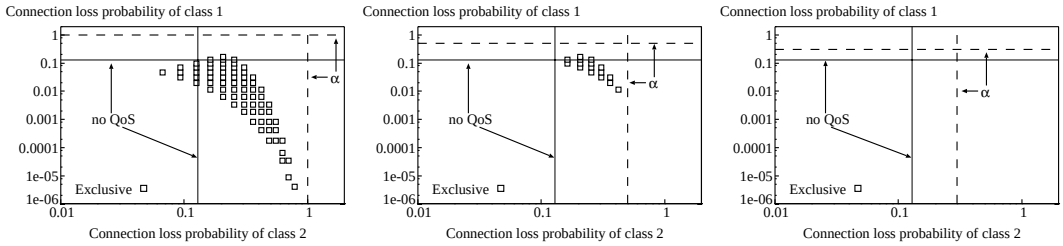

(d) Exclusive wavelength allocation, $\theta = 8$ and $\alpha = 1.0$.

(e) Exclusive wavelength allocation, $\theta = 8$ and $\alpha = 0.5$.

(f) Exclusive wavelength allocation, $\theta = 8$ and $\alpha = 0.3$.

Figure 4.11. Impact of threshold for ring network.

does not change as threshold becomes small. However, as threshold decreases, β becomes large and $P_{s,loss}^{(1)}$ and $P_{s,loss}^{(2)}$ also become large. Note that large β degrades the performance of the shared wavelength allocation. In the case of $\alpha = 0.5$ (see Figs. 4.11(b) and (e)), the shared wavelength allocation can provide more pairs of $P_{s,loss}^{(1)}$ and $P_{s,loss}^{(2)}$ than the exclusive one. With the shared wavelength allocation, $P_{s,loss}^{(1)}$ and $P_{s,loss}^{(2)}$ can be smaller than the connection loss probability provided in no QoS-guaranteed network.

In Figs. 4.11(c) and (f), the shared wavelength allocation can provide some pairs of $P_{s,loss}^{(1)}$ and $P_{s,loss}^{(2)}$ whereas the exclusive one can not provide those. However, the number of pairs of $P_{s,loss}^{(1)}$ and $P_{s,loss}^{(2)}$ is smaller than those in the case of $\theta = 31$ (see Fig. 4.10(c) and Fig. 4.11(c)). This is because small θ results in large β and large $P_{s,loss}^{(3)}$.

From these considerations, the performance of the shared wavelength allocation becomes worse for the uni-directional ring network when the capability of the FWM wavelength conversion is small. However, the shared wavelength allocation

is more effective than the exclusive one for QoS provisioning when low priority class requires a small connection loss probability.

4.5. Conclusions

In this chapter, we proposed the shared wavelength allocation to provide multiple QoS classes in terms of the connection loss probability. We also considered how the method is applied under the limited-range wavelength conversion. For the performance evaluation of the proposed method for a single link, we modeled it as a two-stage queueing system and calculated the connection loss probability of each class with the EQRM. Then we also evaluated the performance of the method for a uni-directional ring network by simulation.

From numerical examples, we found that the shared wavelength allocation is effective for QoS provisioning when the wavelength conversion capability is large. Moreover, we observed that a small number of shared wavelengths makes the connection loss probability less variable despite the increase of the arrival rate of the other classes. As the wavelength conversion capability becomes small, however, the performance of the proposed method becomes worse. Nevertheless, the shared wavelength allocation is more effective for QoS provisioning than the exclusive one when the low priority class requires a small connection loss probability.

Chapter 5

Timer-Based Burst Assembly with Slotted Scheduling

5.1. Introduction

In OBS networks, multiple IP packets are assembled into a burst with variable length at an ingress edge node and is transmitted to its egress one. As shown in the subsection 1.4, a burst is pure payload and has the associated control packet which contains control information such as burst length and routing information [21, 67]. In the Just-Enough-Time (JET) signaling protocol, a source node sends a control packet and then sends the corresponding burst after some offset time (see Fig. 1.6).

As for the performance issue of the JET signaling protocol in the OBS network, several studies have appeared in the literature. In those studies, the Erlang loss system, i.e., the $M/M/c/c$ queueing model, plays an important role for the analysis of the burst loss probability. For example, the burst loss probability for the OBS node without FDLs was analyzed using the $M/M/c/c$ in [13], [58], [61], and [71]. In [68], a probabilistic preemption scheme for service differentiation in the OBS networks was analyzed with a multi-dimensional Markov chain. As for the case where the OBS node has FDLs, an $M/M/c/K$ queueing model is utilized for the analysis of the burst loss probability [14, 34, 71].

[22] discussed the influence of self-similar traffic on assembled burst traffic in OBS core nodes and showed that a Poisson process can be assumed for the

burst arrival process in the time-scale of burst blocking. It is well known that the burst size distribution significantly depends on the burst assembly technique. For example, the burst size distribution approaches to deterministic when the burst assembly is timer-based [22, 72]. [39] analyzed the blocking time distribution for bursts and investigated the effect of three burst-size distributions; the Pareto, Gaussian and exponential ones. However, to the best of our knowledge, the performance analysis in which both the burst assembly technique and burst transmission scheduling are taken into consideration has not been studied yet.

In this chapter, we analyze the performance of the timer-based burst assembly at an edge OBS node without FDLs. A burst is assembled in a round-robin manner, and with the JET signaling protocol, assembled bursts are transmitted into the OBS network at multiples of some fixed interval. In [56], we modeled the edge node as a loss model with deterministic and Poisson arrivals, assuming that assembled bursts are transmitted at fixed intervals from scheduler. In this chapter, we extend the model to the one with geometric and Poisson arrivals, and explicitly derive the burst loss probability, burst throughput, and data throughput. We also investigate those performance measures for uni-directional ring and mesh-torus networks by simulation, and discuss the effectiveness of our analysis in comparison with the Erlang loss model and simulation.

The rest of the chapter is organized as follows. Section 5.2 presents the timer-based burst assembly and burst transmission scheduling, and in Section 5.3, we describe our analytical model for an edge node. In Section 5.4, we present the performance analysis of the model in detail and numerical examples are shown in Section 5.5. Finally, conclusions are presented in Section 5.6.

5.2. Proposed Method

The OBS network considered in the chapter consists of edge and core nodes, as shown in Fig. 5.1. An ingress edge node consists of a burstifier, a scheduler, and a burst switch (see Fig. 5.2). The burstifier has L_{buf} buffers, and IP packets arriving from its access network are stored in the buffers corresponding to their destination edge nodes.

In our scenario, bursts are assembled with multiple IP packets stored in each

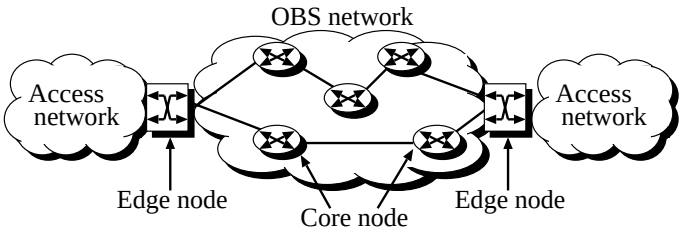

Figure 5.1. OBS network.

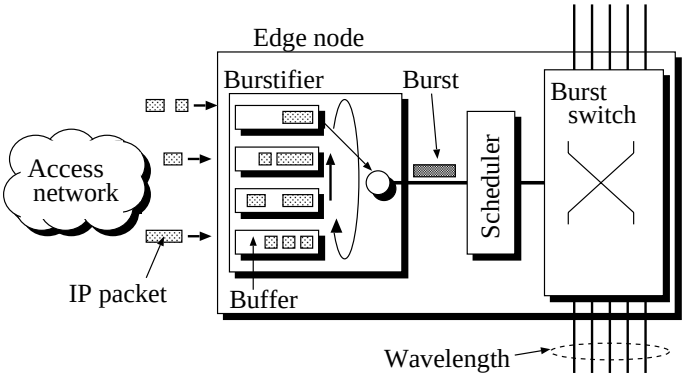

Figure 5.2. Round-robin burst assembly.

buffer, and each burst assembly is processed in round-robin fashion. The burst assembly processing time at each buffer is constant and equal to T. We define the cycle time of a round-robin process as the total processing time at the L_{buf} buffers and thus it is given by $L_{buf}T$. Therefore, in each buffer, a burst is assembled with IP packets stored during the cycle time $L_{buf}T$. Let $D_{\min}$ denote the minimum burst size. If the amount of IP packets just before the assembly is smaller than $D_{\min}$, padding is performed such that the resulting burst size is equal to $D_{\min}$.

The scheduler sends the associated control packet to the destination edge node and then transmits the burst into the OBS network after some offset time. The scheduler sends control packets so that bursts depart from the scheduler at multiples of T as shown in Fig. 5.3. In this figure, we assume that L_{buf} is equal to 4.

Let B_i $(i = 1, \cdots, L_{buf})$ denote the burst assembled in the ith buffer and C_i the control packet associated with B_i. We define Δ_i as the offset time for B_i. Let τ_i $(i = 1, \cdots, L_{buf} - 1)$ and $\tau_{L_{buf}}$ denote the transmission intervals between

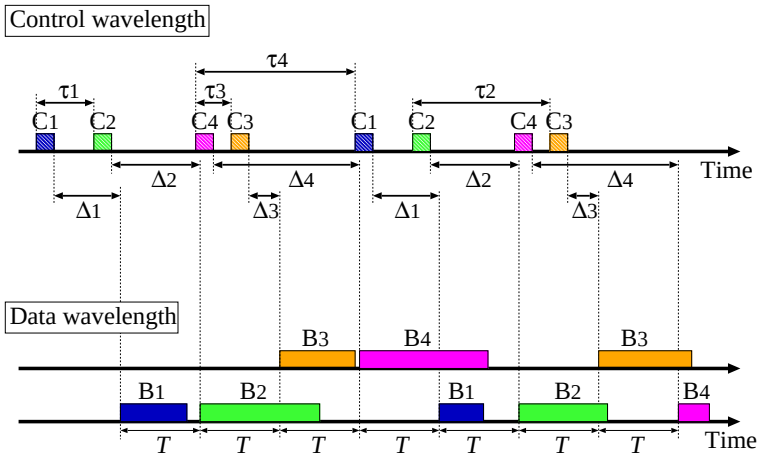

Figure 5.3. Slotted transmission scheduling.

C_i and C_{i+1}, and between $C_{L_{buf}}$ and C_1, respectively.

When Δ_i and Δ_{i+1} $(i = 1, \cdots, L_{buf} - 1)$ satisfy

$$T + \Delta_i \geq \Delta_{i+1}, \tag{5.1}$$

C_i is transmitted before C_{i+1}, and τ_i is set to $T + \Delta_i - \Delta_{i+1}$. On the other hand, when Δ_i and Δ_{i+1} $(i = 1, \cdots, L_{buf} - 1)$ satisfy

$$T + \Delta_i < \Delta_{i+1}, \tag{5.2}$$

C_{i+1} is transmitted before C_i, and τ_i is set to $\Delta_{i+1} - T - \Delta_i$. In terms of $C_{L_{buf}}$ and C_1, i and $i + 1$ in the above are replaced by L_{buf} and 1, respectively, and $\tau_{L_{buf}}$ is determined in the same way.

Note that the order of control-packet transmissions are not always in sequence and that the transmission interval between consecutive control packets depends on the offset times of the corresponding bursts. However, the bursts are transmitted in sequence over the cycle time and each burst transmission starts at a multiple of T.

The assembled bursts are forwarded to the scheduler and then sent to the switch. The timer axis in the scheduler is segmented into a sequence of slots with size T, and it is assumed that the burst forwarding from the scheduler to the switch starts at the slot boundary if there exists at least one burst in the scheduler.

In the burst switch, wavelengths are used not only by bursts from the scheduler but also by those from other OBS nodes. When a control packet arrives at the OBS node and there are no available output wavelengths, the control packet fails in reserving a wavelength and the corresponding burst is lost.

5.3. Queueing Model

We focus on an ingress edge node for the performance analysis of the timer-based burst assembly. In the burstifier of the edge node, there are L_{buf} buffers and IP packets coming from the access network are stored in the buffers. (see Fig. 5.4.)

We assume that IP packets arrive at the edge node from the access network according to a Poisson process with rate λ_{packet} and that the destination edge nodes of the IP packets are equally likely. Because each IP packet is stored in the buffer corresponding to its destination node, IP packets arrive at each buffer according to a Poisson process with rate λ_{packet}/L_{buf}. Moreover, we assume that the mean length of an arriving IP packet is δ_{packet} bits. When the transmission speed of a wavelength is E bps, an IP packet is transmitted with the mean transmission time $1/\mu_{packet} = \delta_{packet}/E$. The processing time of a burst assembly at each buffer is a fixed time equal to T. We assume that the buffer with no IP packet is served with the processing time T. Therefore, a burst is assembled with multiple IP packets which are stored during the cycle time $L_{buf}T$. Hence the mean transmission time of a burst at the switch is given by $\lambda_{packet}T/\mu_{packet} = \lambda_{packet}\delta_{packet}T/E$. We assume that the transmission time of a burst is exponentially distributed with the mean $\lambda_{packet}\delta_{packet}T/E$ [1] .

The assembled bursts are forwarded to the scheduler and then sent to the switch. The timer axis in the scheduler is segmented into a sequence of slots with size T, and it is assumed that the burst forwarding from the scheduler to the switch starts at the slot boundary if there exists at least one burst in the scheduler. Because the packet arrival process at each buffer is Poisson with

[1] [72] reported that with the assumption of Poisson arrivals for IP packets, the distribution of burst length approaches to a deterministic distribution as the timeout value becomes large. In general, however, a multiserver queueing system whose service distribution is general is not analyzable expect for the Erlang loss system. For analytical simplicity, we assume the exponential distribution for the burst-transmission time.

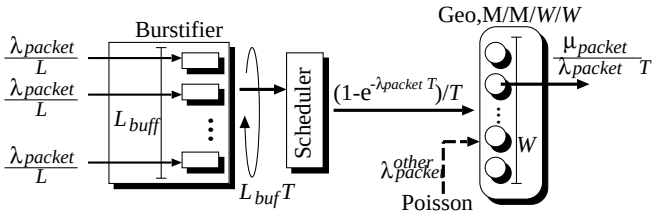

Figure 5.4. Analytical model.

parameter λ_{packet}/L_{buf} and the cycle time is $L_{buf}T$, the probability that there exists a burst in the scheduler at the slot boundary is given by $1 - e^{-\lambda_{packet}T}$.

Note that the burst inter-departure time at the scheduler is geometrically distributed with a mean of $1/(1 - e^{-\lambda_{packet}T})$ slots. That is, denoting A as the burst inter-departure time, we have

$$\Pr\{A = kT\} = (1 - e^{-\lambda_{packet}T})e^{-(k-1)\lambda_{packet}T}, \quad k \geq 1. \tag{5.3}$$

There are W output wavelengths in the switch and two types of bursts are transmitted with the wavelengths; the bursts from the scheduler and those from the other edge nodes. We assume that the OBS network has many edge nodes and that each node's scheduler is not synchronized with other schedulers. If a large number of the burst arrival processes are independent and each burst arrival process contributes a small fraction to the load, the compound burst arrival process can be approximated by a Poisson process [30]. Following [30], we approximate the compound burst arrival process from the other nodes by a Poisson process with rate $\lambda_{packet,o}$.

5.4. Performance Analysis

From the assumptions in Section 5.3, we have a Geo, $M/M/W/W$ queueing model as shown in Fig. 5.4. In this section, we explicitly derive the burst loss probability, burst throughput, and data throughput for the Geo, $M/M/W/W$ system. In the following, we assume that the system is in equilibrium.

Let $N_b(t)$ denote the number of bursts being transmitted in the system at time t. Without loss of generality, we assume that the event of a burst arrival from the scheduler occurs at multiples of T. Fig. 5.5 shows the sample path of

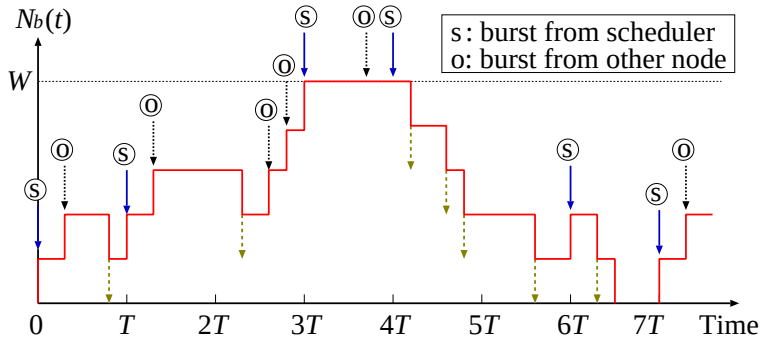

Figure 5.5. Sample path for Geo,$M/M/W/W$ queueing model.

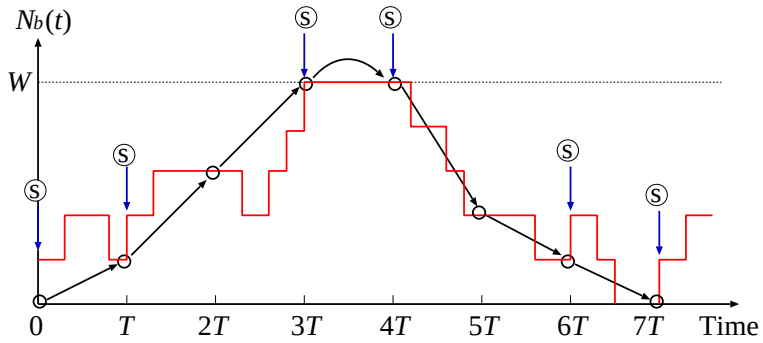

Figure 5.6. Geometric arrivals in the sample path.

$N_b(t)$. In this figure, burst arrivals from the scheduler occur at multiples of T, while those from the other nodes occur at arbitrary points.

First, we focus on the system state just before the slot boundary (white circles in Fig. 5.6). We define the number of bursts in the system just before the nth slot as $N^-_{b,n} = N_b(nT^-)$ $(n = 0, 1, \cdots)$. With the assumptions of Poisson arrivals from the other nodes and the exponential transmission time, the process $\left\{N^-_{b,n} : n = 0, 1, \cdots\right\}$ is a discrete-time Markov chain. We define the steady state probability for the Markov chain as

$$q_k = \lim_{n\to\infty} P_r\{N^-_{b,n} = k\}, \;\; 0 \le k \le W. \tag{5.4}$$

To derive the transition probability of q_k, we consider the state transition between $N^-_{b,n}$ and $N^-_{b,n+1}$. Note that the state transition between $N^-_{b,n}$ and $N^-_{b,n+1}$ consists of two parts: one is the event of a burst arrival from the scheduler at nT

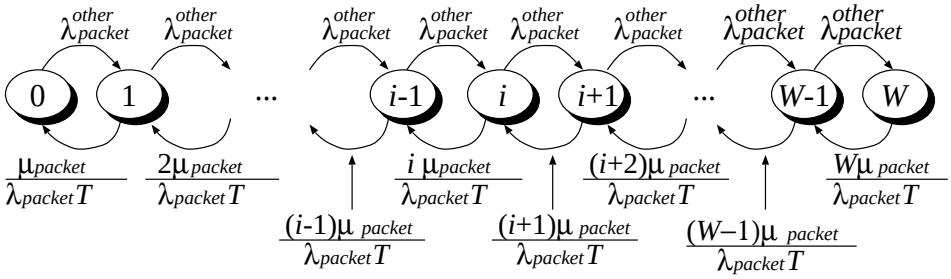

Figure 5.7. State transition diagram.

(the nth slot boundary), and the other is the transition from the state just after the nth slot boundary to the state just before the $n+1$st slot boundary. Note that the latter state transition is the same as an $M/M/W/W$ queueing model in which the arrival process is Poisson with rate λ_{packet}^{other} and the service time is exponentially distributed with the mean $\lambda_{packet}T/\mu_{packet}$. The state transition diagram for the $M/M/W/W$ queueing model is illustrated in Fig. 5.7. Let $\boldsymbol{Q}$ denote the infinitesimal generator of the $M/M/W/W$. $\boldsymbol{Q}$ is a $(W+1)\times(W+1)$ matrix whose (i,j)th element is given by

$$[\boldsymbol{Q}]_{ij} = \begin{cases} \lambda_{packet}^{other}, & 1 \le i \le W, \;\; j = i+1, \\ -\left\{\lambda_{packet}^{other} + \frac{(i-1)\mu_{packet}}{\lambda_{packet}T}\right\}, & 1 \le i \le W+1, \;\; j = i, \\ \frac{(i-1)\mu_{packet}}{\lambda_{packet}T}, & 2 \le i \le W+1, \;\; j = i-1, \\ 0, & \text{otherwise.} \end{cases} \tag{5.5}$$

For s and t $(0 \le s < t < T)$, we define $\boldsymbol{H}(s,t)$ as the $M/M/W/W$ state-transition probability matrix from the state at time s to the state at time t. $\boldsymbol{H}(s,t)$ satisfies the forward Chapman-Kolmogorov equation

$$\frac{\partial \boldsymbol{H}(s,t)}{\partial t} = \boldsymbol{H}(s,t)\boldsymbol{Q}. \tag{5.6}$$

In the following, $\boldsymbol{H}(0,t) \equiv \boldsymbol{H}(t)$ and $\boldsymbol{I}$ is the identity matrix. With the initial condition $\boldsymbol{H}(0) = \boldsymbol{I}$ and (5.6), $\boldsymbol{H}(t)$ is given by $\boldsymbol{H}(t) = e^{\boldsymbol{Q}t}$.

Note that a burst arrival from the scheduler occurs with probability $1 - e^{-\lambda_{packet}T}$. Therefore, the system state just after the nth slot boundary is $\min(N_{b,n}^{-}+1, W)$ with probability $1-e^{-\lambda_{packet}T}$, or $N_{b,n}^{-}$ with probability $e^{-\lambda_{packet}T}$. Since the slot size is T, the transition probabilities for q_k are then given by

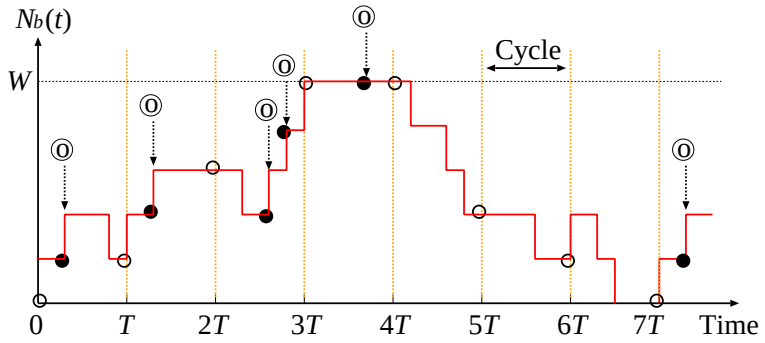

Figure 5.8. Poisson arrivals in the sample path.

$$
\begin{aligned}
U_{ij} &\equiv P_r\{N^-_{b,n+1} = j | N^-_{b,n} = i\} \\
&= \begin{cases} (1 - e^{-\lambda_{packet} T})[\boldsymbol{H}(T)]_{i+1,j} + e^{-\lambda_{packet} T}[\boldsymbol{H}(T)]_{i,j}, \\ \qquad\qquad 0 \le i \le W-1, \;\; 0 \le j \le W, \\ [\boldsymbol{H}(T)]_{W,j}, \\ \qquad\qquad i = W, \;\; 0 \le j \le W. \end{cases}
\end{aligned} \tag{5.7}
$$

With $\boldsymbol{U} = [U_{ij}]$, $\boldsymbol{q} = (q_0, \cdots, q_W)$, and $\boldsymbol{e} = (1, \cdots, 1)^T$, $\boldsymbol{q}$ is determined from the equilibrium equations $\boldsymbol{q} = \boldsymbol{qU}$ and the normalizing condition $\boldsymbol{qe} = 1$. Given that a burst arrival from the scheduler occurs, the burst is lost with probability q_W.

Next, we consider the steady-state probability at an arbitrary point defined as $p_k = \lim_{t\to\infty} P_r\{N_b(t) = k\}$. Note that p_k is the same as the probability that the burst arrivals from the other nodes (Poisson arrivals, black circles in Fig. 5.8) find k bursts in the system (Poisson arrivals see time averages, [65]). We define the nth cycle as the time interval $[nT, (n+1)T)$. From the assumptions in our analytical model, it is clear that the process $N_b(t)$ regenerates itself at nT $(n = 0, 1, \cdots)$. With the renewal-reward theorem [65, p. 60], we have for $k = 0, 1, 2, \cdots$,

$$
p_k = \lim_{t\to\infty} \frac{1}{t} \int_0^t \mathbf{1}_{\{N_b(t)=k\}} dt = \frac{1}{T} \int_0^{T^-} E\left[\mathbf{1}_{\{N_b(t)=k\}}\right] dt, \tag{5.8}
$$

where $\mathbf{1}_{\{X\}}$ is the indicator function of event X. (5.8) implies that the steady state probability at an arbitrary time is equal to the time average of the number of bursts in the system over one cycle. Therefore, we consider the time average of $N_b(t)$ over one cycle.

Let $\{r_k : k = 0, \cdots, W\}$ denote the state probability at the beginning of a cycle. With the steady state probability q_k, r_k is given by the following equations.

$$r_k = \begin{cases} e^{-\lambda_{packet}T} q_0, & k = 0, \\ (1 - e^{-\lambda_{packet}T}) q_{k-1} + e^{-\lambda_{packet}T} q_k, & 0 < k < W, \\ (1 - e^{-\lambda_{packet}T}) q_{W-1} + q_W, & k = W. \end{cases} \tag{5.9}$$

Let $\boldsymbol{p} = (p_0, \cdots, p_W)$ and $\boldsymbol{r} = (r_0, \cdots, r_W)$. For $0 \leq t < T$, we have

$$E\left[\mathbf{1}_{\{N_b(t)=k\}}\right] = \left[\boldsymbol{r} e^{\boldsymbol{Q}t}\right]_k, \tag{5.10}$$

where $[\boldsymbol{x}]_k$ denote the kth element of vector $\boldsymbol{x}$. Substituting (5.10) into (5.8), we obtain

$$\boldsymbol{p} = \frac{1}{T}\boldsymbol{r}\int_0^{T^-} e^{\boldsymbol{Q}t} dt = \frac{1}{T}\boldsymbol{r}\int_0^{T} e^{\boldsymbol{Q}t} dt = \frac{1}{T}\boldsymbol{r}\sum_{k=0}^{\infty}\frac{\boldsymbol{Q}^k T^{k+1}}{(k+1)!}, \tag{5.11}$$

where we use the continuity of $e^{\boldsymbol{Q}t}$ in the second equality.

In (5.11), $\boldsymbol{Q}$ is the infinitesimal generator of $M/M/W/W$ and hence $\boldsymbol{Q}$ is singular. Now we consider the matrix $\boldsymbol{e}\boldsymbol{\pi} - \boldsymbol{Q}$ where $\boldsymbol{\pi}$ is the steady-state probability vector of $M/M/W/W$ such that $\boldsymbol{\pi}\boldsymbol{Q} = \mathbf{0}$ and $\boldsymbol{\pi}\boldsymbol{e} = 1$. Here, $\boldsymbol{e}\boldsymbol{\pi} - \boldsymbol{Q}$ is nonsingular [35] and has an inverse matrix. In addition, $\boldsymbol{Q}$ and $\boldsymbol{\pi}$ satisfy the following equation

$$\boldsymbol{Q}(\boldsymbol{e}\boldsymbol{\pi} - \boldsymbol{Q}) = -\boldsymbol{Q}^2. \tag{5.12}$$

Hence, we have

$$\boldsymbol{Q} = \boldsymbol{Q}^2(\boldsymbol{Q} - \boldsymbol{e}\boldsymbol{\pi})^{-1}. \tag{5.13}$$

With (5.11) and (5.13), $\boldsymbol{p}$ is explicitly given by

$$\boldsymbol{p} = \frac{1}{T}\boldsymbol{r}\left\{\boldsymbol{I}T + (e^{\boldsymbol{Q}T} - \boldsymbol{I} - \boldsymbol{Q}T)(\boldsymbol{Q} - \boldsymbol{e}\boldsymbol{\pi})^{-1}\right\}. \tag{5.14}$$

Because Poisson arrivals see time average (PASTA) [65], the loss probability for the bursts from the other nodes is given by p_W.

With q_W and p_W, the burst loss probability $P_{b,loss}$ is given by the following equation.

$$P_{b,loss} = \frac{(1 - e^{-\lambda_{packet}T}) q_W + \lambda_{packet}^{other} T\, p_W}{1 - e^{-\lambda_{packet}T} + \lambda_{packet}^{other} T}. \tag{5.15}$$

The burst throughput defined as the number of transmitted bursts per unit of time, $T_{hr}^{(b)}$, is given by

$$T_{hr}^{(b)} = \frac{(1 - e^{-\lambda_{packet}T})(1 - q_W)}{T} + \lambda_{packet}^{other}(1 - p_W). \tag{5.16}$$

Finally, the data throughput defined as the amount of transmitted data (bits) per unit of time, $T_{hr}^{(d)}$, is derived as

$$T_{hr}^{(d)} = \lambda_{packet}\delta_{packet}\left\{(1 - e^{-\lambda_{packet}T})(1 - q_W) + \lambda_{packet}^{other}T(1 - p_W)\right\}. \tag{5.17}$$

5.5. Numerical Examples

In our numerical examples, we assume that the transmission speed of each output wavelength E is 10 Gbps and that IP packets with the mean size of 1,250 bytes, i.e. $\delta_{packet} = 10,000$ bits, arrive at the edge node from the access network. Thus, the mean transmission speed of an IP packet, $1/\mu_{packet}$, is 1.0 μs and in the following, the unit of time is 1.0 μs. In addition, we set the minimum burst size $D_{\min}$ is equal to 64 kbytes.

5.5.1 An Edge Node in OBS Network

In this subsection, we assume that the number of buffers L_{buf} is equal to 5. The burst loss probability, burst throughput [number of bursts/s], and data throughput [Gbps] are calculated by the analysis in the previous section and by simulation. The assumptions we made for the simulation are the same as the analysis, except that the IP packet size is constant and equal to 1,250 bytes. Note that the probability distribution of the resulting burst size is not an exponential one.

We also compare the analysis with the Erlang loss system which has been extensively used as a reference model for evaluating the loss performance in the literature [71]. For the Erlang loss system, the burst loss probability, burst throughput, and data throughput are given by

$$P_{b,loss}^{(Erlang)} = \frac{\{\lambda_{packet}T(1/T + \lambda_{packet}^{other})/\mu_{packet}\}^W/W!}{\sum_{k=0}^{W}\{\lambda_{packet}T(1/T + \lambda_{packet}^{other})/\mu_{packet}\}^k/k!}, \tag{5.18}$$

$$T_{hr}^{(b)(Erlang)} = (1/T + \lambda_{packet}^{other})\left\{1 - P_{b,loss}^{(Erlang)}\right\}, \tag{5.19}$$

$$T_{hr}^{(d)(Erlang)} = \lambda_{packet}\delta_{packet}T(1/T + \lambda_{packet}^{other})\left\{1 - P_{b,loss}^{(Erlang)}\right\}. \tag{5.20}$$

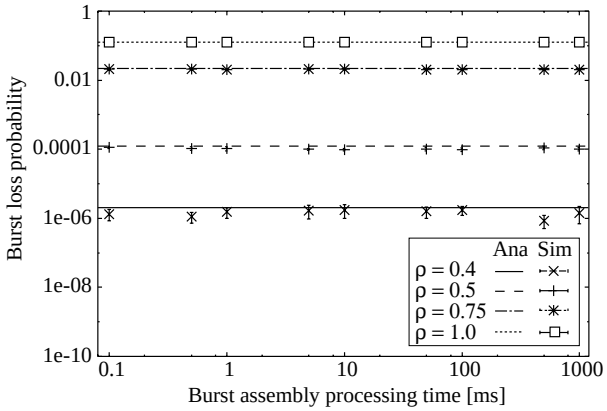

Figure 5.9. Burst loss probability vs. burst assembly processing time.

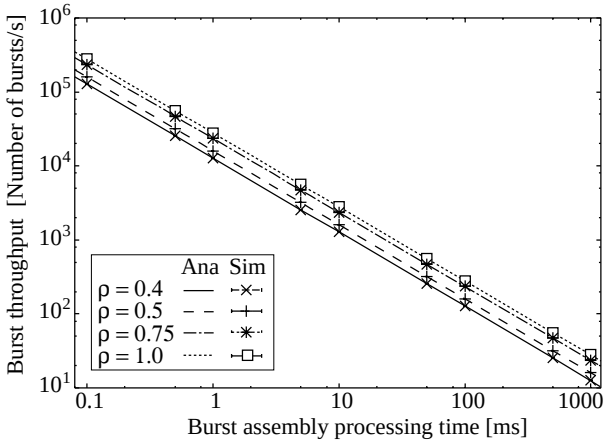

Figure 5.10. Burst throughput vs. burst assembly processing time.

5.5.1.1 Impact of Burst Assembly Processing Time

First, we consider how the burst assembly processing time T affects the burst loss probability, burst throughput, and data throughput. Here, we set $W = 32$ and $\lambda_{packet} = 1.0$. λ_{packet}^{other} is determined so that the system utilization factor $\rho = \lambda_{packet}(1 + \lambda_{packet}^{other} T)/W\mu_{packet}$ is unchanged.

Fig. 5.9 illustrates the loss probability against the burst-assembly processing time with $\rho = 0.4$, 0.5, 0.75, and 1.0, and Figs. 5.10 to 5.11 illustrate the burst and data throughputs, respectively. These results are calculated by our analysis and simulation. From these figures, we observe that the analytical and simulation

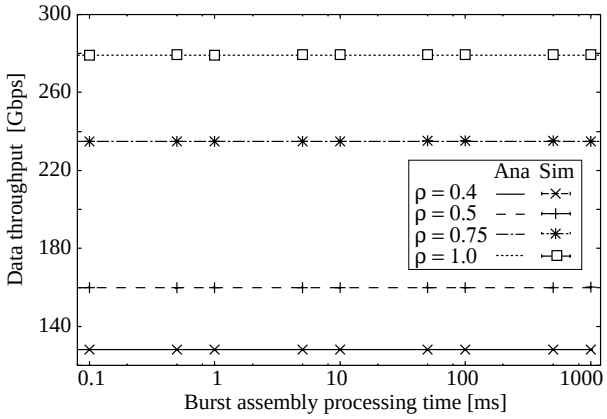

Figure 5.11. Data throughput vs. burst assembly processing time.

results are almost the same in the case of large ρ and that the discrepancy between these two results is small even when $\rho = 0.4$. Table 5.1 shows the results of the Geo,$M/M/W/W$, Erlang, and simulation in the case of small T. The table shows that if T is large and the padding is not used, the result of Geo,$M/M/W/W$ is more close to that of the simulation than the Erlang loss model. These results validate the efficiency of the analysis under the above conditions.

Fig. 5.9 shows that the burst loss probability does not change as the burst assembly processing time becomes large. When the burst assembly processing time is large, large bursts are assembled at the edge node. However, the interval between consecutive burst transmissions also becomes large. Therefore, the burst assembly processing time does not affect the burst loss probability for the timer-based burst assembly. In Fig. 5.9, we also find that the burst loss probability becomes large as the system utilization factor ρ increases.

From Fig. 5.10, we observe that the burst throughput becomes small as the burst assembly processing time increases. This is because the increase of the burst assembly processing time causes a large burst-transmission interval. As a result, the burst-transmission delay becomes large and the number of transmitted bursts per unit of time becomes small. The burst throughput also decreases as the system utilization factor becomes small, however, the impact of the system utilization factor on the burst throughput is smaller than that of the burst assembly processing time. On the other hand, in Fig. 5.11, the data throughput does not change as the burst assembly processing time becomes large.

Table 5.1. Comparison of results of Geo,$M/M/W/W$, Erlang, and simulation in the case of $\rho = 0.5$.

T [ms]	Metrics	Erlang	Geo,$M/M/W/W$	Simulation
0.05	$P_{b,loss}$	1.45e-04	1.22e-04	(3.46±0.12)e-04
	$T_{hr}^{(b)}$	319.95	319.96	319.87±0.14
	$T_{hr}^{(d)}$	159.97	159.98	159.93e±0.07
0.1	$P_{b,loss}$	1.45e-04	1.22e-04	(1.13±0.09)e-04
	$T_{hr}^{(b)}$	159.97	159.98	159.95±0.09
	$T_{hr}^{(d)}$	159.97	159.98	159.95±0.09
0.5	$P_{b,loss}$	1.45e-04	1.22e-04	(1.16±0.08)e-04
	$T_{hr}^{(b)}$	31.99	31.98	31.99±0.03
	$T_{hr}^{(d)}$	159.97	159.98	159.99±0.02

From these observations, the burst loss probability and data throughput are insensitive to the burst assembly processing time while the burst throughput is sensitive to the burst assembly processing time. Note that the decrease of the burst throughput implies the increase of the burst-transmission delay.

5.5.1.2 Impact of Bursts from the Other Nodes

Next, we investigate how the bursts from the other nodes affect the performance of the timer-based burst assembly. Fig. 5.12 shows the relation between the arrival rate of bursts transmitted from the other nodes, λ_{packet}^{other}, and the burst loss probability in the cases of $\lambda_{packet} = 3.0$, 5.0, and 10.0. Figs. 5.13 and 5.14 show the results for the burst and data throughputs, respectively. Here, we set $W = 32$ and $T = 1.0$ ms.

From Fig. 5.12, we observe that the burst loss probability for the timer-based burst assembly increases as the arrival rate of bursts from the other nodes becomes large. This is simply because the system is overloaded. We also observe that the burst loss probability increases as the arrival rate of packets from the access network becomes large. This is due to the large bursts which are assembled with a number of IP packets at the edge node.

Comparing the loss probabilities for our analysis and the Erlang loss system

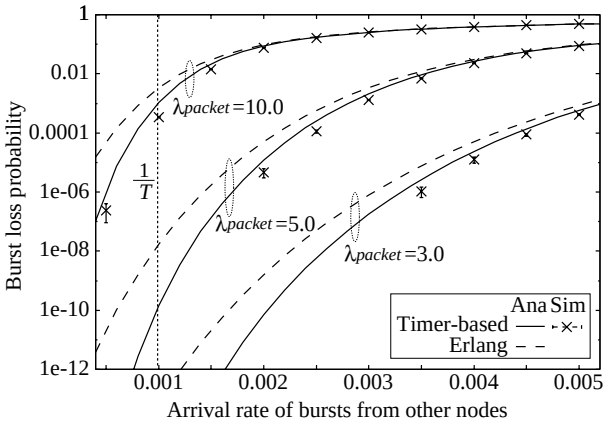

Figure 5.12. Burst loss probability vs. arrival rate of bursts from other nodes.

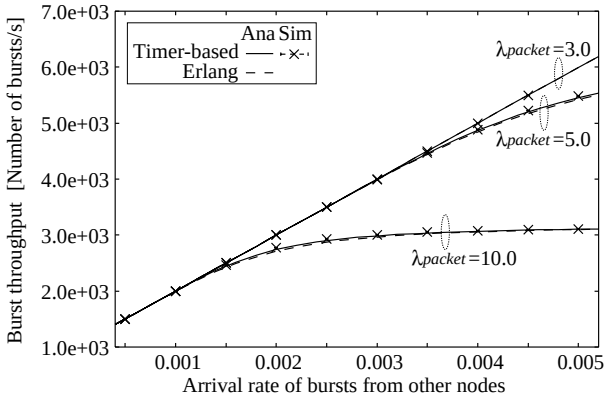

Figure 5.13. Burst throughput vs. arrival rate of bursts from other nodes.

in Fig. 5.12, the burst loss probability for the Erlang loss system is always larger than that for our analysis, while the results for our analysis is remarkably close to the simulation ones even when λ_{packet}^{other} is small. Note that the discrepancy between the Erlang loss system and simulation becomes large when λ_{packet}^{other} decreases. This implies that the accuracy of the Erlang loss system greatly depends on the arrival rate of the bursts from the other node and that our analytical model succeeds in predicting the burst loss probability in the case of small λ_{packet}^{other}, where the Erlang loss model fails in providing the accurate value.

From Figs. 5.13 and 5.14, we observe that the burst and data throughputs become large and converge to constant values as the arrival rate of bursts from

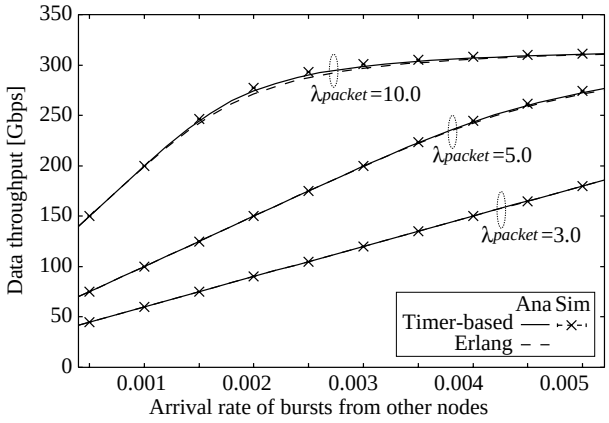

Figure 5.14. Data throughput vs. arrival rate of bursts from other nodes.

the other nodes increases. We also find that the burst throughput becomes small as the arrival rate of IP packets from the access network, λ_{packet}, increases. This is because the burst size becomes large and this results in the increase of the burst loss probability. However, the number of packets assembled into a burst also increases and this causes large data throughput.

5.5.1.3 Impact of the Number of Wavelengths

Fig. 5.15 shows how the number of wavelengths affects the loss probability for the timer-based burst assembly. In this figure, we set $\lambda_{packet} = 10.0$ and $T = 1.0$ ms. The loss probabilities are calculated by the analysis and simulation in the cases of $\lambda_{packet}^{other} = 0.001$, 0.002, 0.003 and 0.004. From this figure, we find again that the results of our analysis are close to the simulation results, while the results for the Erlang loss system are always larger than those for the simulation. On the other hand, the discrepancy among the analysis, Erlang loss model, and simulation becomes small as W becomes large. Therefore, the Erlang loss model is useful for large W, however, our analysis is more useful than the Erlang loss model when the number of wavelengths is not large.

5.5.2 Ring Network

In this subsection, we investigate the effectiveness of our analysis for a unidirectional ring network. In the ring network with $L_{buf} + 1$ nodes, IP packets

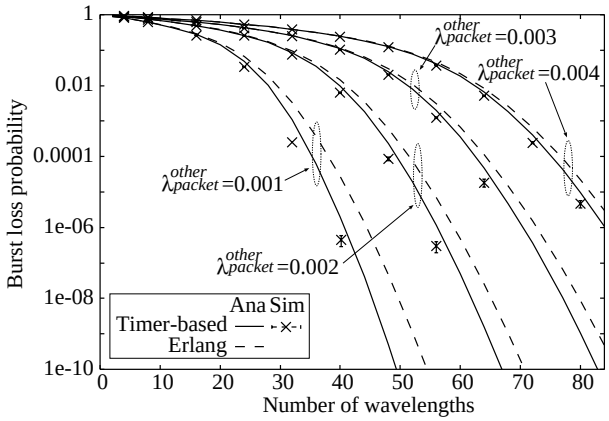

Figure 5.15. Burst loss probability vs. number of wavelengths.

arrive at each node from its access network according to a Poisson process with rate λ_{packet} and the pair of source and destination nodes is uniformly distributed, i.e., any pair is selected with the same probability. In addition, we assume that the processing time of a control packet at each node is 1.0 ms and that the distance between each two nodes is 320 km. Here, the number of wavelengths is W and the burst assembly time T is equal to 1.0 [ms].

Table 5.2 illustrates the burst loss probability for our analysis, Erlang loss model, and simulation at an arbitrary link. Note that in the Geo,$M/M/W/W$ and Erlang loss models, we obtained the value of λ_{packet}^{other} from the simulation results in advance.

From this table, we can see the discrepancy between the analysis and simulation results. This is because the burst arrival process from the other nodes is not a Poisson one in the simulation and the probability distribution of the resulting burst size is not an exponential one. However, the analysis result gives the upper bound of the simulation one and both results show the same tendency. As the numbers of nodes and wavelengths become large, our analysis result becomes close to the simulation one. Moreover in this table, we observe that our analysis can give the better estimate for the burst loss probability than the Erlang loss model. Hence, in the uni-directional ring network, our analytical model is useful for capturing the burst loss behavior in a qualitative sense.

Table 5.2. Comparison of results of Geo,$M/M/W/W$, Erlang, and simulation in uni-directional ring network.

$(L_{buf}+1, W)$	λ_{packet}	Erlang	Geo,$M/M/W/W$	Simulation
(5,8)	3.0	1.77e-01	1.52e-01	(6.24±0.96)e-02
	4.0	2.60e-01	2.36e-01	(1.58±0.02)e-01
(5,16)	7.0	1.72e-01	1.53e-01	(8.69±0.68)e-02
	8.0	2.15e-01	1.97e-01	(1.38±0.02)e-01
(10,16)	3.5	1.34e-01	1.25e-01	(6.54±0.54)e-02
	4.5	1.88e-01	1.78e-01	(1.22±0.05)e-01
(20,32)	4.25	1.07e-01	1.03e-01	(5.24±0.19)e-02
	8.0	2.00e-01	1.95e-01	(1.60±0.01)e-01

5.5.3 Mesh-Torus Network

Finally, we investigate the effectiveness of our analysis for a mesh-torus network with 25 nodes (see Fig. 5.16). We use the same parameters as those in the ring network. In this network, bursts are transmitted from source to destination nodes according to the deterministic routing algorithm as follows [29]. We define G_x and G_y as the shortest distance in the number of links from the destination node along the x and y axes, respectively. When $G_x \geq G_y$ or $G_x = G_y < 2$, we choose a link on the x axis as the next one to get closer to the destination node. When $G_x < G_y$ or $G_x = G_y = 2$, a link on the y axis is chosen. We repeat this procedure until G_x and G_y become zero. Here, each source node has 24 destination nodes and four output links. Note that according to the routing algorithm, each output link of the source node supports burst transmission to six destination nodes. Each node has four pairs of burstifier and scheduler, and the cycle time of round-robin is 6.0 [ms] ($L_{buf} = 6$ and T=1.0 [ms] in our analysis). We preobtained the value of λ_{packet}^{other} for the Geo,$M/M/W/W$ and Erlang loss models from the simulation results. In the following, we focus on any link in this network.

Table 5.3 illustrates the burst loss probability for the analysis, Erlang loss model, and simulation in the cases of $W = 16$ and 32. From this table, we observe the discrepancy between the analysis and simulation results, however, the

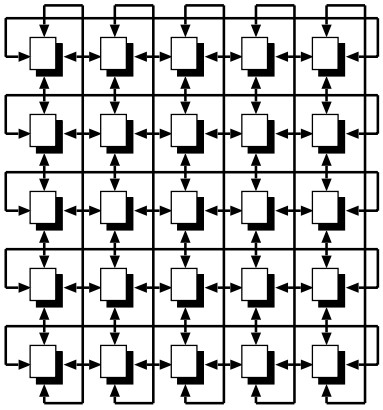

Figure 5.16. Mesh-torus network with 25 nodes.

Table 5.3. Comparison of results of Geo,$M/M/W/W$, Erlang, and simulation in mesh-torus network.

W	λ_{packet}	Erlang	Geo,$M/M/W/W$	Simulation
16	12.0	1.16e-01	1.08e-01	(7.36±0.99)e-02
	15.0	1.60e-01	1.51e-01	(1.47±0.13)e-01
32	26.0	7.99e-02	7.34e-01	(5.92±0.68)e-02
	32.0	1.47e-01	1.40e-01	(1.25±0.11)e-01

discrepancy is smaller than that in the ring network. This is because each node in the mesh-torus network has more input and output links than that in the ring network, and the resulting burst arrival process is more close to a Poisson process. Moreover, our analysis gives the good estimate for the burst loss probability when the number of wavelengths is large and traffic load is heavy. From the above observation, our analytical model is useful for characterizing the burst loss behavior in the mesh-torus network.

5.6. Conclusions

In this chapter, we considered the timer-based burst assembly with the slotted scheduling for the OBS networks. To evaluate its performance at an OBS edge

node, we considered the Geo,$M/M/W/W$ model and explicitly derived the burst loss probability, burst throughput, and data throughput. Numerical examples showed that our analysis is efficient to evaluate the performance of the timer-based burst assembly in comparison with the Erlang loss system. In particular, our analysis is useful for the OBS network where a number of wavelengths are utilized and the arrival rate of bursts transmitted from other nodes is relatively small. Moreover, we observed that our analysis is also effective for large-scale unidirectional ring and mesh-torus networks with a large number of wavelengths.

Chapter 6

Conclusions

The main theme of this dissertation is how the WDM networks should be constructed for the next generation Internet. In order to transmit the data in the WDM networks efficiently, three network architectures such as wavelength routing, OBS, and OPS have been studied and developed. However, the next generation Internet requires ultra high speed and more reliable transmission in order to support future diverse applications. The OPS will provide the efficient utilization of wavelength and the QoS guarantee, but it is difficult to implement the OPS in the near future due to the fact that optical components are still not commercially available. Therefore, further extension and development of the wavelength routing and OBS are required.

In this dissertation, we considered the new network architectures for the wavelength routing and OBS networks, and evaluated their performances with queueing theory and simulation. With the analysis and simulation results, we investigated how the physical constraints affect the proposed methods and discussed the deployment capability of the architectures.

In Chapter 2, we considered the dynamic lightpath configuration method where a lightpath supports multiple LSPs, and analyzed the loss probability of packet flows and wavelength utilization factor under the light and heavy traffic conditions for the symmetric WDM ring networks. In the light traffic case, the numerical results showed that our approximation analysis gives good estimates for the packet-flow loss probability and wavelength utilization factor. With multiple LSPs in a lightpath, the dynamic lightpath configuration method becomes

effective when the lightpath establishment/release time becomes small. As for the design of the threshold in the method, the optimal thresholds which give the smallest loss probability and the largest lightpath utilization factor can be obtained from the light traffic analysis. We also observed in the light traffic case that a small extra holding time is effective when the lightpath establishment/release time is in the order of 10 ms. In the heavy traffic case, we showed that our approximation analysis is useful to estimate the packet-flow loss probability. On the other hand, the resulting estimates of the wavelength utilization factor are not accurate. Further improvement of the approximation is needed for the well estimation of the wavelength utilization factor.

In Chapter 3, we proposed the QoS-guaranteed wavelength allocation method which provides multiple QoS classes for the connection loss probability. We considered three combinations of wavelength selection rules and compared those performances for a single link and a uni-directional ring network by continuous-time Markov chain and simulation. The numerical results showed that our analysis is useful for both the optimal allocation of wavelengths and the best selection of Method. In numerical examples, we observed that each method among the three methods is effective for each different class, i.e., Methods 1, 2, and 3 are effective for the classes 1, 2, and 3. Moreover, under the wavelength conversion constraint, we investigated the robustness of each method and observed that the robustness of Methods 2 and 3 are attractive for QoS provisioning.

In Chapter 4, we proposed the shared wavelength allocation to provide multiple QoS classes in terms of the connection loss probability. We also considered how the method is applied under the limited-range wavelength conversion. For the performance evaluation of the proposed method for a single link, we modeled it as a two-stage queueing system and calculated the connection loss probability of each class with the EQRM. Then we also evaluated the performance of the method for a uni-directional ring network by simulation. From the numerical examples, we found that the shared wavelength allocation is effective for QoS provisioning when the wavelength conversion capability is large. Moreover, we observed that a small number of shared wavelengths makes the connection loss probability less variable despite the increase of arrival rate of the other classes. As the wavelength conversion capability becomes small, however, the performance

of the proposed method becomes worse. Nevertheless, the shared wavelength allocation is more effective for QoS provisioning than the exclusive one when the low priority class requires a small connection loss probability.

In Chapter 5, we considered the timer-based burst assembly with slotted scheduling for OBS networks. To evaluate its performance at an OBS edge node, we considered the Geo,$M/M/W/W$ model and explicitly derived the burst loss probability, burst throughput, and data throughput. The numerical examples showed that our analysis is efficient to evaluate the performance of the timer-based burst assembly in comparison with the Erlang loss system. In particular, our analysis is useful for the OBS network where a number of wavelengths are utilized and the arrival rate of bursts transmitted from other nodes is relatively small. Moreover, we observed that our analysis is also effective for large-scale unidirectional ring and mesh-torus networks with a large number of wavelengths.

Currently, the WDM networks are deploying world-wide and the research for the realization of all-optical Internet has become more active than ever before. The author expects that the proposed methods and their performance analysis will be significantly utilized in order to construct the WDM networks for the next generation Internet.

References

[1] D. O. Awduche, Y. Rekhter, "Multiprotocol Lambda Switching: Combining MPLS Traffic Engineering Control with Optical Crossconnects," *IEEE Commun. Mag.*, vol. 39, no. 3, pp. 111–116, Mar. 2001.

[2] I. Baldine, G. N. Rouskas, H. G. Perros, and D. Stevenson, "JumpStart: A Just–In–Time Signaling Architecture for WDM Burst-Switched Networks," *IEEE Commun. Mag.*, vol. 40, no. 2, pp. 82–89, Feb. 2002.

[3] R. A. Barry and P. A. Humblet, "Models of Blocking Probability in All-Optical Networks with and without Wavelength Changers," *IEEE J. Select. Areas Commun.*, vol. 14, no. 5, pp. 858–867, June 1996.

[4] U. Black, *Optical Networks, Third Generation Transport Systems*. Indiana: Prentice Hall PTR, 2002.

[5] P. Bonenfant, A. R. Moral, "Optical Data Networking", *IEEE Commun. Mag.*, vol. 38, no. 3, pp. 63–70, Mar. 2000.

[6] X. Cao, J. Li, Y. Chen, and C. Qiao, "Assembling TCP/IP Packets in Optical Burst Switched Networks," in *Proc. IEEE Globecom'02*, Nov. 2002, pp. 2808–2812.

[7] T. Chikama, H. Onaka, S. Kuroyanagi, "Photonic Networking Using Optical Add Drop Multiplexers and Optical Cross-Connects," *FUJITSU Sci. Tech. J.*, vol. 35, no. 1, pp. 46–55, July 1999 .

[8] I. Chlamtac, A. Ganz, and G. Karmi, "Purely Optical Networks for Terabit Communication," in *Proc. IEEE INFOCOM'89*, Apr. 1989, pp. 887–896.

[9] I. Chlamtac, V. Elek, A. Fumagalli, and C. Szabó, "Scalable WDM Access Network Architecture Based on Photonic Slot Routing," *IEEE/ACM Trans. Networking*, vol. 7, no. 1, pp. 1–9, Feb. 1999.

[10] A. Detti and M. Listanti, "Impact of Segments Aggregation on TCP Reno Flows in Optical Burst Switching Networks," in *Proc. IEEE INFOCOM'02*, June 2002.

[11] S. S. Dixit, *IP over WDM, Building the Next Generation Optical Internet*. New Jersey: Wiley, 2002.

[12] K. Dolzer, "Assured Horizon – A New Combined Framework for Burst Assembly and Reservation in Optical Burst Switched Networks," in *Proc. NOC'02*, June 2002.

[13] K. Dolzer and C. Gauger, "On Burst Assembly in Optical Burst Switching Networks–A Performance Evaluation of Just-Enough-Time," in *Proc. 17th Int. Teletraffic Congress*, Sept. 2001, pp. 149–160.

[14] P. Fan, C. Feng, Y. Wang, and N. Ge, "Investigation of the Time-Offset Based QoS Support with Optical Burst Switching in WDM Networks," in *Proc. IEEE ICC'02*, May 2002, pp. 2682–2686.

[15] O. Gerstel, G. Sasaki, S. Kutten, and R. Ramaswami, "Worst-case analysis of dynamic wavelength allocation in optical networks," *IEEE/ACM Trans. Networking*, vol. 7, no. 6, pp. 833–846, Dec. 1999.

[16] A. Ge and F. Callegati, "On Optical Burst Switching and Self-Similar Traffic," *IEEE Commun. Lett.*, vol. 4, no. 3, pp. 98–100, Mar. 2000.

[17] O. Gerstel, R. Ramaswami, and G. H. Sasaki, "Cost-Effective Traffic Grooming in WDM Rings," *IEEE/ACM Trans. Networking*, vol. 8, no. 5, pp. 618–630, Oct. 2000.

[18] O. Gerstel, G. H. Sasaki, S. Kutten, and R. Ramaswami, "Worst-Case Analysis of Dynamic Wavelength Allocation in Optical Networks," *IEEE/ACM Trans. Networking*, vol. 7, no. 6, pp. 833–846, Dec. 1999.

[19] N. Ghani, S. Dixit, and T.S. Wang, "On IP-over-WDM Integration," *IEEE Commun. Mag.*, vol. 38, no. 3, pp. 72–84, Mar. 2000.

[20] H. Harai, M. Murata, and H. Miyahara, "Performance Analysis of Wavelength Assignment Policies in All-Optical Networks with Limited-Range Wavelength Conversion," *IEEE J. Select. Areas Commun.*, vol. 16, no. 7, pp. 1051–1060, Sept. 1998.

[21] C. F. Hsu, T. L. Liu, and N. F. Huang, "Performance Analysis of Deflection Routing in Optical Burst-Switched Networks," in *Proc. IEEE INFOCOM'02*, June 2002.

[22] M. Izal and J. Aracil, "On the Influence of Self-Similarity in Optical Burst Switching Traffic," in *Proc. IEEE Globecom'02*, Nov. 2002, pp. 2308–2312.

[23] A. Jukan and H. R. van As, "Quality-of-Service Routing in Optical Networks," in *Proc. ECOC'97*, Sept. 1997, pp. 160–163.

[24] A. Jukan and H. R. van As, "Resource Allocation Strategies with QoS-routing in Optical Networks," in *Proc. ICC'99*, June 1999, pp. 2048–2054.

[25] A. Jukan and H. R. van As, "Service-Specific Resource Allocation in WDM Networks with Quality Constraints," *IEEE J. Select. Areas Commun.*, vol. 18, no. 10, pp. 2051–2061, Oct. 2000.

[26] A. Jukan, QoS-based Wavelength Routing in Multi-Service WDM Networks, Springer, New York, 2000.

[27] A. Jukan and H. R. van As, "Service-Specific Resource Allocation in WDM Networks with Quality Constraints," *IEEE J. Select. Areas Commun.*, vol. 18, no. 10, pp. 2051–2061, Oct. 2000.

[28] L. Kleinrock, *Queueing Systems, Volume I: Theory*. Willey, New York, 1975.

[29] M. Kovačević and A. Acampora, "Benefits of Wavelength Translation in All-Optical Clear-Channel Networks," *IEEE J. Select. Areas Commun.*, vol. 14, no. 5, pp. 868–880, June 1996.

[30] H. Kröner, G. Hébuterne, P. Boyer, and A. Gravey, "Priority Management in ATM Switching Nodes," *IEEE J. Select. Areas Commun.*, vol. 9, no. 3, pp. 418–427, Apr. 1991.

[31] V. G. Kulkarni, *Modeling and Analysis of Stochastic Systems*. Chapman&Hall, London, 1995.

[32] S. Lee, C. H. Lee, and S. Seo, "Blocking Models of All-Optical WDM Networks under Distributed Wavelength Assignment Policies," *IEICE Trans. Commun.*, vol. E84–B, no. 1, pp. 17–25, Jan. 2001.

[33] K. Long, R. S. Tucker, and C. Wang, "A New Framework and Burst Assembly for IP DiffServ over Optical Burst Switching Networks," in *Proc. IEEE Globecom'03*, Dec. 2003, pp. 3159–3164.

[34] X. Lu and B. L. Mark, "A New Performance Model of Optical Burst Switching with Fiber Delay Lines," in *Proc. IEEE ICC'03*, May 2003, pp. 1365–1369.

[35] D. Lucantoni, K. S. Meier-Hellstern, and M. F. Neuts, "A Single Server Queue with Server Vacations and a Class of Non-renewal Arrival Processes," *Adv. Appl. Probab.*, vol. 22, pp. 676–705, 1990.

[36] M. Ma and M. Hamdi, "Providing Deterministic Quality-of-Service Guarantees on WDM Optical Networks," *IEEE J. Select. Areas Commun.*, vol. 36–37, no. 10, pp. 2072–2083, Oct. 2000.

[37] M. W. McKinnon, H. G. Perros, and G. N. Rouskas, "Performance Analysis of Broadcast WDM Networks under IP Traffic," *Perform. Eval.*, vol. 36–37, no. 1–4, pp. 333–358, Aug. 1999.

[38] Y. Miyao, "λ-Ring System: An Application in Survivable WDM Networks of Interconnected Self-Healing Ring Systems," *IEICE Trans. Commun.*, vol. E84–B, no. 6, pp. 1596–1604, June 2001.

[39] D. Morató, M. Izal, J. Aracil, E. Magaña, and J. Miqueleiz, "Blocking Time Analysis of OBS Routers with Arbitrary Burst Size Distribution," in *Proc. IEEE Globecom'03*, Dec. 2003, pp. 2488–2492.

[40] H. T. Mouftah and P. H. Ho, *Optical Networks, Architecture and Survivability*. Massachusetts: Kluwer, 2002.

[41] S. Nakazawa, H. Tamura, K. Kawahara, and Y. Oie, "Performance Analysis of IP Datagram Transmission Delay in MPLS: Impact of Both Number and Bandwidth of LSPs of Layer 2," *IEICE Trans. Commun.*, vol. E85-B no. 1, pp. 165–172, Jan. 2002.

[42] C. Qiao and M. Yoo, "Optical Burst Switching (OBS) – A New Paradigm for an Optical Internet," *J. High Speed Network*, vol. 8, no. 1, pp. 69–84, Jan. 1999.

[43] C. Qiao and M. Yoo, "Choices, Features and Issues in Optical Burst Switching," *Optical Net. Mag.*, vol. 1, no. 2, pp. 36–44, Apr. 2000.

[44] C. Qiao, "Labeled Optical Burst Switching for IP-over-WDM Integration," *IEEE Commun. Mag.*, vol. 38, no. 9, pp. 104–114, Sept. 2000.

[45] B. Ramamurthy and B. Mukherjee, "Wavelength Conversion in WDM Networking," *IEEE J. Select. Areas Commun.*, vol. 16, no. 7, pp. 1061–1073, Sept. 1998.

[46] R. Ramaswami and K. N. Sivarajan, "Optimal Routing and Wavelength Assignment in All-Optical Networks," in *Proc. IEEE INFOCOM'94*, June 1994, pp.970–979.

[47] R. Ramaswami and G. Sasaki, "Multiwavelength Optical Networks with Limited Wavelength Conversion," *IEEE/ACM Trans. Networking*, vol. 6, no. 6, pp. 744–754, Dec. 1998.

[48] R. Ramaswami and K. N. Sivarajan, *Optical Networks: A Practical Perspective*. San Francisco: Morgan Kaufmann Publishers, 1998.

[49] S. Ramesh, G. N. Rouskas, and H. G. Perros, "Computing Blocking Probabilities in Multiclass Wavelength-Routing Networks with Multicast Calls," *IEEE J. Select. Areas Commun.,* vol. 20, no. 1, pp. 89–96, Jan. 2002.

[50] K. Sato, S. Okamoto, and H. Hadama, "Network Performance and Integrity Enhancement with Optical Path Layer Technologies," *IEEE J. Select. Areas Commun.*, vol. 12, no. 1, pp. 159–170, Jan. 1994.

[51] V. Sharma and E. A. Varvarigos, "Limited Wavelength Translation in All-Optical WDM Mesh Networks," in *Proc. IEEE INFOCOM'98,* Mar. 1998, pp. 893–901.

[52] K. Struyve, N. Wauters, P. Falcao, P. Arijs, D. Colle, P. Demeester, and P. Lagasse, "Application, Design, and Evolution of WDM in GTS's Pan-European Transport Network," *IEEE Commun. Mag.*, vol. 38, no. 3, pp. 114–121, Mar. 2000.

[53] S. Subramaniam, M. Azizoğlu, and A. K. Somani, "All-Optical Networks with Sparse Wavelength Conversion," *IEEE/ACM Trans. Networking.*, vol. 4, no. 4, pp. 544–557, Aug. 1996.

[54] S. Subramaniam, A. K. Somani, M. Azizoglu, and R. A. Barry, "A Performance Model for Wavelength Conversion with Non-Poisson Traffic," in *Proc. IEEE INFOCOM'97*, Apr. 1997, pp. 499–506.

[55] T. Tachibana and S. Kasahara, "Performance Analysis of Dynamic Lightpath Configuration for WDM Asymmetric Ring Networks," in *Proc. IFIP Networking 2002*, May 2002, pp. 972–983.

[56] T. Tachibana, T. Ajima, and S. Kasahara, "Round-Robin Burst Assembly and Constant Transmission Scheduling for Optical Burst Switching Networks," in *Proc. IEEE Globecom'03*, Dec. 2003, pp. 2772–2776.

[57] H. Takagi, *Queueing Analysis, Vol. 2: Finite Systems.* Elsevier Science Publishers B, 1993.

[58] J. Teng and G. N. Rouskas, "A Comparison of the JIT, JET, and Horizon Wavelength Reservation Schemes on A Single OBS Node," in *Proc. the First International Workshop on Optical Burst Switching*, Oct. 2003.

[59] V. M. Vokkarane, K. Haridoss, and J. P. Jue, "Threshold-based Burst Assembly Policies for QoS Support in Optical Burst-Switched Networks," in *Proc. SPIE OptiComm'02*, July 2002, pp. 125–136.

[60] V. M. Vokkarane, Q. Zhang, J. P. Jue, and B. Chen, "Generalized Burst Assembly and Scheduling Techniques for QoS Support in Optical Burst-Switched Networks," in *Proc. IEEE Globecom'02*, Nov. 2002.

[61] H. L. Vu and M. Zukerman, "Blocking Probability for Priority Classes in Optical Burst Switching Networks," *IEEE Commun. Lett.*, vol. 6, no. 5, pp. 214–216, May 2002.

[62] J. Y. Wei and R. I. McFarland, "Just-In-Time Signaling for WDM Optical Burst Switching Networks," *J. Lightwave Tech.*, vol. 18, no. 12, pp. 2019–2037, Dec. 2000.

[63] W. Weiershausen, A. Mattheus, and F. Küppers, Realisation of Next Generation Dynamic WDM Networks by Advanced OADM Design, in: D.W. Faulkner, A.L. Harmer (Eds.), *WDM and Photonic Networks*. IOS Press, Amsterdam, 2000, pp. 199–207.

[64] J. White, M. Zukerman, and H. L. Vu, "A Framework for Optical Burst Switching Network Design," *IEEE Commun. Lett.*, vol. 6, no. 6, pp. 268–270, June 2002.

[65] R. W. Wolff, *Stochastic Modeling and the Theory of Queues*. New Jersey: Prentice Hall, 1989.

[66] R. I. Wilkinson, "Theories for Toll Traffic Engineering in the U. S. A.," *Bell Sys. Tech. J.,* pp. 421–514, Mar. 1956.

[67] Y. Xiong, M. Vandenhoute, and H. C. Cankaya, "Control Architecture in Optical Burst-Switched WDM Networks," *IEEE J. Select. Areas Commun.*, vol. 18, no. 10, pp. 1838–1851, Oct. 2000.

[68] L. Yang, Y. Jiang, and S. Jiang, "A Probabilistic Preemptive Scheme for Providing Service Differentiation in OBS Networks," in *Proc. IEEE Globecom'03*, Dec. 2003, pp. 2689–2693.

[69] J. Yates, J. Lacey, D. Everitt, and M. Summerfield, "Limited-Range Wavelength Translation in All-Optical Networks," in *Proc. IEEE INFOCOM'96*, Mar. 1996, pp. 954–961.

[70] M. Yoo and C. Qiao, "Just-Enough-Time (JET): A High Speed Protocol for Bursty Traffic in Optical Networks," in *Proc. IEEE/LEOS Conf. on Technologies for a Global Information Infrastructure*, Aug. 1997, pp. 26–27.

[71] M. Yoo, C. Qiao, and S. Dixit, "QoS Performance of Optical Burst Switching in IP-Over-WDM Networks," *IEEE J. Select. Areas Commun.*, vol. 18, no. 10, pp. 2062–2071, Oct. 2000.

[72] X. Yu, Y. Chen, and C. Qiao, "Study of Traffic Statistics of Assembled Burst Traffic in Optical Burst Switched Networks," in *Proc. Opticomm*, July 2002, pp. 149–159.

[73] Y. Yuki, M. Nakao and H. Ibe, "Study of Wavelength Path Configuration Method for WDM Networks," in *Proc. IEICE Commun. Soc. Conf.'00*, B–10–123, 2000. (in Japanese)

[74] J. Zhou, N. Park, K. J. Vahala, M. A. Newkirk, and B. I. Miller, "Four-Wave Mixing Wavelength Conversion Efficiency in Semiconductor Traveling- Wave Amplifiers Measured to 65nm of Wavelength Shift," *IEEE Photon. Tech. Lett.*, vol. 6, no. 8, pp. 984–987, Aug. 1994.

Appendix

A. Equilibrium State Equations

For simplicity, we consider the case of $W = 2$. Then $\pi(N_r,\ J_{l_1})$'s satisfy the following equilibrium state equations.

(A) $J_{l_1} = I$: l_1 is idle.

$$\lambda^{all}_{flow}\pi(0,\ I) = \mu_r\pi(1,\ I) + p\pi(0,\ R), \tag{6.1}$$

$$\begin{aligned}(\lambda^{all}_{flow} + \mu_r)\pi(N_r,\ I) &= \lambda^{all}_{flow}\pi(N_r - 1,\ I) + \mu_r\pi(N_r + 1,\ I) \\ &\quad + p\pi(N_r,\ R), \qquad (0 < N_r \le T_h),\end{aligned} \tag{6.2}$$

$$\begin{aligned}(\lambda^{all}_{flow} + \mu_r)\pi(N_r,\ I) &= \mu_r\pi(N_r + 1,\ I) \\ &\quad + p\pi(N_r,\ R), \qquad (T_h < N_r < K_r),\end{aligned} \tag{6.3}$$

$$(\lambda^{all}_{flow} + \mu_r)\pi(K_r,\ I) = p\pi(K_r,\ R). \tag{6.4}$$

(B) $J_{l_1} = S$: l_1 is being established.

$$(\lambda^{all}_{flow} + p)\pi(0,\ S) = \mu_r\pi(1,\ S), \tag{6.5}$$

$$\begin{aligned}(\lambda^{all}_{flow} + \mu_r + p)\pi(N_r,\ S) &= \lambda^{all}_{flow}\pi(N_r - 1,\ S) \\ &\quad + \mu_r\pi(N_r + 1,\ S), \qquad (0 < N_r \le T_h),\end{aligned} \tag{6.6}$$

$$\begin{aligned}(\lambda^{all}_{flow} + \mu_r + p)\pi(N_r,\ S) &= \lambda^{all}_{flow}\pi(N_r - 1,\ S) + \lambda^{all}_{flow}\pi(N_r - 1,\ I) \\ &\quad + \mu_r\pi(N_r + 1,\ S), \quad (T_h < N_r < K_r),\end{aligned} \tag{6.7}$$

$$\begin{aligned}(\mu_r + p)\pi(K_r,\ S) &= \lambda^{all}_{flow}\pi(K_r - 1,\ S) + \lambda^{all}_{flow}\pi(K_r - 1,\ I) \\ &\quad + \lambda^{all}_{flow}\pi(K_r,\ I).\end{aligned} \tag{6.8}$$

(C) $J_{l_1} = n$ $(0 \le n \le K_l)$: l_1 is busy.

(a) $n = 0$

$$
\begin{aligned}
(\lambda_{flow}^{all} + h)\pi(0,\ 0) &= \mu_r\pi(1,\ 0) + \mu_l\pi(0,\ 1) + p\pi(0,\ S), && (6.9)\\
(\lambda_{flow}^{all} + \mu_r + h)\pi(N_r,\ 0) &= (\lambda_{flow}^{all} - \lambda_{flow})\pi(N_r - 1,\ 0)\\
&\quad +\mu_r\pi(N_r + 1,\ 0) + \mu_l\pi(N_r,\ 1)\\
&\quad +p\pi(N_r,\ S), \qquad (0 < N_r < K_r), && (6.10)\\
(\lambda_{flow} + \mu_r + h)\pi(K_r,\ 0) &= (\lambda_{flow}^{all} - \lambda_{flow})\pi(K_r - 1,\ 0) + \mu_l\pi(K_r,\ 1)\\
&\quad +p\pi(K_r,\ S). && (6.11)
\end{aligned}
$$

(b) $0 < n < K_l$

$$
\begin{aligned}
(\lambda_{flow}^{all} + \mu_l)\pi(0,\ n) &= \mu_r\pi(1,\ n) + \lambda_{flow}\pi(0,\ n - 1)\\
&\quad +\mu_l\pi(0,\ n + 1), && (6.12)\\
(\lambda_{flow}^{all} + \mu_r + \mu_l)\pi(N_r,\ n) &= (\lambda_{flow}^{all} - \lambda_{flow})\pi(N_r - 1,\ n)\\
&\quad +\mu_r\pi(N_r + 1,\ n) + \lambda_{flow}\pi(N_r,\ n - 1)\\
&\quad +\mu_l\pi(N_r,\ n + 1), \quad (0 < N_r < K_r), && (6.13)\\
(\lambda_{flow} + \mu_r + \mu_l)\pi(K_r,\ n) &= (\lambda_{flow}^{all} - \lambda_{flow})\pi(K_r - 1,\ n)\\
&\quad +\lambda_{flow}\pi(K_r,\ n - 1) + \mu_l\pi(K_r,\ n + 1). && (6.14)
\end{aligned}
$$

(c) $n = K_l$

$$
\begin{aligned}
(\lambda_{flow}^{all} + \mu_l)\pi(0,\ K_l) &= \mu_r\pi(1,\ K_l) + \lambda_{flow}\pi(0,\ K_l - 1), && (6.15)\\
(\lambda_{flow}^{all} + \mu_r + \mu_l)\pi(N_r,\ K_l) &= \lambda_{flow}^{all}\pi(N_r - 1,\ K_l) + \mu_r\pi(N_r + 1,\ K_l)\\
&\quad +\lambda_{flow}\pi(N_r,\ K_l - 1), \quad (0 < N_r < K_r), && (6.16)\\
(\mu_r + \mu_l)\pi(K_r,\ K_l) &= \lambda_{flow}^{all}\pi(K_r - 1,\ K_l) && (6.17)\\
&\quad +\lambda_{flow}\pi(K_r,\ K_l - 1).
\end{aligned}
$$

(D) $J_{l_1} = R$: l_1 is being released.

$$
\begin{aligned}
(\lambda_{flow}^{all} + p)\pi(0,\ R) &= \mu_r\pi(1,\ R) + h\pi(0,\ 0), && (6.18)\\
(\lambda_{flow}^{all} + \mu_r + p)\pi(N_r,\ R) &= \lambda_{flow}^{all}\pi(N_r - 1,\ R) + \mu_r\pi(N_r + 1,\ R)\\
&\quad +h\pi(N_r,\ 0), \qquad (0 < N_r < K_r), && (6.19)\\
(\mu_r + p)\pi(K_r,\ R) &= \lambda_{flow}^{all}\pi(K_r - 1,\ R) + h\pi(K_r,\ 0). && (6.20)
\end{aligned}
$$

B. Equilibrium State Equations for Method 2

Let $1_{\{X\}}$ denote the indicator function of event X, that is,

$$1_{\{X\}} = \begin{cases} 1, & \text{if } X \text{ occurs,} \\ 0, & \text{otherwise.} \end{cases}$$

When $M = 3$ for Method 2, equilibrium state equations are as follows.

$$\lambda_{conn}\pi(0,0,0) = \mu_{conn}\left\{\pi(1,0,0) + \pi(0,1,0) + \pi(0,0,1)\right\}, \tag{6.21}$$

$$\begin{aligned}
&(\lambda_{conn} + N_q^{(1)}\mu_{conn})\pi(N_q^{(1)},0,0) \\
&\quad = \mu_{conn}\left\{\pi(N_q^{(1)},1,0) + \pi(N_q^{(1)},0,1)\right\} \\
&\qquad + 1_{\{N_q^{(1)} < \bar{W}_q^{(1)}\}}(N_q^{(1)}+1)\mu_{conn}\pi(N_q^{(1)}+1,0,0) \\
&\qquad + \lambda_{conn}^{(1)}\pi(N_q^{(1)}-1,0,0), \qquad (N_q^{(1)} > 0),
\end{aligned} \tag{6.22}$$

$$\begin{aligned}
&(\lambda_{conn} + N_q^{(2)}\mu_{conn})\pi(0,N_q^{(2)},0) \\
&\quad = \mu_{conn}\left\{\pi(1,N_q^{(2)},0) + \pi(0,N_q^{(2)},1)\right\} \\
&\qquad + 1_{\{N_q^{(2)} < \bar{W}_q^{(2)}\}}(N_q^{(2)}+1)\mu_{conn}\pi(0,N_q^{(2)}+1,0) \\
&\qquad + \lambda_{conn}^{(2)}\pi(0,N_q^{(2)}-1,0), \qquad (N_q^{(2)} > 0),
\end{aligned} \tag{6.23}$$

$$\begin{aligned}
&(\lambda_{conn} + N_q^{(3)}\mu_{conn})\pi(0,0,N_q^{(3)}) \\
&\quad = \mu_{conn}\left\{\pi(1,0,N_q^{(3)}) + \pi(0,1,N_q^{(3)})\right\} \\
&\qquad + 1_{\{N_q^{(3)} < \bar{W}_q^{(3)}\}}(N_q^{(3)}+1)\mu_{conn}\pi(0,0,N_q^{(3)}+1) \\
&\qquad + (\lambda_{conn}^{(2)} + \lambda_{conn}^{(3)})\pi(0,0,N_q^{(3)}-1), \qquad (N_q^{(3)} > 0),
\end{aligned} \tag{6.24}$$

$$\begin{aligned}
&\{\lambda_{conn} + (N_q^{(2)} + N_q^{(3)})\mu_{conn}\}\pi(0,N_q^{(2)},N_q^{(3)}) \\
&\quad = \mu_{conn}\pi(1,N_q^{(2)},N_q^{(3)}) + 1_{\{N_q^{(2)} < \bar{W}_q^{(2)}\}}(N_q^{(2)}+1)\mu_{conn}\pi(0,N_q^{(2)}+1,N_q^{(3)}) \\
&\qquad + 1_{\{N_q^{(3)} < \bar{W}_q^{(3)}\}}(N_q^{(3)}+1)\mu_{conn}\pi(0,N_q^{(2)},N_q^{(3)}+1) \\
&\qquad + (\lambda_{conn}^{(2)} + \lambda_{conn}^{(3)})\pi(0,N_q^{(2)},N_q^{(3)}-1) \\
&\qquad + 1_{\{N_q^{(3)} = \bar{W}_q^{(3)}\}}\lambda_{conn}^{(2)}\pi(0,N_q^{(2)}-1,N_q^{(3)}), \qquad (N_q^{(2)}, N_q^{(3)} > 0),
\end{aligned} \tag{6.25}$$

$$\begin{aligned}
&\{\lambda_{conn} + (N_q^{(1)} + N_q^{(2)})\mu_{conn}\}\pi(N_q^{(1)},N_q^{(2)},0) \\
&\quad = \mu_{conn}\pi(N_q^{(1)},N_q^{(2)},1) + 1_{\{N_q^{(1)} < \bar{W}_q^{(1)}\}}(N_q^{(1)}+1)\mu_{conn}\pi(N_q^{(1)}+1,N_q^{(2)},0) \\
&\qquad + 1_{\{N_q^{(2)} < \bar{W}_q^{(2)}\}}(N_q^{(2)}+1)\mu_{conn}\pi(N_q^{(1)},N_q^{(2)}+1,0) \\
&\qquad + \lambda_{conn}^{(1)}\pi(N_q^{(1)}-1,N_q^{(2)},0)
\end{aligned}$$

$$+1_{\{N_q^{(1)}=\bar{W}_q^{(1)}\}}\lambda_{conn}^{(1)}\pi(N_q^{(1)},N_q^{(2)}-1,0), \qquad (N_q^{(1)},N_q^{(2)}>0), \tag{6.26}$$

$$\begin{aligned}
&\{\lambda_{conn}+(N_q^{(1)}+N_q^{(3)})\mu_{conn}\}\pi(N_q^{(1)},0,N_q^{(3)})\\
&\quad=\mu_{conn}\pi(N_q^{(1)},1,N_q^{(3)})+1_{\{N_q^{(1)}<\bar{W}_q^{(1)}\}}(N_q^{(1)}+1)\mu_{conn}\pi(N_q^{(1)}+1,0,N_q^{(3)})\\
&\qquad+1_{\{N_q^{(3)}<\bar{W}_q^{(3)}\}}(N_q^{(3)}+1)\mu_{conn}\pi(N_q^{(1)},0,N_q^{(3)}+1)+\lambda_{conn}^{(1)}\pi(N_q^{(1)}-1,0,N_q^{(3)})\\
&\qquad+(\lambda_{conn}^{(2)}+\lambda_{conn}^{(3)})\pi(N_q^{(1)},0,N_q^{(3)}-1), \qquad (N_q^{(1)},N_q^{(3)}>0),
\end{aligned} \tag{6.27}$$

$$\begin{aligned}
&\Big\{1_{\{\Gamma\}}\lambda_{conn}^{(1)}+1_{\{\Theta\}}\lambda_{conn}^{(2)}+1_{\{N_q^{(3)}<\bar{W}_q^{(3)}\}}\lambda_{conn}^{(3)}+(N_q^{(1)}+N_q^{(2)}+N_q^{(3)})\mu_{conn}\Big\}\times\\
&\qquad\pi(N_q^{(1)},N_q^{(2)},N_q^{(3)})\\
&\quad=1_{\{N_q^{(1)}<\bar{W}_q^{(1)}\}}(N_q^{(1)}+1)\mu_{conn}\pi(N_q^{(1)}+1,N_q^{(2)},N_q^{(3)})\\
&\qquad+1_{\{N_q^{(2)}<\bar{W}_q^{(2)}\}}(N_q^{(2)}+1)\mu_{conn}\pi(N_q^{(1)},N_q^{(2)}+1,N_q^{(3)})\\
&\qquad+1_{\{N_q^{(3)}<\bar{W}_q^{(3)}\}}(N_q^{(3)}+1)\mu_{conn}\pi(N_q^{(1)},N_q^{(2)},N_q^{(3)}+1)\\
&\qquad+\lambda_{conn}^{(1)}\pi(N_q^{(1)}-1,N_q^{(2)},N_q^{(3)})+(\lambda_{conn}^{(2)}+\lambda_{conn}^{(3)})\pi(N_q^{(1)},N_q^{(2)},N_q^{(3)}-1)\\
&\qquad+1_{\{N_q^{(1)}=\bar{W}_q^{(1)}\}}\lambda_{conn}^{(1)}\pi(N_q^{(1)},N_q^{(2)}-1,N_q^{(3)})\\
&\qquad+1_{\{N_q^{(3)}=\bar{W}_q^{(3)}\}}\lambda_{conn}^{(2)}\pi(N_q^{(1)},N_q^{(2)}-1,N_q^{(3)})\\
&\qquad+1_{\{N_q^{(2)}=\bar{W}_q^{(2)},N_q^{(3)}=\bar{W}_q^{(3)}\}}\lambda_{conn}^{(1)}\pi(N_q^{(1)},N_q^{(2)},N_q^{(3)}-1),\\
&\qquad\qquad\qquad\qquad (N_q^{(1)},N_q^{(2)},N_q^{(3)}>0).
\end{aligned} \tag{6.28}$$

In (6.28), the sets of events Γ and Θ are given by

$$\begin{aligned}
\Gamma&=\{N_q^{(1)}<\bar{W}_q^{(1)}\}\cup\{N_q^{(2)}<\bar{W}_q^{(2)}\}\cup\{N_q^{(3)}<\bar{W}_q^{(3)}\},\\
\Theta&=\{N_q^{(2)}<\bar{W}_q^{(2)}\}\cup\{N_q^{(3)}<\bar{W}_q^{(3)}\}.
\end{aligned}$$